DOI:
10.1038/s41563-019-0371-y

Document Version
Peer reviewed version

A mechano-signalling network linking microtubules, myosin-IIA filaments and integrin-based adhesions

Nisha Bte Mohd Rafiq*[1,2], Yukako Nishimura*[1], Sergey V. Plotnikov[3], Visalatchi Thiagarajan[1], Zhen Zhang[1], Shidong Shi[1], Meenubharathi Natarajan[1], Virgile Viasnoff[1,4,5], Pakorn Kanchanawong#[1,6], Gareth E. Jones#[2] and Alexander D. Bershadsky#[1,7]

*Co-first authors
#Co-corresponding authors

[1]Mechanobiology Institute, National University of Singapore, Singapore 117411, Singapore
[2]Randall Centre for Cell & Molecular Biophysics, King's College London, London SE1 1UL, UK
[3]Department of Cell and Systems Biology, University of Toronto, Toronto, Ontario, Canada M5S 3G5
[4]CNRS UMI 3639, 5A Engineering drive 1, 117411 Singapore
[5]Department of Biological Sciences, National university of Singapore, 14 Science Drive 4, Singapore 117543
[6]Deparment of Biomedical Engineering, National University of Singapore, Singapore 117411
[7]Department of Molecular Cell Biology, Weizmann Institute of Science, Rehovot 76100, Israel

Keywords: actomyosin contractility, focal adhesions, GEF-H1, KANK, podosomes, SIM

Lead contact and correspondence to: alexander.bershadsky@weizmann.ac.il

Abstract

The interrelationship between microtubules and the actin cytoskeleton in mechanoregulation of integrin-mediated adhesions is poorly understood. Here, we show that the effects of microtubules on two major types of cell-matrix adhesions, focal adhesions and podosomes, are mediated by KANK family proteins connecting the adhesion protein talin with microtubule tips. Both total microtubule disruption and microtubule uncoupling from adhesions by manipulations with KANKs trigger a massive assembly of myosin-IIA filaments, augmenting focal adhesions and disrupting podosomes. Myosin-IIA filaments are indispensable effectors in the microtubule-driven regulation of integrin-mediated adhesions. Myosin-IIA filament assembly depends on Rho activation by the RhoGEF, GEF-H1, which is trapped by microtubules when they are connected with integrin-mediated adhesions via KANK proteins but released after their disconnection. Thus, microtubule capturing by integrin-mediated adhesions modulates the GEF-H1-dependent effect of microtubules on the assembly of myosin-IIA filaments. Subsequent actomyosin reorganization then remodels the focal adhesions and podosomes, closing the regulatory loop.

Main

The cytoskeleton is a composite material comprised of several types of fibrillar structures and molecular motors [1]. The coordinated function of these cytoskeletal elements is poorly understood. We focus here on the crosstalk between microtubules and the specialized domains of the actin cytoskeleton, focal adhesions and podosomes.

Focal adhesions are elongated micron-sized clusters of transmembrane integrin molecules associated with a complex network of plaque proteins that connect them to bundles of actin filaments[2-4]. It was shown long ago that disruption of microtubules by microtubule-depolymerizing agents leads to a substantial increase in the size and in some cases the number of mature focal adhesions [5,6], whilst microtubule outgrowth following washout of microtubule-depolymerizing drugs leads to a transient decrease in size or even the disappearance of focal adhesions [7]. Different facets of these phenomena have been investigated and several mechanisms were suggested (See Supplementary Information). Recent studies revealed that novel components of focal adhesions, KANK1 and KANK2, can physically connect focal adhesions and microtubule tips. Indeed, KANKs interact with a major integrin-associated protein, talin, and, via α and β liprins, with the cortical microtubule docking complex (liprins, ELKS, LL5β), which in turn bind to CLASP end-tracking proteins[8-12]. In addition, KANK proteins can bind directly to the microtubule plus-end motor KIF21A [8,11] and, at least in Drosophila, to EB1 [13].

Podosomes are another integrin-based cell-matrix adhesions common in cells of monocytic origin but found also in cells of several other types[14,15]. The characteristic structural feature of a podosome is a submembranous actin core formed due to Arp2/3-dependent actin polymerization. The actin core is associated with an approximately ring-shaped cluster of adhesion proteins including transmembrane integrin molecules and the plaque molecules (paxillin, talin, vinculin etc.) linking

3

integrins to the actin network, essentially similar to those in focal adhesions. Unlike focal adhesions, podosomes integrity does not require actomyosin-dependent traction forces [16]. Importantly, in contrast to the case for focal adhesions, disruption of microtubules in macrophage-like cells results in a rapid disassembly of podosomes [17,18]. Several mechanisms involved in this process has been proposed (see Supplementary Information).

The contrast between the effects of microtubule disruption on focal adhesions and podosomes led to a suggestion that microtubules regulate these integrin adhesions using different mechanisms. In this study we surprisingly find a common mechanism underlying the effect of microtubules on both focal adhesions and podosomes. We present evidence that the common mechanism operates via KANK family proteins and the GEF-H1-dependent local regulation of myosin-IIA filament assembly by microtubules.

4

Phenocopying microtubule disruption by hindering KANK's function

We addressed the effect of perturbations of the microtubule network on focal adhesions and podosomes. Human fibrosarcoma cell line, HT1080 display a well-developed system of focal adhesions, while the human monocytic THP1 cell line, which upon treatment with transforming growth factor-beta 1 (TGFβ1) undergo differentiation into macrophage-like cells, form numerous podosomes [19]. We used THP1 cells treated with TGFβ1 in all the experiments presented in this paper.

Treatment with 1 μM nocodazole disrupted microtubules completely in both HT1080 and THP1 cells (Figure 1). To uncouple microtubules from adhesion structures in a more physiological manner, we experimentally perturbed KANK1 and KANK2 proteins connecting microtubule tips with integrin adhesions [8,10] (Figure 1). We then compared the effects of total microtubule disruption on podosomes and focal adhesions with those caused by depletion of KANK1 or KANK2 (Figure 1 and Supplementary Figure 1). In agreement with previous studies, we found that disruption of microtubules led to an increase of focal adhesion number and size in HT1080 cells (Figure 1A, B and R), but completely disrupted podosomes in TGFβ1-stimulated THP1 cells (Figure 1G, H, S and T).

As shown by gene expression profiling (Supplementary Table 1), both KANK1 and KANK2 isoforms are expressed in HT1080 and THP1 cells. Expression of two other isoforms, KANK3 and KANK4 was negligible. We confirmed previous observations on the localization of GFP-KANK1 and 2 around focal adhesion plaques [8,9] (Figure 1L and M). We further demonstrated that in THP1 cells, GFP-KANK1 localize to the external ring surrounding podosomes (Panel O in Figure 1 and Supplementary Figure 1A). Similar localization of KANK1 around podosomes was also observed in phorbol 12-myristate 13-acetate (PMA)-stimulated murine macrophage RAW 264.7 macrophages (Supplementary Figure 2A). Association of KANK2 with podosomes in

THP1 cell was less prominent than that of KANK1, even though a small number of podosomes were surrounded by KANK2-positive rings (Figure 1P).

In HT1080 cells, knockdown of either KANK1 or KANK2 produced an increase in focal adhesion size similar to total disruption of microtubules by nocodazole (Figure 1A-F and R). The double knockdown of KANK1 and KANK2 affected focal adhesions more strongly than the knockdown of KANK1 or KANK2 alone (Figure 1R , Supplementary Figure 1C). In THP1 cells, knockdown of KANK1 and KANK2 produced different effects (Figure 1G-K). Only the knockdown of KANK1 induced pronounced disruption of podosomes in THP1 cells, phenocopying the effect of total microtubule disruption. Knockdown of KANK2 did not significantly affect podosome number in THP1 cells (Figure 1K, S and T) even though it increased the cell projection area (Supplementary Figure 1B).

In addition to KANK1/2 knockdown, we uncoupled microtubules from integrin adhesions by overexpression of KANK1/2 truncated constructs, GFP-KANK1-KN and GFP-KANK2-KN, which bind to talin but not to microtubules [8,9] (Figure 1C). We anticipated that these constructs would compete with endogenous KANK1 and 2 for binding to talin. Indeed, expression of either GFP-KANK1-KN or GFP-KANK2-KN in HT1080 cells resulted in localization of these constructs to focal adhesions and elimination of endogenous KANK2 from this location (Figure 1N, Supplementary Figures 1D and E). Then we examined how such treatment affected focal adhesions. Overexpression of GFP-KANK1-KN or GFP-KANK2-KN led to an increase in focal adhesion size (Figure 1N, R and Supplementary Figure 1E), similarly to KANK1/2 knockdowns. An increase in focal adhesion size upon overexpression of KN domains of KANK1 or KANK2 was also observed in human colon adenocarcinoma line (HT-29) cells and human umbilical vein endothelial cells (HUVECs) (Supplementary Figure 2E-K).

We then overexpressed GFP-KANK1-KN or GFP-KANK2-KN in THP1 cells and found that excess of KN domain of either KANK1 or KANK2 led to a significant reduction in

podosome number and the appearance of focal adhesion-like structures, resembling the effects of KANK1 knockdown (Figure 1Q, S, T, Supplementary Figure 1F). Both exogenous GFP-KANK1-KN and GFP-KANK2-KN were localized to the few residual podosomes and to newly-formed focal adhesion-like structures. This suggests that the KN domains of KANK1 and KANK2 are similar and compete with endogenous KANK1 for binding to talin in podosomes. Similar effects were also observed in another podosome-forming cell type, RAW 264.7 macrophages, in which overexpression of GFP-KANK1-KN led to elimination of podosomes and formation of numerous focal adhesion-like structures (Supplementary Figure 2B-D).

To understand why KANK2, unlike KANK1, is poorly localized to podosomes, in spite of the functional similarity of their KN domains, we examined the role of the liprin-binding coiled-coil domains of KANK1 and KANK2 [8,9]. We created a chimeric construct of KANK2 (KANK2/CC-KANK1) in which its own coiled-coil domain was substituted with that of KANK1 (Supplementary Figure 3A). Such chimeric construct localized to podosome rings much better than KANK2 (Supplementary Figure 3B and C). Moreover, while wild-type KANK2 did not rescue podosomes in KANK1-depleted cells, the GFP fusion of KANK2/CC-KANK1 induced formation of podosomes in cells lacking KANK1 (Supplementary Figure 3D, E and F). This suggests that the differential role of KANK1 and KANK2 in podosome regulation depends on differences in their liprin-binding domains.

We further performed additional rescue experiments on KANK1-depleted THP1 cells and KANK2-depleted HT1080 cells using various deletion mutants of KANK1 and KANK2, respectively (Supplementary Figure 4A and F). The constructs (GFP-KANK1ΔANKR, GFP-KANK2 (1-670)) containing the talin-binding domain together with the coil-coiled liprin-binding domain rescued the effects of KANK1 and KANK2 knockdowns respectively, similarly to the full-length KANK1 or KANK2 (Supplementary Figure 4B, C, G, H, K-M). Of note here, the C-terminal regions of KANK1 and KANK2 containing ankyrin repeats known to be involved in binding KIF21A kinesin [11], appeared to be dispensable for the KANK1 effect on podosomes

and KANK2 effect on focal adhesions. At the same time, the constructs consisting of talin-binding domain alone (GFP-KANK1-KN, GFP-KANK2-KN), or constructs lacking a talin-binding domain (GFP-KANK1-CC-Cter, GFP-KANK2ΔKN), which cannot link talin-containing structures with microtubules, did not rescue the effects of KANK1 knockdown on podosomes and KANK2 knockdown on focal adhesions (Supplementary Figure 4D, E, I, J, K-M).

KANKs control focal adhesion by linking them to microtubules

To study the role of KANK proteins in microtubule targeting to focal adhesions, we plated HT1080 cells onto patterned substrata consisting of 4 μm diameter fibronectin islands (Figure 2A). Cells spreading on such substrata form focal adhesions only within these islands (Figure 2B). In control cells, microtubule tips are concentrated at such islands but not at circular areas of similar dimension lacking focal adhesions (Figure 2C, E, F and Supplementary Movie 1). In cells depleted of KANK1 and KANK2, the microtubule tips were randomly distributed (Figure 2D, E and G, Supplementary Movie 2).

While disruption of microtubules resulted in augmentation of focal adhesions, microtubule outgrowth after nocodazole washout led to transient disassembly of focal adhesions ([7,20] and Supplementary Movie 3). To elucidate the role of KANK-mediated microtubule targeting in the negative regulation of focal adhesions, we used the technique of rapamycin-induced dimerization to link two parts of KANK1 protein: the KN talin-binding domain and the remaining part of the molecule (ΔKN) (Figure 2H). Transfection of HT1080 cells with mApple-KN-FRB and FKBP-ΔKN-mEmerald resulted in localization of mApple-KN-FRB (green) to focal adhesions and diffuse distribution of FKBP-ΔKN-mEmerald (red)(Figure 2I). The addition of rapamycin, which links mApple-KN-FRB with FKBP-ΔKN-mEmerald, led to accumulation of FKBP-ΔKN-mEmerald to KN-containing adhesions and subsequently triggered transient disassembly of focal adhesion as manifested by disappearance of vinculin (Figure 2I and I', Supplementary Movie 4). Coupling of

microtubules to focal adhesions by rapamycin-induced dimerization of KANK1 domains, also resulted in a rapid decrease of traction forces exerted by cell (Figure 2J), which, in view of focal adhesion mechanosensitivity, could be the cause of focal adhesion disassembly.

Myosin-II filaments mediate microtubule effects on adhesions

We found that disruption of microtubules or uncoupling them from integrin adhesions resulted in massive formation of new myosin-II filaments visualized by SIM using myosin-II regulatory light chain or myosin-IIA heavy chain labeling (Figure 3). This effect was especially dramatic in THP1 cells, which normally contain only a peripheral rim of myosin-II filaments associated with circumferential actin bundles. (Figure 3A, Supplementary Movie 5). Upon addition of nocodazole, disassembly of podosomes followed a drastic increase in the number of new myosin-II filaments (Figure 3A, A', J, K, Supplementary Movie 5). The newly-formed myosin-II filaments aligned in registry forming "stacks" [21] (Figure 3A, E and Supplementary Movie 5). Simultaneously, short actin filament bundles associated with newly formed focal adhesion-like structures appeared (Figure 3E and L). In HT1080 cells, the disruption of microtubules also significantly increased the amount of myosin-II filaments located in the central part of the cell. This increase was accompanied by growth of focal adhesions (Figure 3B, B', Supplementary Movie 6). The epithelial HT-29 cells also responded to microtubule disruption by augmentation of myosin-II filaments (Supplementary Figure 2E, F) in agreement with [22].

Knockdown of KANK1 in THP1 cells also produced a significant increase of the number of myosin-IIA filaments organized into stacks, as well as formation of focal adhesion-like structures (Figure 3G and L). In HT1080 cells, KANK2 knockdown resulted in significant increase in formation of myosin-II filaments and focal adhesion area (Supplementary Figure 5A and C).

To ascertain whether myosin-IIA filament assembly and disassembly are consequential or causal factors that account for the changes in focal adhesions and podosomes, we interfered with myosin-II filament formation by siRNA-mediated knockdown of myosin-IIA. In THP1 cells lacking myosin-IIA, podosomes were insensitive to disruption of microtubules by nocodazole or their disconnection from integrin adhesions by depletion of KANK1 (Figure 3C-K). Consistent with previous studies [23,24], we found that myosin IIA-depleted HT1080 cells essentially lack mature focal adhesions but contain small nascent adhesions at the cell periphery. The size of these adhesions did not increase upon either treatment with nocodazole or by KANK2 knockdown (Supplementary Figure 5A-C). Thus, we conclude that depletion of myosin-IIA filaments abolished the effect of microtubule disruption, or disconnection from integrin-mediated adhesions by KANK1/2 knockdown, on both focal adhesions and podosomes.

Unlike myosin-IIA, the knockdown of myosin-IIB did not prevent the effects of microtubule disruption or disconnection from integrin adhesions on both focal adhesions and podosomes (Supplementary Figure 5D-K).

Recovery of microtubules following nocodazole washout in HT1080 cells led to a rapid decrease in myosin-II filament number and the traction forces exerted by cells on a substrate, which returned to the control level 20 minutes following the washout (Supplementary Figure 6A-D, Supplementary Movie 7 and Supplementary Movie 8). The drop in traction forces preceded the decrease in focal adhesion size, while the recovery of traction forces preceded the enlargement of focal adhesions (Supplementary Figure 6D) consistent with the concept of focal adhesion mechanosensitivity[25].

Finally, we found that effect of microtubule recovery on myosin-II filaments and focal adhesions is reduced in HT1080 cells lacking KANK2. KANK2-depleted HT1080 cells did not demonstrate a pronounced drop in the amount of myosin-II filaments and focal adhesion area under condition of microtubule outgrowth

(Supplementary Figure 6E-G, Supplementary Movie 9). Together with data on decrease of traction force and focal adhesions upon chemically-induced dimerization of KANK domains (Figure 2H-J), these data suggest that the microtubule effect on myosin-II filaments and focal adhesions depends on local interactions of microtubules with focal adhesions via KANK proteins.

Microtubules control integrin adhesions via Rho-ROCK axis

Microtubule disruption as well as KANK1 depletion resulted in an increase in the fraction of RhoA-GTP in both HT1080 and THP1 cells (Supplementary Figure 7A and B) in agreement with previous studies [26,27]. KANK2 knockdown also led to increased RhoA-GTP levels in HT1080 cells but not in THP1 cells Supplementary Figure 7A and B) consistent with the lack of the effect KANK2 knockdown on podosomes in these cells (Figure 1K, S and T).

We further found that Rho activation by the small peptide CN03, mimicked the disruptive effect of microtubule disassembly or KANK1 depletion on podosomes (Supplementary Figure 7C, C', Supplementary Movie 10). Inhibition of ROCK by Y-27632 or thiazovivin, did not affect podosomes in control THP1 cells, but prevented the podosome disruption after nocodazole treatment (Figure 4C and D, Supplementary Figure 7D, E, G-K, Supplementary Movie 11, Supplementary Movie 12 and Supplementary Movie 13). Moreover, addition of Y-27632 to THP1 cells incubated with nocodazole and demonstrating enhanced level of myosin-II filaments along with complete lack of podosomes, rapidly disassembled myosin-II filaments and subsequently rescued podosomes (Figure 4C and D, Supplementary Figure 7F and F', Supplementary Movie 14).

Inhibition of ROCK by Y-27632 also led to rescue of podosomes in KANK1 knockdown THP1 cells (Figure 4A-D, Supplementary Movie 15). Rescued podosomes were functionally active in terms of their ability to degrade extracellular matrix. The podosomes of control THP1 cell actively degrade fluorescent gelatin in

agreement with previous studies [28]. The depletion of KANK1 induced elimination of podosomes and formation of focal adhesions, which also degraded gelatin (c.f. [29]) but far weaker than podosomes. Treatment of KANK1-depleted cells with Y-27632 not only rescued morphologically normal podosomes but also restored the gelatin degradation pattern (Figure 4E).

Data showing podosome rescue in KANK1 knockdown cells by treatment with Y-27632 make it possible to check that KANK1 is indeed responsible for targeting of microtubules to podosomes. We plated podosome-forming THP1 cells on micro-patterned substrata so that podosomes were formed only inside the small adhesive islands. In THP1 cells transfected with control siRNA, microtubule tips overlap with podosomes at adhesive islands at the lowest focal plane (z= 0 μm) (Figure 4I). In cells lacking KANK1, podosomes were absent and microtubule tips were not found at the z=0 μm plane, where focal adhesion-like structure were located (Figure 4J). Treatment with Y-27632 by itself affected neither podosome formation nor localization of microtubules to podosome-containing islands (Figure 4K). In KANK1 knockdown cells treated with Y-27632, the recovered podosomes, unlike the control ones, were not colocalized with microtubule tips at z=0 μm plane (Figure 4L). Quantification of the association of microtubule tips with podosomes at micro-patterned adhesive islands is given in Figure 7C-D. These data (quantified in Supplementary Figure 8) showed that KANK1 is indeed necessary for targeting of microtubules to podosomes. In addition, these results show that functional podosomes can be maintained without a connection to microtubules if Rho/ROCK-dependent myosin-II filament formation is suppressed.

Whilst disruption of podosomes is induced by disruption of microtubules, disruption of focal adhesion occurs upon microtubule outgrowth. We showed above that this process was preceded by the decrease of traction forces due to disassembly of myosin-II filaments (Supplementary Figure 6A-D). Expression of either constitutively active RhoA (Q63L), or constitutively active ROCK mutant (rat Rok-

alpha 1-543aa) known to activate myosin-II filament formation prevented the disruptive effect of microtubule outgrowth on focal adhesions in HT1080 cells (Supplementary Figure 7L-N, Supplementary Movie 16). Thus, we conclude that microtubules regulate focal adhesions through the same pathway as podosomes, via modulation of Rho/ROCK activity.

Microtubule capturing by adhesions control GEF-H1 function

The Rho nucleotide exchange factor, GEF-H1 is associated with microtubules in both THP1 and HT1080 cells as well as HUVECs, and demonstrated diffuse distribution upon microtubule disruption (Figure 5A and B, Supplementary Figure 9A, B and F), in agreement with previous observations [30-32]. Remarkably, diffuse localization of GEF-H1 was also observed upon knockdown of KANK1 in THP1 cells and HUVECs, or KANK1 and KANK2 in HT1080 cells, even though microtubule integrity was well preserved (Figure 5A-C, Supplementary Figure 9A-G). Moreover, overexpression of KANK1-KN talin-binding domain reproduced the effect of KANK1 knockdown on GEF-H1 localization in THP1 cells (Figure 5D). Thus, not only the disruption of microtubules but merely the uncoupling of microtubules from integrin adhesions led to release of GEF-H1.

Next, we investigated whether GEF-H1 depletion prevents the effects of KANK knockdowns on the myosin-II filaments and integrin adhesions in both THP1 and HT1080 cells.

GEF-H1 knockdown THP1 cells essentially preserved the phenotype of control cells, having myosin-II filaments at the periphery and podosomes in the central area. The integrity of the microtubule network was also unchanged (Figure 5F and G, Supplementary Figure 9H and I). Disruption of microtubules in GEF-H1 knockdown cells however did not result in augmentation of myosin-II filaments and did not lead to podosome disassembly and formation of focal adhesion-like structures. Moreover, double knockdown of GEF-H1 and KANK1 also did not lead to a reduction

in podosome number, unlike the knockdown of KANK1 alone. Finally, GEF-H1 knockdown also prevented the effect of overexpression of KANK1 talin-binding domain, GFP-KANK1-KN (Figure 5H-P, Supplementary Figure 9J-M).

In HT1080 cells lacking GEF-H1, the disruption of microtubules by nocodazole as well as disconnection of microtubules from adhesions by KANK2 knockdown only weakly, if at all, increased focal adhesion size above its level in cells with knockdown of GEF-H1 alone. Similarly, knockdown of GEF-H1 reduced the increase of focal adhesion size in cells overexpressing the GFP-KANK2-KN (Supplementary Figure 10A-H and K, graph in Supplementary Figure 11). Whilst in control HT1080 cells, microtubule outgrowth produced transient disassembly of focal adhesions, in GEF-H1-depleted HT1080 cells, focal adhesion disruption upon microtubule recovery was less pronounced (Supplementary Figure 10I-K, Supplementary Movie 17). Altogether, these results show that both the protective effect of microtubules on podosomes and suppressive effect on focal adhesions are mediated via GEF-H1 regulation.

Of note in this study, possible off-target effects of Dharmacon SMARTpool siRNAs against myosin-IIA and GEF-H1 were excluded by validation experiments using individual siRNAs taken from the corresponding SMARTpools (Supplementary Figure 11).

14

In this study, we have discovered a mechanism for the microtubule-mediated regulation of both focal adhesions and podosomes operating via KANK family proteins and GEF-H1-dependent reorganization of myosin-II filaments (Figure 6). KANKs are required for targeting of microtubules to both types of integrin adhesions by linking talin to the liprin-containing cortical microtubule docking complex ([8,10] and this study). Both depletion of KANKs and their displacement from talin by overexpression of talin-binding KN domain of KANKs faithfully reproduce the contrasting effects of total microtubule disruption: elimination of podosomes and augmentation of focal adhesions in several cell types. This indicates that both supportive effect of microtubules on podosomes and suppressive effect on focal adhesions are mediated by KANKs. Indeed, linking the microtubules and focal adhesions by rapamycin-induced dimerization of KN domain with the remaining part of KANK, leads to disassembly of focal adhesions. The coiled-coil liprin-binding domain of KANK proteins, together with KN domain were necessary and sufficient to restore the effect of microtubules on integrin adhesions in KANK-depleted cells. KANK1 and KANK2 isoforms are not entirely equivalent. While the KN domains of KANK1 and KANK2 were shown to be functionally similar, the coiled-coil domains are different, which explains the differential effects of KANK1 and KANK2 knockdowns on podosomes.

Studying the effects of microtubule disruption or uncoupling from integrin adhesions using SIM microscopy, we demonstrate that the major consequence of such treatments is a dramatic increase in the number of myosin-II filaments. Moreover, a burst of microtubule polymerization resulted in a transient decrease in the number of myosin-II filaments. The magnitude of traction forces exerted by cells essentially follows the quantity of myosin-II filaments, which explains the changes in traction force upon KANK2 knockdown and its rescue observed in [9].

We demonstrated that the effects of microtubule disruption or uncoupling from talin on podosomes and focal adhesions can be efficiently abolished by various pharmacological and genetic manipulations affecting myosin-IIA filament assembly.

In particular, disassembly of myosin-II filament by ROCK inhibition recovered functionally active podosomes in spite of their uncoupling from microtubules or even total microtubule disruption. These experiments show that KANK-mediated links between integrin adhesions and microtubules controls the integrin adhesions indirectly via regulation of the assembly of myosin-II filaments, which then remodels these adhesions.

How does microtubule disruption or their uncoupling from adhesions affect myosin-II filament assembly? We investigated the role of the RhoGEF, GEF-H1 known to be associated with microtubules [30,31,33] in this process. We have shown that knockdown of GEF-H1 renders the level of myosin-II filament polymerization independent of microtubule integrity or their association with adhesion structures. In GEF-H1 knockdown cells, neither microtubule disruption nor KANK depletion, nor its displacement from talin led to podosome disassembly or focal adhesion growth. It is suggested that GEF-H1 undergoes inactivation when associated with microtubules and is rapidly activated upon microtubule disruption [30,34]. Our experiments showed that GEF-H1 can be released from microtubules and apparently activated not only upon microtubule disruption but also upon uncoupling microtubules from integrin adhesions by KANK knockdown or displacement from talin. Previous studies have already demonstrated that knockdown of KANK1 [27] and KANK2 [35] led to activation of Rho but overlooked the role of GEF-H1 in such activation. Our experiments suggest that it is not merely the presence of KANK in the cytoplasm but its simultaneous binding to talin and microtubules that is required for suppression of Rho activity, most probably by arresting GEF-H1 on microtubules (Figure 6).

It remains to be studied which changes in biochemistry or mechanics of microtubules induced by their uncoupling from integrin adhesions are responsible for release and activation of GEF-H1. It is possible that disconnection of microtubules from adhesions intensifies their dynamics and consequently the GEF-H1 turnover. Coupling/uncoupling of microtubules from integrin adhesions can also

alter the organization of microtubule lattice affecting the release of GEF-H1 from the microtubule wall. Indeed, recent studies demonstrated that microtubule bending can modify the lattice triggering tubulin acetylation [36,37].

Proteins associated with microtubules can participate in the regulation of GEF-H1 release. Of note, knockdown of EB1, a plus-end tracking protein possibly involved in microtubule connection to integrin adhesions, was shown to promote release of GEF-H1 from microtubules [38]. In addition, depletion of vimentin intermediate filaments was shown to result in GEF-H1-dependent Rho activation [32], suggesting yet another avenue for such regulation.

The question of why myosin-IIA filaments affect podosomes and focal adhesions in such a different and contrasting manner remains open. Myosin-IIA filaments promote assembly of mechanosensitive focal adhesions by generation of traction forces [25,39] and stabilizing the focal adhesion-associated stress fibers [40-42]. The sensitivity of the actin core of podosomes to mechanical factors differs from that of focal adhesion plaques. Podosomes can form in the absence of traction forces in cells plated on a fluid lipid bilayer [16] and in the presence of inhibitors of myosin-II filament formation ([43] and this study). The excess of myosin-II filaments may induce collapse of the Arp2/3 branched actin networks at the podosome cores and their rapid transformation into actomyosin bundle-like structures. Submembranous myosin-II filaments may also reduce membrane curvature [44] and therefore antagonize podosome integrity.

Microtubules control the directional migration of fibroblasts [45] regulating focal adhesion turnover [46]. Podosomes are required for migration of some cell types [47] and their integrity depends on microtubules[17]. Our study shows that both turnover of focal adhesions and maintenance of podosomes are controlled by linking of microtubules to these adhesions via KANK proteins. Such linking regulates the Rho/ROCK signaling axis and hence the myosin-IIA filament assembly in a GEF-H1 dependent manner. It is reasonable to suggest that such regulation can operate

locally. Indeed, the formation of focal adhesions on rigid substrates creates a positive feedback loop involving activation of Rho, enhancement of myosin-II driven contractility and further growth of mechanosensitive focal adhesions[48]. To break this self-activating loop and control tension homeostasis [49], microtubule-dependent mechanism of local inhibition of Rho activation upon touching the focal adhesions seems plausible. At the trailing edge, the same mechanism could trigger the disassembly of focal adhesions and then promote the burst of myosin-II contractility upon detachment of microtubules from these adhesions, which results in tail retraction [9,50,51]. In podosome-forming cells, microtubule-driven suppression of myosin-II activity can promote formation of podosomes at the leading edge, permitting directional cell movement [47].

Conclusions

We demonstrated that interactions between two major elements of the cytoskeleton, microtubules and the actomyosin network, is mediated by integrin-based adhesions, which at the same time are strongly affected by these interactions. Linking microtubules with the cytoplasmic domains of integrin locally regulate Rho/ROCK signaling that affects the formation of myosin-IIA filaments. Myosin-IIA filaments in turn operate as effectors controlling integrin-based adhesions. This feedback regulatory loop consisting of an interwoven mix of signaling and mechanical events provides a basis for understanding the entire cytoskeleton as a smart composite material.

Acknowledgements

We thank Anna Akhmanova (Utrecht University, Netherlands), Reinhard Fäasler (Max Plank Institute for Biochemistry, Martinsried, Germany), Clare M. Waterman (National Institutes of Health, USA), Ronen Zaidel-Bar (Mechanobiology Institute, Singapore) and Mark Dodding for providing constructs used in this study. We are grateful to Anna Akhmanova for useful discussions and constructive criticism. We thank Diego Pitta de Araujo (MBI Science Communications Unit) for help with Figure 6. This research is supported by the National Research Foundation, Prime Minister's Office, Singapore and the Ministry of Education under the Research Centres of Excellence programme through the Mechanobiology Institute, Singapore (ref no. R-714-006-006-271) (A.D.B, N.B.M.R., T.V., and N.M.) and Singapore Ministry of Education Academic Research Fund Tier 3 MOE Grant No. MOE2016-T3-1-002 (A.D.B, Y.N.). ADB also acknowledges support from and from Maimonides Israeli-France grant (Israeli Ministry of Science Technology and Space) and EU Marie Skłodowska-Curie Network InCeM (Project ID: 642866) at the Weizmann Institute of Science. N.B.M.R is also funded by a joint National University of Singapore-King's College London graduate studentship. G.E.J. is supported by the Medical Research Council, UK (G1100041, MR/K015664) and the generous provision of a visiting professorship from the Mechanobiology Institute, Singapore. P.K. and Z.Z. are funded by the Ministry of Education Academic Research Fund Tier 2 (MOE-T2-1-124), the Mechanobiology Institute seed funding, the National Research Foundation Fellowship (NRF-NRFF-2011-04), and the National Research Foundation Competitive Research Programme (NRF2012NRF-CRP001-084).

Author contributions

A.D.B. conceived and designed the project together with V.V., P.K. and G.E.J.

N.B.M.R and Y.N. equally designed and performed all experiments and prepared the manuscript; T.V., Z.Z., S.S., and N.M. provided assistance in carrying out experiments

and discussed results. A.D.B., N.B.M.R, Y.N. together with V.V., P.K. and G.E.J. discussed results and prepared the manuscript.

Conflict of interest statement

The authors declare no competing financial interest.

20

Materials and Methods

Cell culture and cell transfection procedures

THP1 human monocytic leukemia cell line was obtained from Health Protection Agency Culture Collections (Porton Down, Salisbury, UK) and cultured in Roswell Park Memorial Institute media (RPMI-1640) supplemented with 10% heat-inactivated FBS and 50 μg/ml 2-Mercaptoethanol (Sigma-Aldrich) at 37°C and 5% CO_2. The suspended THP-1 cells were differentiated into adherent macrophage-like cells with 1 ng/ml human recombinant cytokine TGFβ1 (R&D Systems) for 24 or 48 hours on fibronectin-coated glass substrates. No apparent difference between the phenotype of cells stimulated for 24 or 48 hours were detected. For the imaging samples, 35-mm ibidi (Cat. 81158) glass-bottomed dishes were coated with 1 μg/ml of fibronectin (Calbiochem, Merck Millipore) in phosphate buffered saline (PBS) for 1-2 hours at 37°C, washed with PBS twice, and immersed in complete medium prior to seeding of cells. RAW 264.7 murine macrophage cell line was purchased from American Type Culture Collection (Manassas, VA, USA) and cultured in the same media used for THP1 cells. For imaging, cells were scraped from the culture dishes, re-plated at the appropriate cell density and differentiated by addition of 100 ng/ml phorbol 12-myristate 13-acetate (PMA, Sigma-Aldrich) on glass bottom dishes for at least 24 hours.

HT1080 human fibrosarcoma cell line was obtained from American Type Culture Collection (Manassas, VA, USA) and cultured in MEM supplemented with 10% heat-inactivated FBS, Non-essential amino acid and Sodium Pyruvate (Sigma-Aldrich), in an incubator at 37°C and 5% CO_2. HT-29 human colon adenocarcinoma cell line was gifted from Dr. Sudhakar Jha (Cancer Science Institute, Singapore) and cultured in DMEM supplemented with 10% heat-inactivated FBS and penicillin-streptomycin (Thermo Fisher Scientific), in an incubator at 37°C and 5% CO2. Primary human umbilical vein endothelial cells (HUVECs) was a gift from Dr. Roger Kamm (Singapore-MIT Alliance for Research and Technology, Singapore), which was originally purchased from American Type Culture Collection (Manassas, VA, USA).

HUVECs were cultured using EGM-2 BulletKit media (catalogue no. CC-3162, Lonza, MA). All cells were plated on fibronectin-coated surfaces for 24 hours prior to imaging, or 48 hours for knockdown experiments.

Cells were transiently transfected prior to stimulation with the expression vectors plasmids using electroporation (Neon Transfection System, Life Technologies) in accordance to manufacturer's instructions. Specifically, two pulses of 1400V of 20 ms duration were used for THP1 cells, one pulse of 950V of 50 ms was used for HT1080 cells, two pulses of 1300V of 20 ms duration for HT-29 cells, one pulse of 1200V of 40 ms duration for HUVECs and one pulses of 1680V of 20 ms duration for RAW 264.7 macrophages. For siRNA-mediated knockdown, THP1 cells were transfected at the following concentrations: 150nM for KANK1 siRNA (Dharmacon, ON-TARGETplus SMARTpool siRNA, catalogue no. L-012879-01-0005), 100nM for KANK2 siRNA (Dharmacon, ON-TARGETplus SMARTpool siRNA, catalogue no. L-027345-00-0005), 150nM for MYH9 siRNA (Dharmacon, ON-TARGETplus SMARTpool siRNA catalogue no. L-007668-00-0005), 150nM for MYH9 siRNA (Dharmacon, ON-TARGETplus siRNA catalogue no. LQ-007668-00-0002, containing following individual siRNA; J-007668-05 (#05), J-007668-06 (#06), J-007668-07 (#07) and J-007668-08 (#08)), 150nM for MYH10 siRNA (Dharmacon, ON-TARGETplus SMARTpool siRNA catalogue no. L-023017-00-0005), 150nM for GEF-H1 siRNA (Dharmacon, ON-TARGETplus SMARTpool siRNA, catalogue no. L-009883-00-0005), and 150nM for GEF-H1 individual siRNA (GEF-H1 #09 siRNA) (Dharmacon, ON-TARGETplus siRNA, catalogue no. J-009883-09-0002). For control experiments, cells were transfected with non-targeting pool siRNA (Dharmacon, ON-TARGETplus, catalogue no. D-001810-10) at a concentration similar to gene-targeted siRNAs. For siRNA-mediated knockdown in HUVECs, cells were transfected at the following concentration: 100nM for KANK1 siRNA (Dharmacon, ON-TARGETplus SMARTpool siRNA, catalogue no. L-012879-01-0005). HT1080 cells were transfected at the following concentrations: 25nM for KANK1, 25nM for KANK2 siRNA, 50nM for MYH9 siRNA and 50nM for GEF-H1 siRNA (Dharmacon,

see above) using DharmaFECT 1 transfection reagent (Dharmacon, catalogue no. T-2001) following the manufacturer's protocols.

Plasmids

Expression vectors for fluorescent protein fusion constructs are described in Supplementary Information.

For generation of EGFP-KANK2/CC-KANK1 chimeric construct, the liprin-binding coiled-coil domain corresponding to amino acid residues 188-238 of full-length KANK2 [9] was substituted with amino acid residues of 257-500 of full-length KANK1 [8]. The EGFP-KANK2/CC-KANK1 construct was cloned by Epoch Life Science Inc (USA). For generation of constructs used in the rapamycin-induced dimerization of KN and ΔKN of KANK1 protein, KN domain of KANK1 corresponding to amino acid residues 1-68 [8] was fused with mApple fluorescence tag and FKBP12-rapamycin binding (FRB) domain of mammalian target of rapamycin (mTOR) (mApple-KN-FRB). The rest of KANK1, ΔKN, corresponding to amino acid residues 69-1352 [8], was fused with mEmerald fluorescence tag and FK506 binding protein (FKBP12) rapamycin-binding domain (FKBP-ΔKN-mEmerald). The mApple-KN-FRB and FKBP-ΔKN-mEmerald constructs were cloned by Epoch Life Science Inc (USA).

Live cell observations

Pharmacological treatments were performed using the following concentrations of inhibitors or activators: 1 μM for Nocodazole (Sigma-Aldrich), 30-100 μM for Y-27632 dihydrochloride (Sigma-Aldrich), 8 μM for Thiazovivin (Sigma-Aldrich), and 1 μg/ml for Rho Activator II (CN03, Cytoskeleton), 1 μg/ml rapamycin (CAS number 53123-88-9, Santa Cruz). For THP1 cells, duration of the treatment with the inhibitors was 1 hour. In some cases, cells were pre-treated with one inhibitor for 30 min and then another inhibitor was added for additional 1 hour. For nocodazole-washout experiments, transfected HT1080 cells were plated on

collagen I- coated coverslips for overnight. One hour prior to imaging, nocodazole in fresh L-15 medium (Leibovitz, Sigma-Aldrich) with 10% FBS was added to the cells. The coverslips were mounted in a perfusion chamber (CM-B25-1, Chamlide CMB chamber). Nocodazole was washed-out by fresh L-15 medium with FBS just prior to the start of the acquisition. For immunofluorescence observations, the cells were fixed 30 minutes following nocodazole washout.

Immunoblotting

Cells were lysed in RIPA buffer 48 hours after transfection and extracted proteins were separated by SDS-PAGE in 4-20% SDS-polyacrylamide gel (Thermo Fisher Scientific) and transferred to PVDF membranes (Bio-Rad) at 75V for 2 hours. Subsequently, the PVDF membranes were blocked for 1 hour with 5% non-fat milk (Bio-Rad) or bovine serum albumin (BSA, Sigma-Aldrich), then incubated overnight at 4°C with appropriate antibodies: anti-KANK1 (Bethyl Laboratories, catalogue no. A301-882A, dilution 1:1000); anti-KANK2 (Sigma-Aldrich, catalogue no. HPA015643, dilution 1:1000); Anti-non muscle myosin-IIA (Sigma-Aldrich, catalogue no. M8064, dilution 1:1000); anti-GEF-H1 (Cell Signaling Technology, catalogue no. 4145, dilution 1:1000); anti-α-tubulin (Sigma-Aldrich, catalogue no. T6199, dilution 1:3000); anti-GAPDH (Santa Cruz Biotechnology, Inc., catalogue no. sc-32233, dilution 1:3000); anti-RhoA (Santa Cruz Biotechnology, Inc., catalogue no sc-418, dilution 1:1000); anti-non muscle myosin-IIB (Developmental Studies Hybridoma Bank, CMII 23, dilution 1:1000).

Subsequently, the PVDF membranes were washed 3 times (10 minutes each) and probed by incubation for 1 hour with the appropriate secondary antibodies conjugated with horseradish peroxidase (Bio-Rad). The membranes were then washed three times (15 minutes at room temperature each), developed using Pierce™ ECL western blotting substratum (Thermo Fisher Scientific) and imaged by a ChemiDoc imaging system (Bio-Rad).

Uncropped images of the western blots presented in Figure 1D, Figure 1I, Figure 3I, Figure 5E, Supplementary Figure 5A, Supplementary Figure 7A, Supplementary Figure 10A of this paper are shown in Supplementary Figures 12 and 13.

RhoA activity assay

THP1 and HT1080 cells were lysed in RIPA buffer for five minutes on ice as described in [52], then centrifuged at 15,000g for five minutes at 4°C. The supernatant was incubated with Glutathione-agarose beads coated with GST-tagged Rho-binding domain of Rhotekin (provided by Dr. Boon Chuan Low (National University of Singapore) at 4°C for 30 minutes. The beads were washed three times with chilled RIPA buffer before being boiled in Laemmli buffer. Pulled-down RhoA was immunoblotted using respective antibodies as described above, and normalized to total RhoA in the whole cell lysates.

Immunofluorescence Microscopy

HT1080 cells were pre-fixed for 3 min at 37°C using 0.3 % Glutaraldehyde and 0.2% TritonX-100 in PHEM buffer (60 mM PIPES, 27 mM HEPES, 10 mM EGTA, 8 mM $MgSO_4 \times 7H_2O$, pH 7.0), and then post-fixed for 15 min at 37°C using 4 % PFA (Sigma-Aldrich) in PHEM buffer. After fixation, free aldehyde groups were quenched with 5 mg/ml Sodium borohydride (Sigma-Aldrich) for 5 min, and cells were washed 3 times for 5 min in PBS and blocked for 30 min in blocking solution (2 % Bovine Serum Albumin in PBS, Sigma-Aldrich). THP1 Cells were fixed for 15 min with 3.7% PFA in PBS, washed twice in PBS, permeabilized for 10 minutes with 0.5% triton X-100 (Sigma-Aldrich) in PBS, and then washed twice again in PBS. For microtubule visualization, cells were fixed and simultaneously permeabilized for 15 min at 37°C in a mixture of 3% PFA–PBS, 0.25% Triton-X-100 and 0.2% glutaraldehyde in PBS, and then washed twice with PBS for 10 min. Before immunostaining, samples were quenched for 15 min on ice with 1 mg/ml sodium borohydride in cytoskeleton buffer (10 mM MES, 150 mM NaCl, 5 mM EGTA, 5 mM $MgCl_2$, 5 mM glucose, pH 6.1). For GEF-H1 visualization, cells were fixed with 100%

methanol for 5 min at -20°C. Fixed cells were blocked with 5% BSA or 5% FBS for 1 hour at room temperature or overnight at 4°C prior to incubation with the following primary antibodies: anti-tubulin (Sigma-Aldrich, catalogue no. T6199, dilution 1:300); anti-paxillin (BD catalogue no. 610569, dilution 1:200); anti-vinculin (Sigma-Aldrich, catalogue no. V9131, dilution 1:400); anti-KANK2 (Sigma-Aldrich, catalogue no. HPA015643, dilution 1:200); anti-non muscle heavy chain of myosin-IIA (Sigma-Aldrich, catalogue no. M8064, dilution 1:800); anti-GEF-H1 (Abcam, catalogue no. ab155785, dilution 1:100); anti-non muscle myosin-IIB (Developmental Studies Hybridoma Bank, CMII 23, dilution 1:100). Samples were washed with PBS three times and incubated with Alexa Fluor-conjugated secondary antibodies (Thermo Fisher Scientific) for 1 hour at room temperature, followed by three washes in PBS. F-actin was visualized by Alexa Fluor 488 Phalloidin (Thermo Fisher Scientific), Phalloidin-TRITC (Sigma-Aldrich) or Alexa Fluor 647 Phalloidin (Thermo Fisher Scientific).

Fluorescence Microscopy

For structured illumination microscopy, two types of equipment were used: 1) spinning-disc confocal microscopy coupled with the Live super-resolution (SR) module (Roper Scientific), Nikon Eclipse Ti-E inverted microscope with Perfect Focus System, controlled by MetaMorph software (Molecular device) supplemented with a 100x oil 1.45 NA CFI Plan Apo Lambda oil immersion objective and sCMOS camera (Prime 95B, Photometrics), 2) Nikon N-SIM microscope, based on a Nikon Ti-E inverted microscope with Perfect Focus System controlled by Nikon NIS-Elements AR software supplemented with a 100x oil immersion objective (1.40 NA, CFI Plan-ApochromatVC) and EMCCD camera (Andor Ixon DU-897). For Total Internal Reflection Fluorescence (TIRF) microscopy, samples were imaged using a Nikon Ti-E inverted microscope controlled by Nikon NIS-Elements AR software, supplemented with a 60x 1.49 NA, Apo TIRF oil immersion objective lens and sCMOS camera (Orca Flash 4.0, Hamamatsu Photonics).

Traction Force Microscopy

To prepare polyacrylamide gel substrates, 25 mm round coverslips were activated by treatment with 1.2% 3-(Methacryloyloxy)propyltrimethoxysilane (Shin-Etsu Silicon, KBE-503) in 100 % methanol for 1h followed by extensive 100 % methanol washing. Then, freshly mixed solution of 0.145% bis/12% acrylamide with 100 nm yellow-green fluorescent beads (FluoSpheres, 0.1μm, Thermo Fisher Scientific, Cat# F8803) was placed on dried- and activated- coverslips to give an adhered gel with stiffness of 16kPa. Coverslips with attached gel substrate were washed three times with 0.1M HEPES-NaOH buffer (pH 7.5) and conjugated with collagen I (Thermo Fisher Scientific, A1048301) using sulfo-SANPAH (Thermo Fisher Scientific) to facilitate cell attachment. HT1080 cells were plated on the polyacrylamide gel 2 hours prior to the experiment and images of focal adhesions by RFP-Zyxin and beads were acquired by spinning disk confocal microscope equipped with a 60X water immersion objective (NA1.2, UPlanApo, Nikon) as described above. After acquisition, 0.5 % trypsin-EDTA was added into chamber to remove all cells from the substrate, and then images of beads were captured again. The traction stress field was computed as described previously [53].

For the traction force measurement shown in Figure 5H, a modified version of the traction force set was used. A thin layer (approximately 7 μm) of soft PDMS (Dow Corning, LOT#0008602722) was spin coated onto a glass coverslip. The pre-polymer mix, CY 52-276A and CY 52-276B were used at a 1:1 ratio. Sylgard 184 crossslinker was used to tune the stiffness of the gel for proper force measurement of cells (~95kPa). The gel mixture was spin coated on cleaned coverslips at 300 rpm for 20 secs, followed by 800 rpm for 10 secs and then 6000 rpm for 1 minute. The coverslip with the gel was then cured for 1 hour at 80°C. The surface of the cured gel was then silanized with (3-aminopropyl) triethoxysilane for 2 hours. The coverslips were then incubated with carboxylate-modified dark red (660/680) beads (FluoSpheres, 0.04μm, Thermo Fisher Scientific, LOT#1871942) at a concentration of 0.00025% in a solution of 0.1M sodium bicarbonate for 30 minutes. The coverslips with attached beads were then rinsed and incubated with

10 μg/mL of fibronectin solution (dissolved in bicarbonate buffer) at room temperature for 30 minutes. The online Image J plugin was used to extract and compute the force from the displacement field obtained from live cell imaging (See https://sites.google.com/site/qingzongtseng/tfm for plugin software details).

Micro-patterning of adhesive islands using UV-induced molecular adsorption

Adhesive islands with a diameter of 4 μm were printed in square lattices with a period of 8 μm. Clean glass coverslips were sealed with NOA 73 liquid adhesive to plastic-containing dishes by UV treatment for 2 minutes, and were then treated with oxygen plasma for 5 minutes. The coverslips were coated with PLL-g-PEG (PLL(20)-g[3.5]-PEG(5), SuSoS AG, Dübendorf, Switzerland) at 100 μg/mL in PBS for at least 8 hours followed by multiple washes with PBS. For micropattern printing, PRIMO system (Alveole, France) mounted on an inverted microscope (Nikon Eclipse Ti-E, Japan) equipped with a motorized scanning stage (Physik Instrumente, Germany) was used as Digital Micro-mirror Device (DMD) to create a UV pattern at 105 μm above the focal plane of the microscope. After alignment of specimen with the UV pattern by using the Leonardo software (Alveole, France), a solution of photoinitiator (PLPP, Alveole, France) was incubated on the dishes. Depending on the UV exposure and time, the UV-activated photoinitiator molecules locally cleaved the PEG chains, which permits subsequent local deposition of proteins. The dishes were washed with PBS multiple times prior to incubation with labeled fibronectin (Rhodamine Fibronectin, Cytoskeleton, Inc., 50 μg/ml) or unlabeled fibronectin mixed with Fibrinogen Alexa 647 (ThermoFisher Scientific, 50 μg/mL) at a ratio of 20:1 for 10 minutes. After several washes with PBS, HT1080 or THP1 cells were plated on these micropatterned lattices for SIM imaging.

Matrix degradation assay

50% sulphuric-acid-washed coverslips were coated with 50 μg/ml poly-D-Lysine for 30 minutes at room temperature, and then fixed with 0.5% glutaraldehyde for

15 minutes. 0.2% gelatin warmed at 37°C was mixed with Oregon Green 488 conjugated-pig gelatin at 6:1 ratio. Coverslips were coated with gelatin mix for 10 minutes, washed with 1xPBS and then quenched with 5 mg/ml sodium borohydride for 15 minutes followed by numerous washes. For matrix degradation assay, cells were seeded on the gelatin-coated coverslips for 8 hours, fixed and stained as described above (See "immunofluorescence microscopy"). Dark spots on the fluorescently-labeled gelatin correspond to areas of matrix that were degraded by cells.

Image processing and data analysis

The number of podosomes was quantified automatically by applying an ImageJ-based plugin for counting nuclei (ITCN) to images of the podosome core (F-actin). Quantification was validated by manual analysis of the first 5-10 cells in the specimen. The automated procedure usually detected more than 90% of the podosomes identified by manual counting. Line intensity profiles (arbitrary unit, a.u.) measuring the mean intensity of GFP or mCherry fluorescence per area (μm^2) by ImageJ Plugin, background-subtracted and normalized per maximal intensity in the field, yielding values ranging from 0 (lowest) to 1 (highest). For the measurement of the area of focal adhesions visualized by fluorescently-labeled paxillin or vinculin, a custom-written software (https://github.com/KanchanawongLab) developed in Interactive Data Language (IDL; Harris Geospatial Inc.) was used as described previously [54]. Briefly, the images were first background subtracted using the Sternberg rolling ball algorithm. Subsequently, focal adhesions were segmented using Otsu thresholding algorithm. The software determines the areas of individual focal adhesions. The total area of focal adhesion per cell was calculated by summing the values of individual focal adhesions. Manual curation was also performed to exclude segmented non-FA regions.

To analyze microtubules, fluorescence images of cells labeled by mApple-MAP4 were processed as described previously [55]. The enhanced images were then

binarized to extract the microtubule traces by a threshold calculated using Otsu's method. For the analysis of myosin-II filaments (labeled by GFP-MRLC) and F-actin core in podosomes (labeled by mCherry-UtrCH), segmentation was performed by binarization using Otsu's threshold. The amounts of myosin-II, MAP4 and F-actin were computed as the total numbers of their segmented pixels.

Gene Expression profile

The transcriptomes of THP1 and HT1080 were mapped, quantified and indicated as fragments per Kilobase million (FPKM) using the RNA-Seq technology. Briefly, the total RNA of THP1 and HT1080 cell lysates was extracted using the RNeasy Mini Kit (Qiagen) according to manufacturer's protocol. The extracted RNA was processed and analyzed by BGI Tech Solutions Co., Ltd (http://en.genomics.cn/index) .

Statistical analyses

The methods for statistical analysis and sizes of the samples (n) are specified in the results section or figure legends for all of the quantitative data. Differences were accepted as significant for $P < 0.05$. Prism version 6 (GraphPad Software) was used to plot, analyze and represent the data.

The quantitative data were presented in the figures as bar graphs or scatter dot plots showing mean ± SD, or box-and-whiskers plots. In box-and-whiskers plots, whiskers extend from the minimum to maximum values, the box extends from the 25^{th} to the 75^{th} percentile and the line within the box represents the median.

30

Data Availability Statement

All data generated or analysed during this study are included in this published article (and its supplementary information files). Raw datasets generated during and/or analysed during the current study are available from the corresponding author on reasonable request.

31

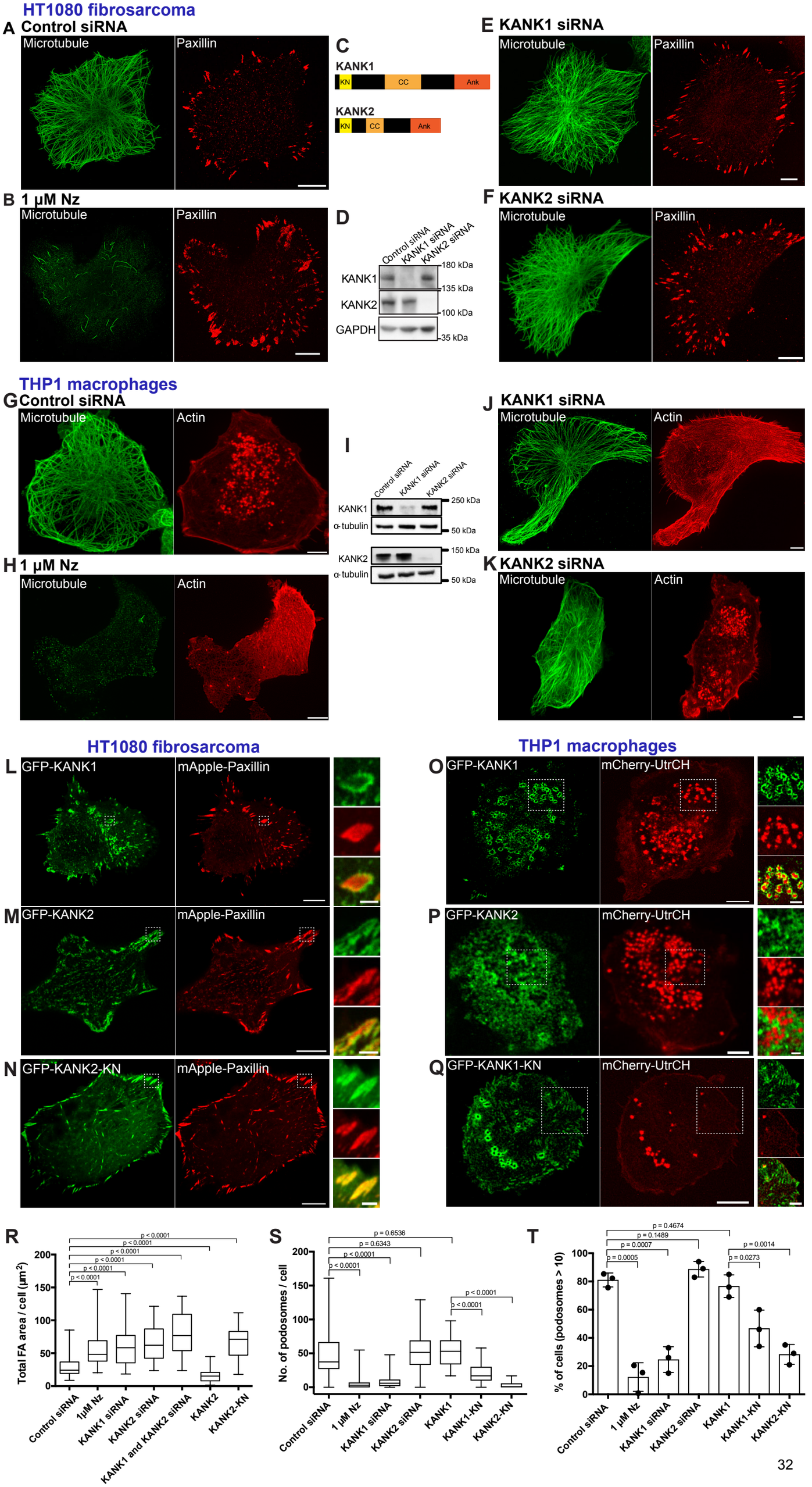
HT1080 fibrosarcoma
A Control siRNA
Microtubule
Paxillin
B 1 μM Nz
Microtubule
Paxillin
C
KANK1
KN
CC
Ank
KANK2
KN
CC
Ank
D
Control siRNA
KANK1 siRNA
KANK2 siRNA
KANK1
KANK2
GAPDH
180 kDa
135 kDa
100 kDa
35 kDa
E KANK1 siRNA
Microtubule
Paxillin
F KANK2 siRNA
Microtubule
Paxillin
THP1 macrophages
G Control siRNA
Microtubule
Actin
H 1 μM Nz
Microtubule
Actin
I
Control siRNA
KANK1 siRNA
KANK2 siRNA
KANK1
α-tubulin
250 kDa
50 kDa
KANK2
α-tubulin
150 kDa
50 kDa
J KANK1 siRNA
Microtubule
Actin
K KANK2 siRNA
Microtubule
Actin
HT1080 fibrosarcoma
L GFP-KANK1
mApple-Paxillin
M GFP-KANK2
mApple-Paxillin
N GFP-KANK2-KN
mApple-Paxillin
THP1 macrophages
O GFP-KANK1
mCherry-UtrCH
P GFP-KANK2
mCherry-UtrCH
Q GFP-KANK1-KN
mCherry-UtrCH
R
Total FA area / cell (μm²)
p < 0.0001
Control siRNA
1μM Nz
KANK1 siRNA
KANK2 siRNA
KANK1 and KANK2 siRNA
KANK2
KANK2-KN
S
No. of podosomes / cell
p = 0.6536
p = 0.6343
p < 0.0001
p < 0.0001
p < 0.0001
p < 0.0001
Control siRNA
1 μM Nz
KANK1 siRNA
KANK2 siRNA
KANK1
KANK1-KN
KANK2-KN
T
% of cells (podosomes > 10)
p = 0.4674
p = 0.1489
p = 0.0007
p = 0.0005
p = 0.0014
p = 0.0273
Control siRNA
1 μM Nz
KANK1 siRNA
KANK2 siRNA
KANK1
KANK1-KN
KANK2-KN

Figure 1:

Effects of microtubule uncoupling from integrin adhesions by manipulations with KANK proteins

(A) Control HT1080 cell show microtubules (α-tubulin, green) and focal adhesions (paxillin, red). (B) Disruption of microtubules with 1 μM nocodazole augmented focal adhesion size. (C) KANK protein domains: Talin-binding (KN), coiled-coil (CC), and ankyrin repeats (Ank). (D) Western blots showing KANK1/2 levels in HT1080 cells; loading control, GAPDH. (E-F) Knockdowns of KANK1 (E) or KANK2 (F) in HT1080 cells increased focal adhesion size compared to control (A) but did not disrupt microtubules. (G) Microtubules (green) and podosome cores (actin, red) in control THP1 cells. (H) Disappearance of podosomes upon microtubule disruption with 1 μM nocodazole. (I) Western blots showing KANK1/2 levels in THP1 cells; loading control, α-tubulin. (J-K) Knockdowns of KANK1 (J) but not KANK2 (K) in THP1 cells induced disassembly of podosomes without disruption of microtubules. Co-localization of (L) GFP-KANK1 and (M) GFP-KANK2 (green) with focal adhesions (mApple-paxillin, red) in HT1080 cells. (N) Talin-binding domain of KANK2 (GFP-KANK2-KN, green) localized to paxillin-containing focal adhesions (red). Localization of (O) GFP-KANK1 and (P) GFP-KANK2 (green) relative to podosome cores (mCherry-UtrCH, red) in THP1 cells. (Q) GFP-KANK1-KN (green) expression reduced the number of podosomes and augmented focal adhesions-like structures (actin, red). Scale bars (A, B, E, F and L-N), 10 μm; (G, H, J, K and O-Q), 5 μm; magnified images (L-Q), 2 μm. (R-T) Quantitative changes in focal adhesions and podosomes in cells treated as indicated. Each condition was triple-repeated. (R) The total areas of focal adhesions (μm^2) per cell (n≥36 cells) in HT1080 cells. (S-T) The podosome numbers per cell in THP1 cells (n≥70 cells) are presented as box-and-whiskers plots (S) and the percentage of cells containing ≥10 podosomes - as mean ± SD (T). Nz-nocodazole. p-values calculated using two-tailed Student's *t*-test.

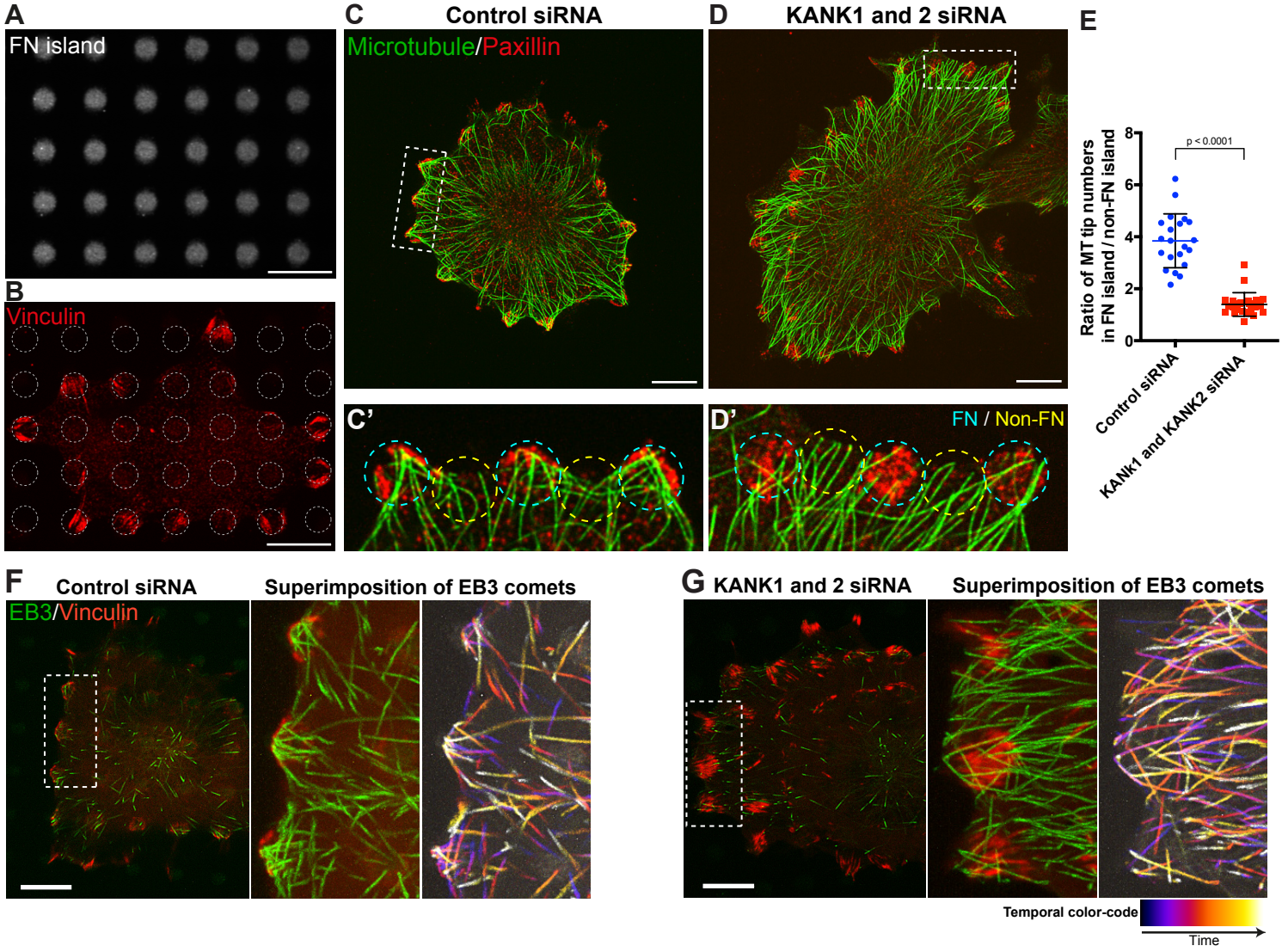
A
FN island
B
Vinculin
C
Control siRNA
Microtubule/Paxillin
C'
D
KANK1 and 2 siRNA
D'
FN / Non-FN
E
Ratio of MT tip numbers in FN island / non-FN island
p < 0.0001
Control siRNA
KANk1 and KANK2 siRNA
F
Control siRNA
Superimposition of EB3 comets
EB3/Vinculin
G
KANK1 and 2 siRNA
Superimposition of EB3 comets
Temporal color-code
Time

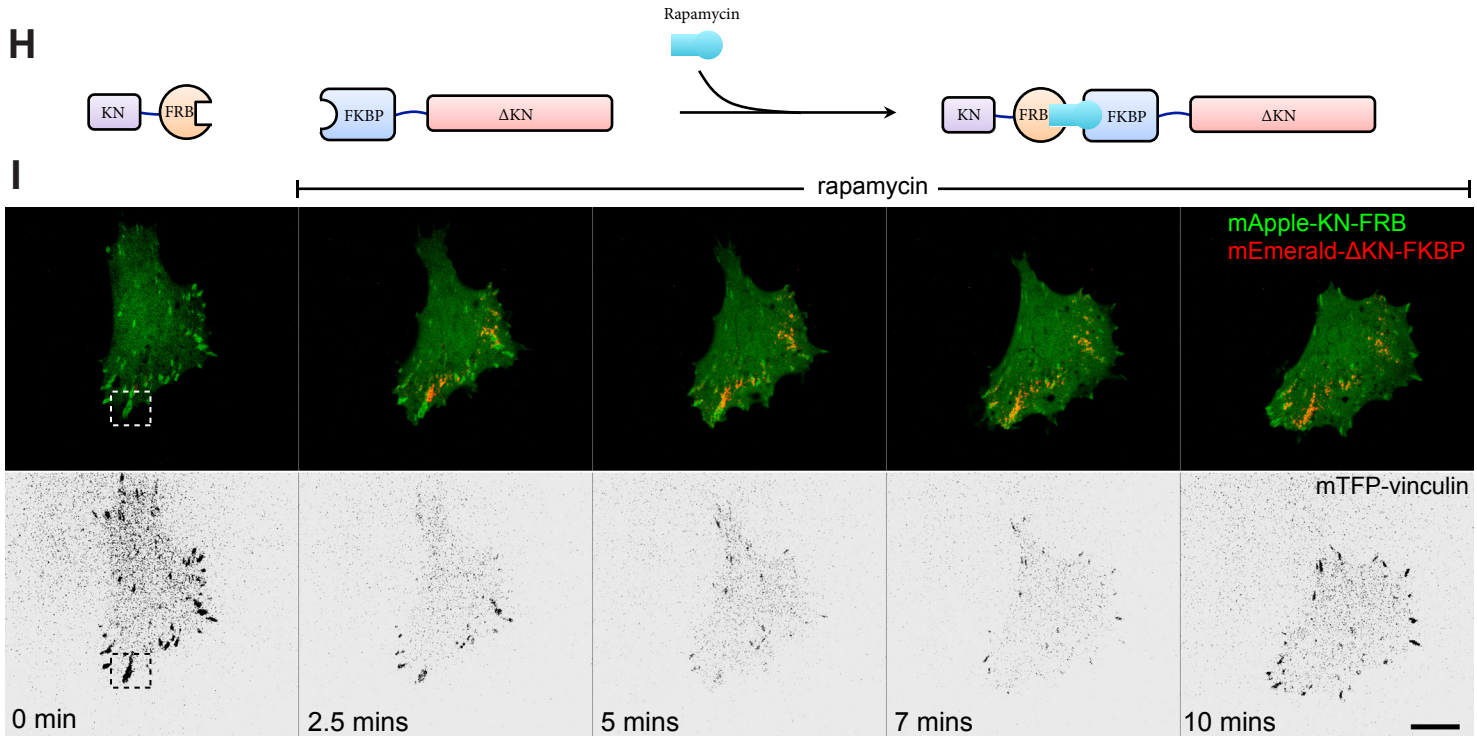
H
KN
FRB
FKBP
ΔKN
Rapamycin
I
rapamycin
mApple-KN-FRB
mEmerald-ΔKN-FKBP
mTFP-vinculin
0 min
2.5 mins
5 mins
7 mins
10 mins

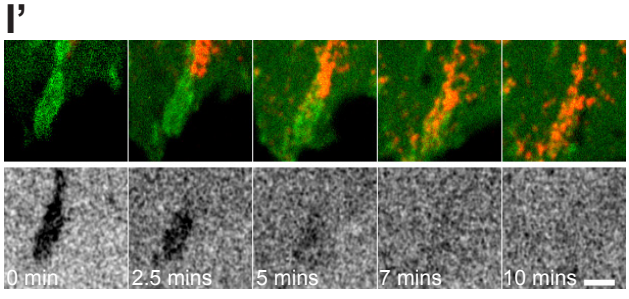
I'
0 min
2.5 mins
5 mins
7 mins
10 mins

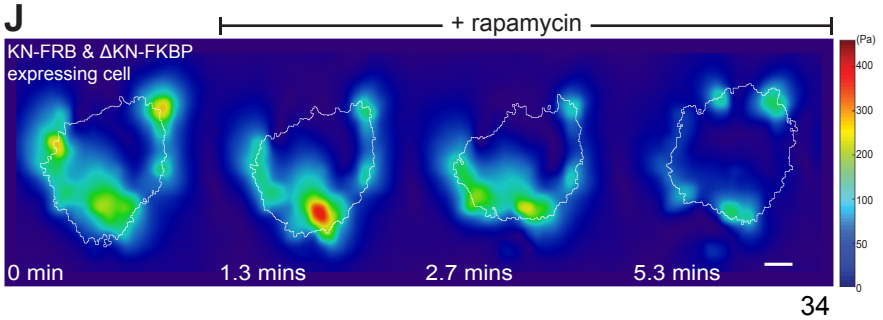
J
+ rapamycin
KN-FRB & ΔKN-FKBP
expressing cell
(Pa)
0 min
1.3 mins
2.7 mins
5.3 mins

Figure 2: KANK proteins are required for targeting microtubules to focal adhesions

(A) Fluorescently-labeled fibronectin-coated islands (white) restricted localization of focal adhesions (B, vinculin, red) in HT1080 cells. (C) Control and (D) KANK1 and 2 knockdown cells showing microtubules (α-tubulin, green) and focal adhesions (paxillin, red). The cyan dotted circles in C' and D' correspond to adhesive islands. Yellow dotted circles mark similar areas between the adhesive islands. Scale bars, 10 μm. (E) The ratios of the numbers of microtubule tips overlapping with islands containing focal adhesions versus circles without focal adhesions. Dots represent control (n=21) or knockdown (n=23) cells (7-13 islands/cell were assessed). p-value calculated using two-tailed Student's *t*-test is indicated. (F) Control (n=21 cells) and (G) KANK1+KANK2-depleted (n=18 cells) HT1080 cells displaying EB3-decorated microtubule tips (mKO-EB3, green) and focal adhesions (GFP-vinculin, red). Frames from time-lapse Supplementary Movies 1 and 2, respectively. The superimpositions of EB3 comet images from the boxed areas (60 frames taken every second) are shown at high magnification in green and temporal color-code, respectively. Each condition was repeated twice. Scale bars, 10 μm. (H-I-I') Transient disassembly of focal adhesions upon the enforced targeting of microtubules. (H) A scheme depicting rapamycin-mediated formation of a link between two parts of KANK1 molecule. (I) The cell triple-transfected with mApple-KN-FRB (green), FKBP-ΔKN-mEmerald (red) and mTFP-vinculin (black). Rapamycin (5 μg/ml) triggered localization of FKBP-ΔKN to KN-FRB-containing focal adhesions, accompanied by gradual disappearance of vinculin. Typical sequence; 27 cells from n=6 experiments were examined. Scale bar, 10 μm. (I') High magnification of the area boxed in (I). Scale bar, 2 μm. See Supplementary Movie 4. (J) Decrease of traction forces exerted by cell (in spectrum scale) upon coupling of FKBP-ΔKN and KN-FRB after rapamycin addition. Typical sequence; 10 cells were examined. The cell edges are marked by white lines. Scale bar, 10 μm.

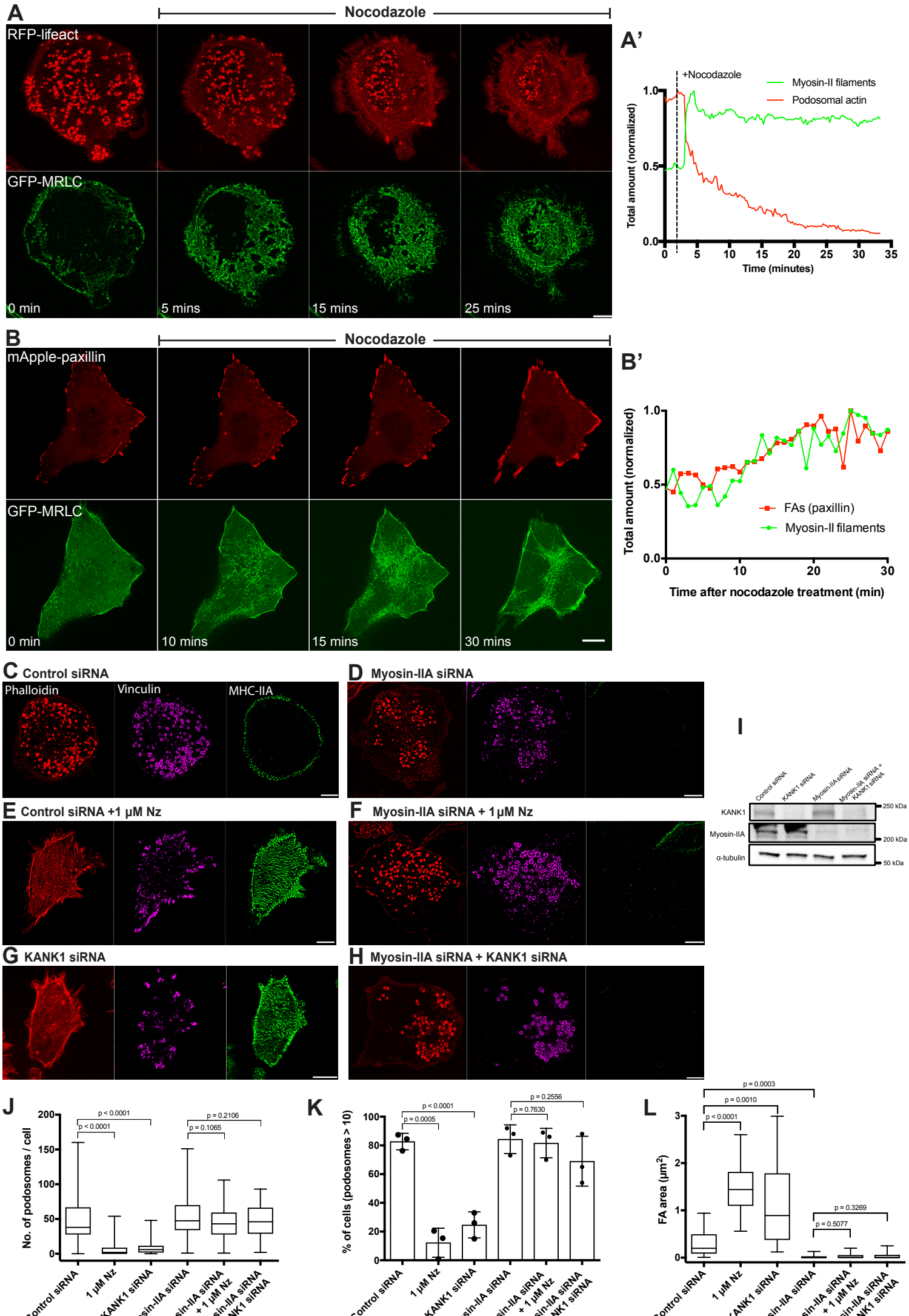
A
Nocodazole
RFP-lifeact
GFP-MRLC
0 min
5 mins
15 mins
25 mins
A'
+Nocodazole
Myosin-II filaments
Podosomal actin
Total amount (normalized)
Time (minutes)
B
Nocodazole
mApple-paxillin
GFP-MRLC
0 min
10 mins
15 mins
30 mins
B'
FAs (paxillin)
Myosin-II filaments
Total amount (normalized)
Time after nocodazole treatment (min)
C Control siRNA
Phalloidin
Vinculin
MHC-IIA
D Myosin-IIA siRNA
E Control siRNA +1 μM Nz
F Myosin-IIA siRNA + 1 μM Nz
G KANK1 siRNA
H Myosin-IIA siRNA + KANK1 siRNA
I
Control siRNA
KANK1 siRNA
Myosin-IIA siRNA
Myosin-IIA siRNA + KANK1 siRNA
KANK1
Myosin-IIA
α-tubulin
250 kDa
200 kDa
50 kDa
J
No. of podosomes / cell
p < 0.0001
p < 0.0001
p = 0.2106
p = 0.1065
K
% of cells (podosomes > 10)
p < 0.0001
p = 0.0005
p = 0.2556
p = 0.7630
L
FA area (μm²)
p = 0.0003
p = 0.0010
p < 0.0001
p = 0.3269
p = 0.5077
Control siRNA
1 μM Nz
KANK1 siRNA
Myosin-IIA siRNA
Myosin-IIA siRNA + 1 μM Nz
Myosin-IIA siRNA + KANK1 siRNA

Figure 3: Myosin-II filaments mediate the effect of microtubules on integrin-based adhesions

(A and B) Addition of 1 μM nocodazole induced the assembly of numerous myosin-II filaments labeled by GFP-MRLC (green) in THP1 (A) and HT1080 (B) cells, which correlates with the disruption of podosomes (red) (A) and increase in focal adhesion size (red) (B). Focal adhesions and podosome cores were marked by mApple-paxillin and RFP-lifeact, respectively. Scale bars, 5 (A) and 10 (B) μm. Graphs A' and B' show the changes in fluorescence intensity of myosin-II filaments (green), podosomes (A') and focal adhesions (B') upon microtubule disruption by nocodazole. See Supplementary Movies 5 and 6. For details of the quantification procedures, see Materials and Method. (C-H) Effect of knockdown of myosin-IIA heavy chain (MYH9) in THP1 cells. (C) Cells transfected with control siRNA showed circumferential assembly of myosin-II filaments (green) and numerous podosomes visualized by actin (red) and vinculin (purple) staining. (D) Knockdown of MYH9 led to complete disappearance of myosin-IIA filaments but did not affect podosomes. (E and G) Microtubule disruption (E) or their uncoupling from podosomes by endogeneous KANK1 depletion (G) induced assembly and alignment of myosin-II filaments as well as disruption of podosomes and formation of focal adhesion-like structures. (F and H). Cells lacking myosin-IIA and either treated with nocodazole (F) or KANK1-depleted (H) preserved the podosomes and do not form focal adhesions Scale bars, 5μm. (I) Western blots showing KANK1 and myosin-IIA levels in cells treated as indicated. Loading control, α-tubulin. Each condition was triple-repeated. (J-L) Quantification of the podosome numbers per cell (box-and-whiskers plots, n≥57 cells) (J), percentage of cells containing ≥10 podosomes (mean ± SD; n=3 independent samples) (K) and area of focal adhesions (L) in cells treated as indicated (n=10 cells for each condition). Nz-nocodazole. The p-values calculated using two-tailed Student's *t*-test are indicated.

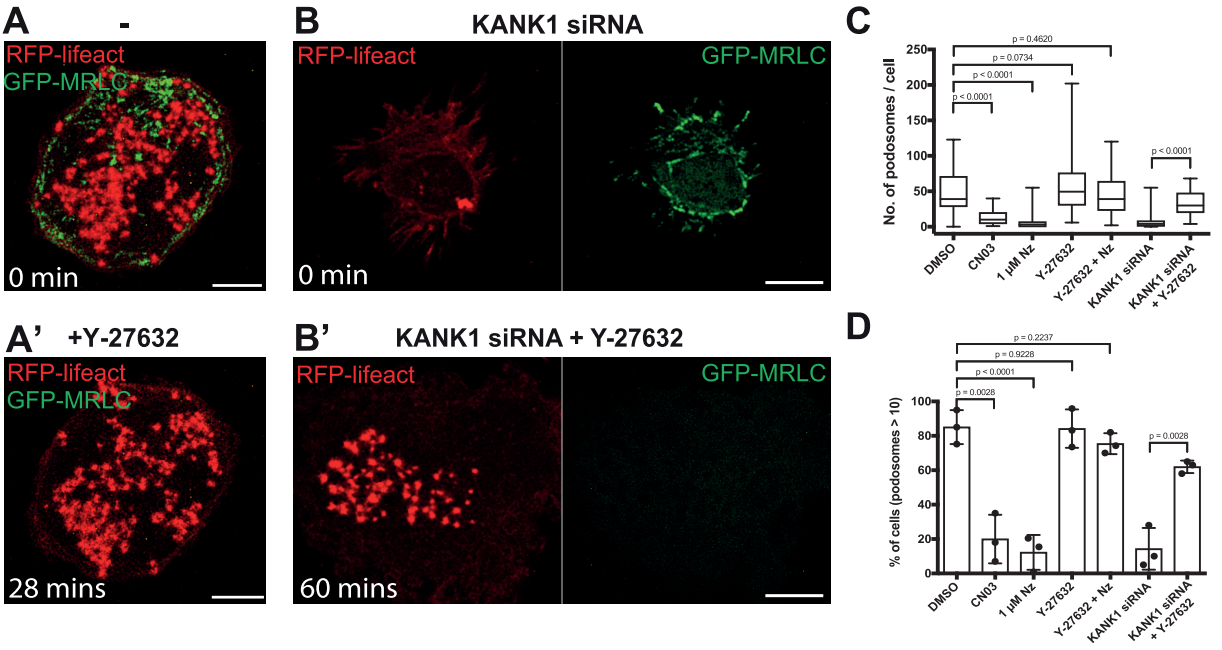
A -
RFP-lifeact
GFP-MRLC
0 min
B KANK1 siRNA
RFP-lifeact
GFP-MRLC
0 min
C
No. of podosomes / cell
p = 0.4620
p = 0.0734
p < 0.0001
p < 0.0001
p < 0.0001
DMSO
CN03
1 µM Nz
Y-27632
Y-27632 + Nz
KANK1 siRNA
KANK1 siRNA + Y-27632
A' +Y-27632
RFP-lifeact
GFP-MRLC
28 mins
B' KANK1 siRNA + Y-27632
RFP-lifeact
GFP-MRLC
60 mins
D
% of cells (podosomes > 10)
p = 0.2237
p = 0.9228
p < 0.0001
p = 0.0028
p = 0.0028
DMSO
CN03
1 µM Nz
Y-27632
Y-27632 + Nz
KANK1 siRNA
KANK1 siRNA + Y-27632

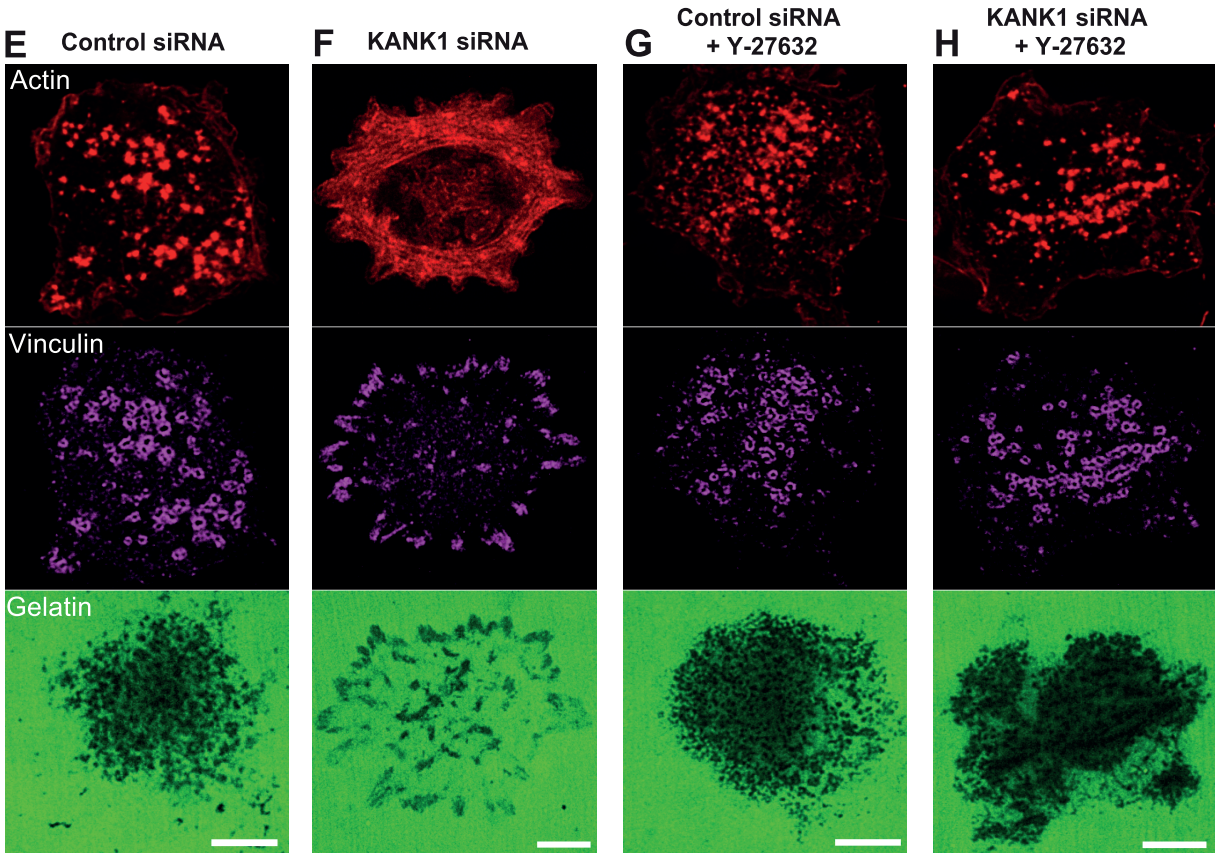
E Control siRNA
F KANK1 siRNA
G Control siRNA + Y-27632
H KANK1 siRNA + Y-27632
Actin
Vinculin
Gelatin

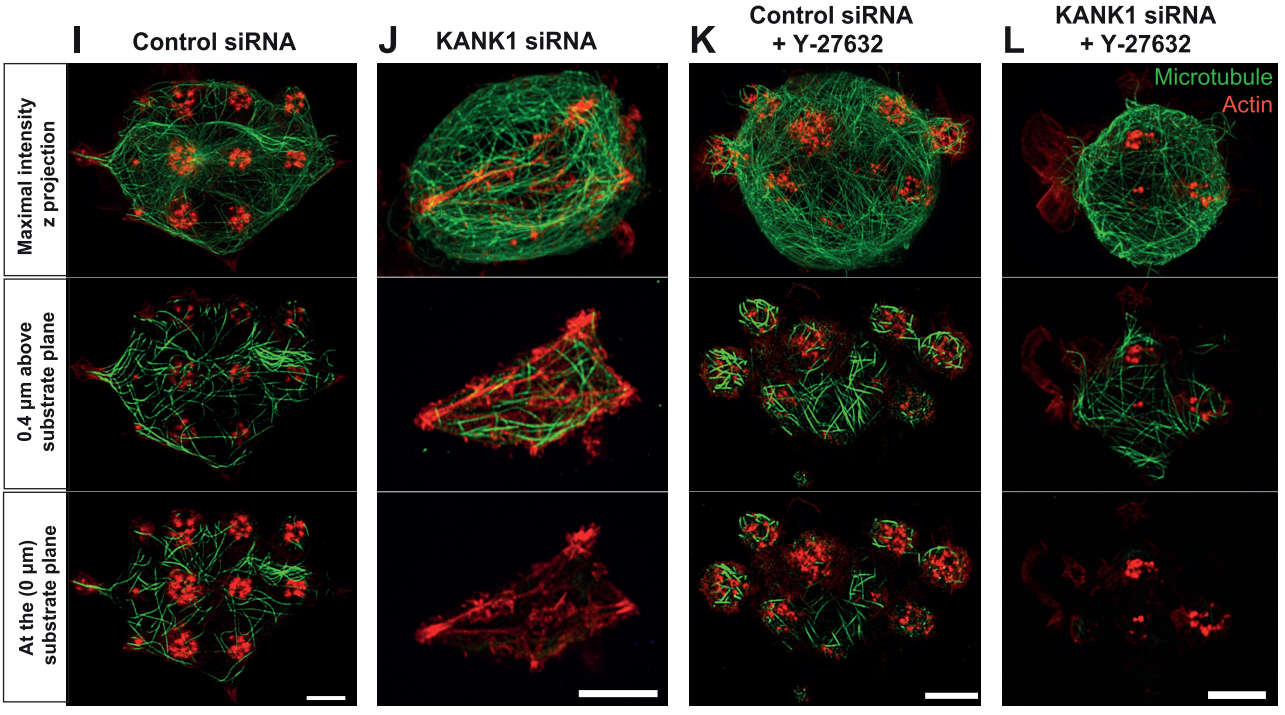
I Control siRNA
J KANK1 siRNA
K Control siRNA + Y-27632
L KANK1 siRNA + Y-27632
Maximal intensity z projection
0.4 µm above substrate plane
At the (0 µm) substrate plane
Microtubule
Actin

Figure 4: Recovery of functional podosomes in KANK1-depleted cells upon ROCK inhibition

(A and A') Podosome actin cores (RFP-lifeact, red) and myosin-II filaments (GFP-MRLC, green) in THP1 cell before (A) and after (A') addition of 30 μM Y-27632. See Supplementary Movie 12. (B and B') KANK1-depleted cell shown before (B) and after (B') incubation with Y-27632. Scale bars, 5 μm. See Supplementary Movie 15. (C and D) The number of podosomes (box-and-whiskers plots, n≥52 cells) (C) and the percentage of cells containing ≥10 podosomes (mean ± SD; n=3 independent samples) (D) in cells treated as indicated (see A, B and Supplementary Figure 7C-F). Nz-nocodazole. CN03-RhoA activator. "Y-27632+Nz" represents pooled results of experiments, in which Y-27632 was added before or after nocodazole. The p-values calculated using two-tailed Student's *t*-test are indicated. (E-H) Matrix degradation by recovered podosomes. Cells were stained for actin (red) and vinculin (purple), while matrix degradation is seen as dark areas in the fluorescent gelatin substrates (green). (I-L) Depletion of KANK1 abolishes targeting of microtubules to podosomes in THP1 cells. The cells were plated on adhesive islands (as in Figure 2A) for ordered localization of podosomes. Microtubules (α-tubulin, green) and actin (red) were labeled. Upper row shows z projection of all microtubules and actin structures; middle and lower rows show the microtubules and actin in the same cell at z=0.4 μm and z=0.0 μm focal planes, respectively. Microtubules can be seen at the z=0.0 focal plane in cells transfected with control siRNA (I, K) but not in cells transfected with KANK1 siRNA (J, L). Scale bars, 5μm. See quantification in Supplementary Figure 8. Each condition was triple-repeated.

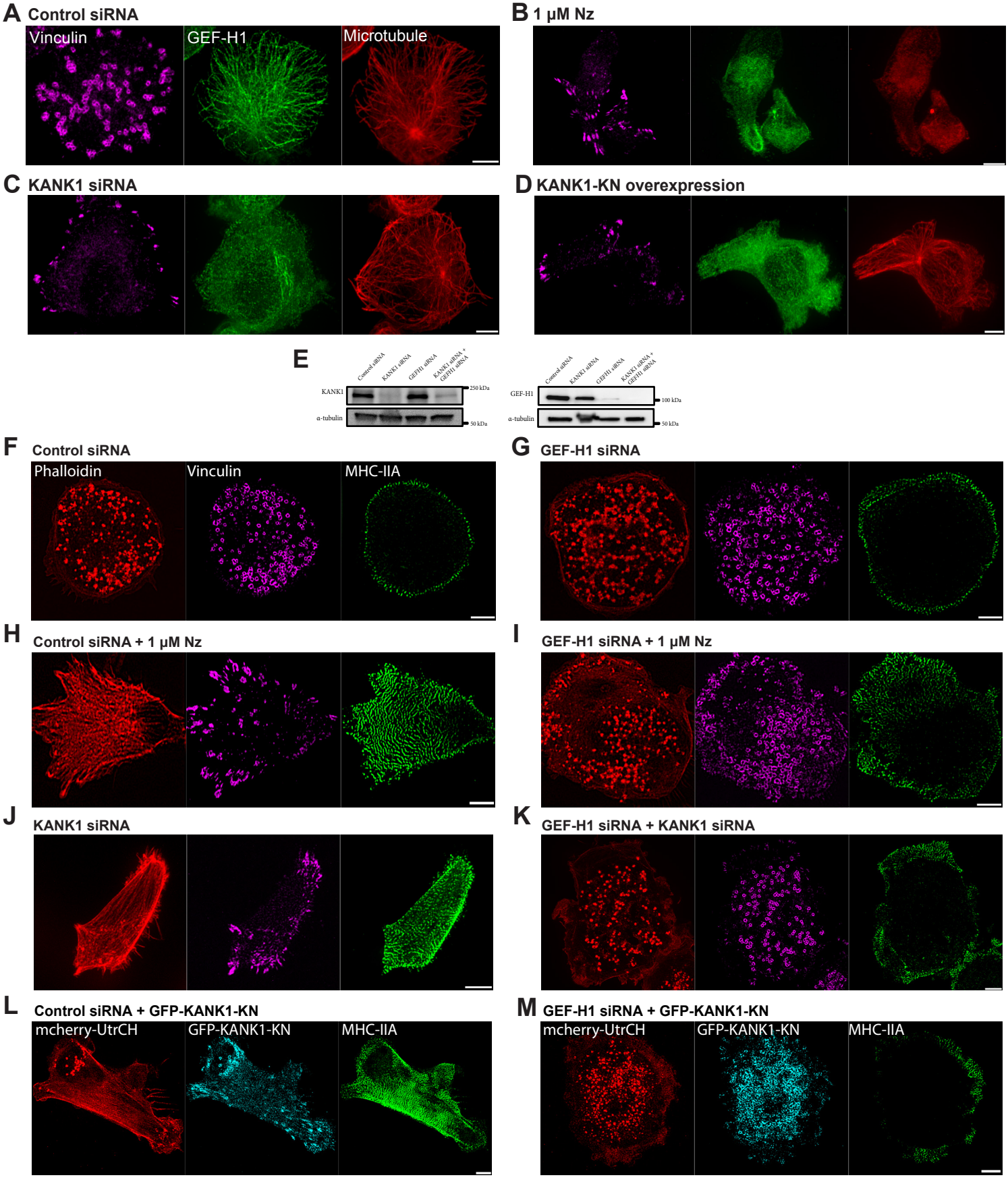
A Control siRNA
Vinculin
GEF-H1
Microtubule
B 1 µM Nz
C KANK1 siRNA
D KANK1-KN overexpression
E
Control siRNA
KANK1 siRNA
GEF-H1 siRNA
KANK1 siRNA + GEF-H1 siRNA
KANK1
250 kDa
α-tubulin
50 kDa
GEF-H1
100 kDa
F Control siRNA
Phalloidin
Vinculin
MHC-IIA
G GEF-H1 siRNA
H Control siRNA + 1 µM Nz
I GEF-H1 siRNA + 1 µM Nz
J KANK1 siRNA
K GEF-H1 siRNA + KANK1 siRNA
L Control siRNA + GFP-KANK1-KN
mcherry-UtrCH
GFP-KANK1-KN
MHC-IIA
M GEF-H1 siRNA + GFP-KANK1-KN
N
No. of podosomes / cell
p = 0.1622
p = 0.1929
p < 0.0001
p < 0.0001
p < 0.0001
Control siRNA
1 µM Nz
GEF-H1 siRNA
GEF-H1 siRNA + 1 µM Nz
KANK1 siRNA
KANK1 siRNA + GEF-H1 siRNA
Control siRNA + KANK1-KN
GEF-H1 siRNA + KANK1-KN
O
% of cells (podosomes > 10)
p = 0.1006
p = 0.5037
p < 0.0001
p = 0.0007
p = 0.0028
P
FA area (µm²)
p = 0.2979
p = 0.1950
p < 0.0001
p = 0.002
p < 0.0001

Figure 5: Function of GEF-H1 in KANK-mediated regulation of integrin-based adhesions

(A-D) Uncoupling of microtubules from integrin adhesions results in release of GEF-H1 from microtubules in THP1 cells. Vinculin (purple), GEF-H1 (green) and α-tubulin (red) were visualized by immunofluorescence staining. In control cell, vinculin labels podosomes, while GEF-H1 localizes to microtubules (A). Disruption of microtubules by nocodazole (B), KANK1 knockdown (C) or KANK1 displacement by overexpression of KANK1-KN (D) resulted in diffuse GEF-H1 distribution over the entire cell. (E) Western blot demonstrating siRNA-mediated depletion of GEF-H1, KANK1, and both of them in THP1 cells. α-tubulin is used as loading control. (F-M) Actin (red) was visualized by phalloidin staining (F-K) or mCherry-UtrCH (L, M); vinculin (purple) and myosin-IIA filaments (green) – by immunofluorescence staining. GFP-KANK1-KN shown in cyan (L, M). Both control (F) and GEF-H1-depleted (G) cells display podosomes and peripheral myosin-II filaments. Disruption of microtubules (H, I), knockdown of KANK1 (J, K) and overexpression of KANK1-KN (L, M) resulted in disappearance of podosomes (and formation of focal adhesions) as well as massive assembly of myosin-IIA filaments in GEF-H1-containing (H, J, L) but not in GEF-H1 depleted (I, K, M) cells. Scale bars, 5 μm. Each condition was triple-repeated. (N-P) Quantification of the number of podosomes (box-and-whiskers plots, n≥80 cells) (N), percentage of cells containing ≥10 podosomes (mean ± SD; n=3 independent samples) (O), and average area of focal adhesions (n=11 cells for each condition) (P) in THP1 cells treated as indicated. Nz=nocodazole. The p-values calculated using two-tailed Student's *t*-test are indicated.

ROCK

Rho

Myosin-II
Filaments

GEF-H1
(active)

Actin

GEF-H1
(inactive)

Microtubule

KN

Talin

KANK

CLASP

Liprin

ELKS

LL5β

Membrane

α

β

Integrin

Extracellular matrix

Figure 6: Interplay between microtubules, myosin-IIA filaments, and integrin adhesions

Microtubules are coupled to integrin-containing adhesions via links formed by KANK family proteins between integrin-binding protein talin and the cortical microtubule docking complex (liprins, ELKS, LL5β). KANK protein binds talin via KN domain and liprin via coiled-coil domain. The microtubule docking complex captures the microtubule plus end through interaction with CLASP proteins [8]. The guanine nucleotide exchange factor GEF-H1 is associated with microtubules. Our findings suggest that coupling of microtubules to integrin adhesions via KANK suppresses GEF-H1 ability to release from microtubules. In such situations, the levels of Rho-GTP and activity of ROCK are low, and as a result, only few myosin-IIA filaments are located in the proximity of adhesions. Such conditions are permissive for podosomes but limit the growth of focal adhesions. Uncoupling of microtubule tips from integrin adhesions by depletion or displacement of KANK, leads to release of GEF-H1 from microtubules, its activation, and consequent activation of the Rho/ROCK signaling axis. As a result, the assembly of myosin-IIA filaments is significantly activated, which is inimical to podosome existence but favorable for the formation and growth of stress fiber-associated focal adhesions.

References

1 Kasza, K. E. *et al.* The cell as a material. *Curr Opin Cell Biol* **19**, 101-107, doi:10.1016/j.ceb.2006.12.002 (2007).

2 Geiger, B., Spatz, J. P. & Bershadsky, A. D. Environmental sensing through focal adhesions. *Nature reviews. Molecular cell biology* **10**, 21-33, doi:10.1038/nrm2593 (2009).

3 Kanchanawong, P. *et al.* Nanoscale architecture of integrin-based cell adhesions. *Nature* **468**, 580-584, doi:10.1038/nature09621 (2010).

4 Horton, E. R. *et al.* The integrin adhesome network at a glance. *Journal of cell science* **129**, 4159-4163, doi:10.1242/jcs.192054 (2016).

5 Bershadsky, A., Chausovsky, A., Becker, E., Lyubimova, A. & Geiger, B. Involvement of microtubules in the control of adhesion-dependent signal transduction. *Current biology : CB* **6**, 1279-1289 (1996).

6 Enomoto, T. Microtubule disruption induces the formation of actin stress fibers and focal adhesions in cultured cells: possible involvement of the rho signal cascade. *Cell structure and function* **21**, 317-326 (1996).

7 Ezratty, E. J., Partridge, M. A. & Gundersen, G. G. Microtubule-induced focal adhesion disassembly is mediated by dynamin and focal adhesion kinase. *Nature cell biology* **7**, 581-590, doi:10.1038/ncb1262 (2005).

8 Bouchet, B. P. *et al.* Talin-KANK1 interaction controls the recruitment of cortical microtubule stabilizing complexes to focal adhesions. *eLife* **5**, doi:10.7554/eLife.18124 (2016).

9 Sun, Z. *et al.* Kank2 activates talin, reduces force transduction across integrins and induces central adhesion formation. *Nature cell biology* **18**, 941-953, doi:10.1038/ncb3402 (2016).

10 Chen, N. P., Sun, Z. & Fassler, R. The Kank family proteins in adhesion dynamics. *Curr Opin Cell Biol* **54**, 130-136, doi:10.1016/j.ceb.2018.05.015 (2018).

11 van der Vaart, B. *et al.* CFEOM1-associated kinesin KIF21A is a cortical microtubule growth inhibitor. *Developmental cell* **27**, 145-160, doi:10.1016/j.devcel.2013.09.010 (2013).

12 Lansbergen, G. *et al.* CLASPs attach microtubule plus ends to the cell cortex through a complex with LL5beta. *Developmental cell* **11**, 21-32, doi:10.1016/j.devcel.2006.05.012 (2006).

13 Clohisey, S. M., Dzhindzhev, N. S. & Ohkura, H. Kank Is an EB1 interacting protein that localises to muscle-tendon attachment sites in Drosophila. *PloS one* **9**, e106112, doi:10.1371/journal.pone.0106112 (2014).

14 Murphy, D. A. & Courtneidge, S. A. The 'ins' and 'outs' of podosomes and invadopodia: characteristics, formation and function. *Nature reviews. Molecular cell biology* **12**, 413-426, doi:10.1038/nrm3141 (2011).

15 Cox, S. & Jones, G. E. Imaging cells at the nanoscale. *The international journal of biochemistry & cell biology* **45**, 1669-1678, doi:10.1016/j.biocel.2013.05.010 (2013).

16 Yu, C. H. *et al.* Integrin-matrix clusters form podosome-like adhesions in the absence of traction forces. *Cell reports* **5**, 1456-1468, doi:10.1016/j.celrep.2013.10.040 (2013).
17 Linder, S., Hufner, K., Wintergerst, U. & Aepfelbacher, M. Microtubule-dependent formation of podosomal adhesion structures in primary human macrophages. *Journal of cell science* **113 Pt 23**, 4165-4176 (2000).
18 Meddens, M. B. *et al.* Actomyosin-dependent dynamic spatial patterns of cytoskeletal components drive mesoscale podosome organization. *Nature communications* **7**, 13127, doi:10.1038/ncomms13127 (2016).
19 Monypenny, J. *et al.* Role of WASP in cell polarity and podosome dynamics of myeloid cells. *European journal of cell biology* **90**, 198-204, doi:10.1016/j.ejcb.2010.05.009 (2011).
20 Kaverina, I., Krylyshkina, O. & Small, J. V. Microtubule targeting of substrate contacts promotes their relaxation and dissociation. *The Journal of cell biology* **146**, 1033-1044 (1999).
21 Hu, S. *et al.* Long-range self-organization of cytoskeletal myosin II filament stacks. *Nature cell biology* **19**, 133-141, doi:10.1038/ncb3466 (2017).
22 Ito, S. *et al.* Induced cortical tension restores functional junctions in adhesion-defective carcinoma cells. *Nature communications* **8**, 1834, doi:10.1038/s41467-017-01945-y (2017).
23 Vicente-Manzanares, M., Zareno, J., Whitmore, L., Choi, C. K. & Horwitz, A. F. Regulation of protrusion, adhesion dynamics, and polarity by myosins IIA and IIB in migrating cells. *The Journal of cell biology* **176**, 573-580, doi:10.1083/jcb.200612043 (2007).
24 Even-Ram, S. *et al.* Myosin IIA regulates cell motility and actomyosin-microtubule crosstalk. *Nature cell biology* **9**, 299-309, doi:10.1038/ncb1540 (2007).
25 Riveline, D. *et al.* Focal contacts as mechanosensors: externally applied local mechanical force induces growth of focal contacts by an mDia1-dependent and ROCK-independent mechanism. *The Journal of cell biology* **153**, 1175-1186 (2001).
26 Ren, X. D., Kiosses, W. B. & Schwartz, M. A. Regulation of the small GTP-binding protein Rho by cell adhesion and the cytoskeleton. *The EMBO journal* **18**, 578-585, doi:10.1093/emboj/18.3.578 (1999).
27 Kakinuma, N., Roy, B. C., Zhu, Y., Wang, Y. & Kiyama, R. Kank regulates RhoA-dependent formation of actin stress fibers and cell migration via 14-3-3 in PI3K-Akt signaling. *The Journal of cell biology* **181**, 537-549, doi:10.1083/jcb.200707022 (2008).
28 Linder, S. The matrix corroded: podosomes and invadopodia in extracellular matrix degradation. *Trends in cell biology* **17**, 107-117, doi:10.1016/j.tcb.2007.01.002 (2007).
29 Wang, Y. & McNiven, M. A. Invasive matrix degradation at focal adhesions occurs via protease recruitment by a FAK-p130Cas complex. *The Journal of cell biology* **196**, 375-385, doi:10.1083/jcb.201105153 (2012).

30 Krendel, M., Zenke, F. T. & Bokoch, G. M. Nucleotide exchange factor GEF-H1 mediates cross-talk between microtubules and the actin cytoskeleton. *Nature cell biology* **4**, 294-301, doi:10.1038/ncb773 (2002).
31 Kwan, K. M. & Kirschner, M. W. A microtubule-binding Rho-GEF controls cell morphology during convergent extension of Xenopus laevis. *Development* **132**, 4599-4610, doi:10.1242/dev.02041 (2005).
32 Jiu, Y. *et al.* Vimentin intermediate filaments control actin stress fiber assembly through GEF-H1 and RhoA. *Journal of cell science* **130**, 892-902, doi:10.1242/jcs.196881 (2017).
33 Ren, Y., Li, R., Zheng, Y. & Busch, H. Cloning and characterization of GEF-H1, a microtubule-associated guanine nucleotide exchange factor for Rac and Rho GTPases. *The Journal of biological chemistry* **273**, 34954-34960 (1998).
34 Chang, Y. C., Nalbant, P., Birkenfeld, J., Chang, Z. F. & Bokoch, G. M. GEF-H1 couples nocodazole-induced microtubule disassembly to cell contractility via RhoA. *Molecular biology of the cell* **19**, 2147-2153, doi:10.1091/mbc.E07-12-1269 (2008).
35 Gee, H. Y. *et al.* KANK deficiency leads to podocyte dysfunction and nephrotic syndrome. *The Journal of clinical investigation* **125**, 2375-2384, doi:10.1172/JCI79504 (2015).
36 Portran, D., Schaedel, L., Xu, Z., Thery, M. & Nachury, M. V. Tubulin acetylation protects long-lived microtubules against mechanical ageing. *Nature cell biology* **19**, 391-398, doi:10.1038/ncb3481 (2017).
37 Xu, Z. *et al.* Microtubules acquire resistance from mechanical breakage through intralumenal acetylation. *Science* **356**, 328-332, doi:10.1126/science.aai8764 (2017).
38 Samereier, M. *et al.* EB1 contributes to proper front-to-back polarity in neutrophil-like HL-60 cells. *European journal of cell biology* **96**, 143-153, doi:10.1016/j.ejcb.2017.01.006 (2017).
39 Bershadsky, A., Kozlov, M. & Geiger, B. Adhesion-mediated mechanosensitivity: a time to experiment, and a time to theorize. *Curr Opin Cell Biol* **18**, 472-481, doi:10.1016/j.ceb.2006.08.012 (2006).
40 Oakes, P. W., Beckham, Y., Stricker, J. & Gardel, M. L. Tension is required but not sufficient for focal adhesion maturation without a stress fiber template. *The Journal of cell biology* **196**, 363-374, doi:10.1083/jcb.201107042 (2012).
41 Choi, C. K. *et al.* Actin and alpha-actinin orchestrate the assembly and maturation of nascent adhesions in a myosin II motor-independent manner. *Nature cell biology* **10**, 1039-1050, doi:10.1038/ncb1763 (2008).
42 Oakes, P. W. & Gardel, M. L. Stressing the limits of focal adhesion mechanosensitivity. *Curr Opin Cell Biol* **30**, 68-73, doi:10.1016/j.ceb.2014.06.003 (2014).
43 Rafiq, N. B. *et al.* Podosome assembly is controlled by the GTPase ARF1 and its nucleotide exchange factor ARNO. *The Journal of cell biology* **216**, 181-197, doi:10.1083/jcb.201605104 (2017).
44 Elliott, H. *et al.* Myosin II controls cellular branching morphogenesis and migration in three dimensions by minimizing cell-surface curvature. *Nature cell biology* **17**, 137-147, doi:10.1038/ncb3092 (2015).

45 Vasiliev, J. M. *et al.* Effect of colcemid on the locomotory behaviour of fibroblasts. *J Embryol Exp Morphol* **24**, 625-640 (1970).
46 Small, J. V., Geiger, B., Kaverina, I. & Bershadsky, A. How do microtubules guide migrating cells? *Nature reviews. Molecular cell biology* **3**, 957-964, doi:10.1038/nrm971 (2002).
47 Jones, G. E., Zicha, D., Dunn, G. A., Blundell, M. & Thrasher, A. Restoration of podosomes and chemotaxis in Wiskott-Aldrich syndrome macrophages following induced expression of WASp. *The international journal of biochemistry & cell biology* **34**, 806-815 (2002).
48 Ballestrem, C., Magid, N., Zonis, J., Shtutman, M. & Bershadsky, A. in *Cell Motility* 75-99 (John Wiley & Sons, Ltd, 2004).
49 Weng, S., Shao, Y., Chen, W. & Fu, J. Mechanosensitive subcellular rheostasis drives emergent single-cell mechanical homeostasis. *Nature materials* **15**, 961-967, doi:10.1038/nmat4654 (2016).
50 Ballestrem, C., Hinz, B., Imhof, B. A. & Wehrle-Haller, B. Marching at the front and dragging behind: differential alphaVbeta3-integrin turnover regulates focal adhesion behavior. *The Journal of cell biology* **155**, 1319-1332, doi:10.1083/jcb.200107107 (2001).
51 Rid, R., Schiefermeier, N., Grigoriev, I., Small, J. V. & Kaverina, I. The last but not the least: the origin and significance of trailing adhesions in fibroblastic cells. *Cell motility and the cytoskeleton* **61**, 161-171, doi:10.1002/cm.20076 (2005).
52 Pan, C. Q., Liou, Y.-c. & Low, B. C. Active Mek2 as a regulatory scaffold that promotes Pin1 binding to BPGAP1 to suppress BPGAP1-induced acute Erk activation and cell migration. *Journal of cell science* **123**, 903-916, doi:10.1242/jcs.064162 (2010).
53 Sabass, B., Gardel, M. L., Waterman, C. M. & Schwarz, U. S. High resolution traction force microscopy based on experimental and computational advances. *Biophysical journal* **94**, 207-220, doi:10.1529/biophysj.107.113670 (2008).
54 Liu, J. *et al.* Talin determines the nanoscale architecture of focal adhesions. *Proceedings of the National Academy of Sciences of the United States of America* **112**, E4864-4873, doi:10.1073/pnas.1512025112 (2015).
55 Zhang, Z., Nishimura, Y. & Kanchanawong, P. Extracting microtubule networks from superresolution single-molecule localization microscopy data. *Molecular biology of the cell* **28**, 333-345, doi:10.1091/mbc.E16-06-0421 (2017).

Supplementary information for

A mechano-signalling network linking microtubules, myosin-IIA filaments and integrin-based adhesions

Nisha Bte Mohd Rafiq*[1,2], Yukako Nishimura*[1], Sergey V. Plotnikov[3], Visalatchi Thiagarajan[1], Zhen Zhang[1], Shidong Shi[1], Meenubharathi Natarajan[1], Virgile Viasnoff[1,4,5], Pakorn Kanchanawong[#1,6], Gareth E. Jones[#2] and Alexander D. Bershadsky[#1,7]

[1]Mechanobiology Institute, National University of Singapore, Singapore 117411, Singapore
[2]Randall Centre for Cell & Molecular Biophysics, King's College London, London SE1 1UL, UK
[3]Department of Cell and Systems Biology, University of Toronto, Toronto, Ontario, Canada M5S 3G5
[4]CNRS UMI 3639, 5A Engineering drive 1, 117411 Singapore
[5]Department of Biological Sciences, National university of Singapore, 14 Science Drive 4, Singapore 117543
[6]Deparment of Biomedical Engineering, National University of Singapore, Singapore 117411
[7]Department of Molecular Cell Biology, Weizmann Institute of Science, Rehovot 76100, Israel

*Co-first authors
[#]Co-corresponding authors

Table of Contents:

Supplementary notes

Previous studies on dynamics of focal adhesions and podosomes and their regulation by microtubules

Microtubule-driven alterations in cell-matrix adhesions are thought to be responsible for many microtubule-mediated changes in cell shape, polarization and migration [1-6].

Several mechanisms were suggested to explain the regulation of focal adhesions by microtubules. These include functions of kinesin-1 [7,8], Eg5 kinesin [9], MYPT1 and HDAC6 [10], FAK and dynamin [11,12] and APC [13]. In addition, microtubules were shown to be associated with Rho activator GEF-H1, and microtubule disruption results in activation of Rho/ROCK signaling axis [14-16]. Moreover, growing microtubules are targeted to focal adhesions so that their plus ends form multiple transient contacts with these structures [7,17].

Crosstalk between microtubules and podosomes was addressed in several studies. In particular, it was proposed that kinesins KIF1C [18,19] and KIF9 [20], along with CLASPs [19,21] are involved in this regulation.

Myosin-IIA filaments are required for maturation and integrity of focal adhesions [22-28]. At the same time, activation of myosin-IIA by a number of pathways promote podosome turnover and disassembly [29-33]. Involvement of myosin-IIA filaments in microtubule-dependent regulation of focal adhesions and podosomes require further investigation.

Additional information on constructs used in this study

Expression vectors for fluorescent protein fusion constructs were kindly provided by several laboratories, as follows: EGFP-KANK1, EGFP-KANK1-KN, EGFP-KANK1ΔANKR and EGFP-KANK1 CC-Cter [34] from Dr. Anna Akhmanova (Utrecht University, Utrecht, The Netherlands); EGFP-KANK2, EGFP-KANK2-KN, EGFP-KANK2 (1-670) and EGFP-KANK2ΔKN [35], from Dr. Reinhard Fässler (Max Planck Institute of Biochemistry, Germany); GFP-Vinculin, mCherry-Vinculin, mTFP-vinculin, mApple-MAP4, mKO-EB3, GFP-paxillin and mApple-Paxillin from Dr. Michael W. Davidson (Florida State University, FL, USA); GFP-RhoAQ63L, from Dr. Clare M. Waterman (National Institutes of Health, USA); FLAG-ROKα1-543, from Dr. Ronen Zaidel-Bar (Mechanobiology Institute, Singapore); human GFP-Myosin regulatory light chain (MRLC), from Dr. Mark Dodding (King's College London,

UK). Microtubule-binding domain of E-MAP-115/ensconsin (GFP-ensconsin) [36]; RFP-Zyxin [37], mouse GFP-MRLC [38], mCherry-UtrCH [39], RFP-Lifeact and GFP-β-actin [31] were described previously.

A

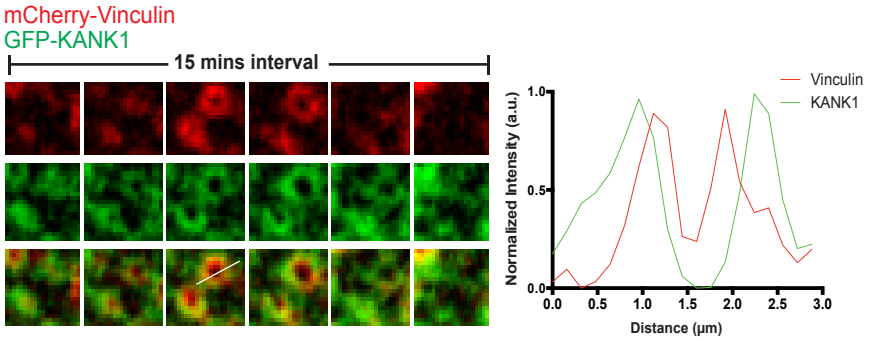
mCherry-Vinculin
GFP-KANK1
15 mins interval
Normalized Intensity (a.u.)
Distance (μm)
Vinculin
KANK1

B

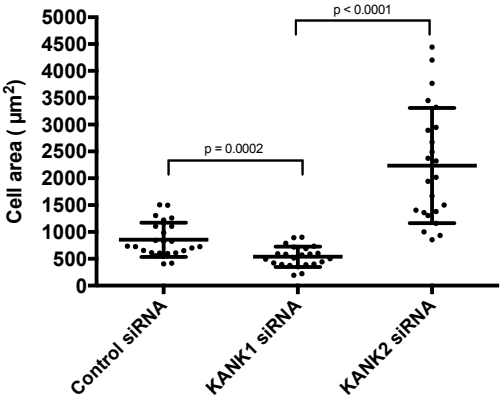
Cell area (μm²)
p < 0.0001
p = 0.0002
Control siRNA
KANK1 siRNA
KANK2 siRNA

C

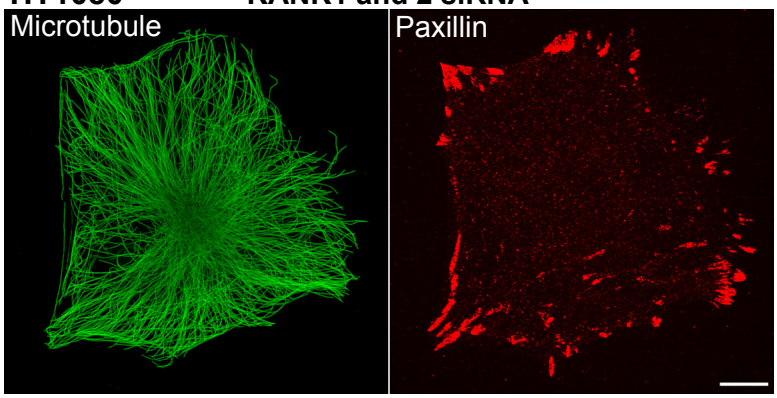
HT1080
KANK1 and 2 siRNA
Microtubule
Paxillin

D

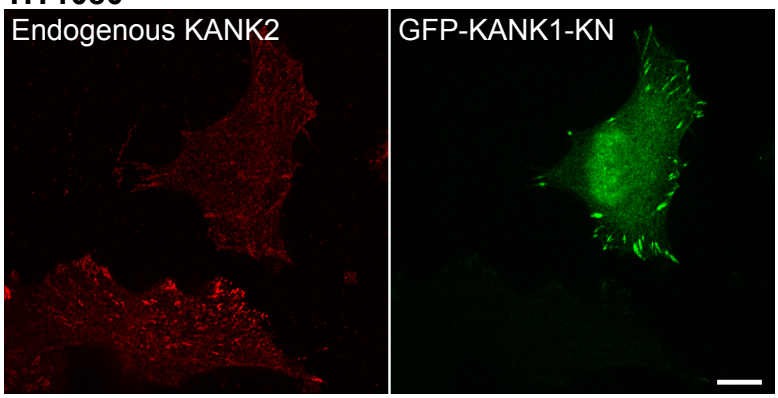
HT1080
Endogenous KANK2
GFP-KANK1-KN

E

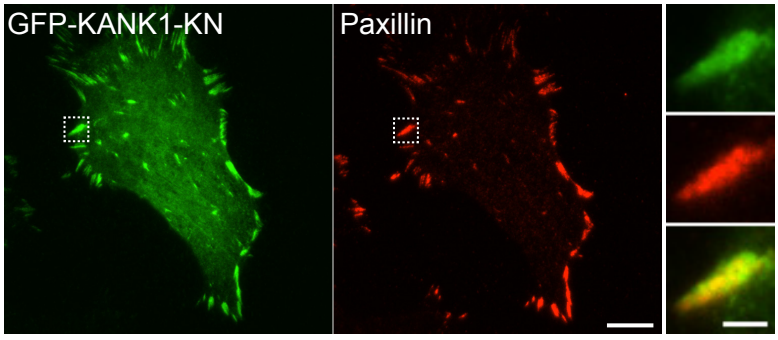
HT1080
GFP-KANK1-KN
Paxillin
E'

F

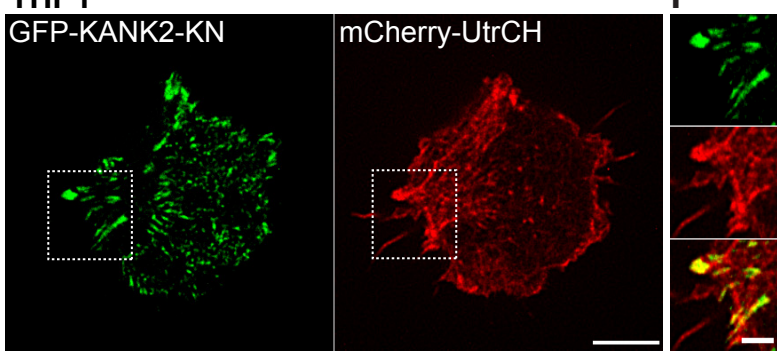
THP1
GFP-KANK2-KN
mCherry-UtrCH
F'

Supplementary Figure 1

Supplementary results on the localization and functions of KANK1 and KANK2. (A) Localization and dynamics of GFP-KANK1 at podosomes in THP1 cell. Six columns (from left to right) represent the sequence of podosome images taken at 3 minute-intervals for 15 minutes. Labeling by mCherry-vinculin (red), GFP-KANK1 (green) and their merged images are shown. Graph on the right represents the line scan profile of vinculin (red) and KANK1 (green) across the podosome shown in the third column (6^{th} minute). KANK1 is located to the outer ring surrounding the vinculin ring of podosome. (B) Effects of knockdown of KANK1 and KANK2 on THP1 cells projected area (μm^2). KANK1 knockdown slightly decreases cell size while KANK2 knockdown markedly increased it. Each dot corresponds to individual cell (mean ± SD; n≥23 cells for each condition). The p-values calculated using two-tailed Student's *t*-test are indicated. Each condition was triple-repeated. (C) KANK1 and KANK2 double knockdown in HT1080 cell labeled with α-tubulin (green) and paxillin (red) antibodies. The cell preserved well-developed microtubule network (left) and form large focal adhesions (right). The measurements of focal adhesion area are shown in Figure 1R. Images are representative of n≥3 independent experiments. (D) Overexpression of talin-binding GFP-KANK1-KN in HT1080 cell resulted in displacement of endogenous KANK2 from the focal adhesions. Two cells labeled with antibody against KANK2 (red) are shown. GFP-KANK1-KN (green) is expressed only in the upper cell (shown in the right image). Note that the lower cell which does not express GFP-KANK1-KN displays prominent KANK2-positive focal adhesions while the upper cell expressing GFP-KANK1-KN contains less of endogenous KANK2 in focal adhesions. Images are representative of two independent experiments. (E) Localization of talin-binding GFP-KANK1-KN domain (green) to focal adhesions marked by mApple paxillin (red) in HT1080 cell. The enlarged images of boxed focal adhesion (E') demonstrate that KANK1-KN labeling overlapped with that of paxillin at the focal adhesion (merged image). Scale bars in C-E, 10 μm; magnified images in E, 2 μm. Images are representative of n≥3 independent experiments. (F) Overexpression of GFP-KANK2-KN (green) in THP1 cell. The actin is labeled by mCherry-UtrCH (red). KANK2-KN resulted in total disruption of podosomes and appearance of focal adhesion-like structures containing KANK2-KN. Scale bar, 5μm. (F') The enlarged images of boxed areas showing localization of GFP-KANK2-KN, actin and their merge. Scale bar, 2 μm.

RAW 264.7 macrophages

A Control

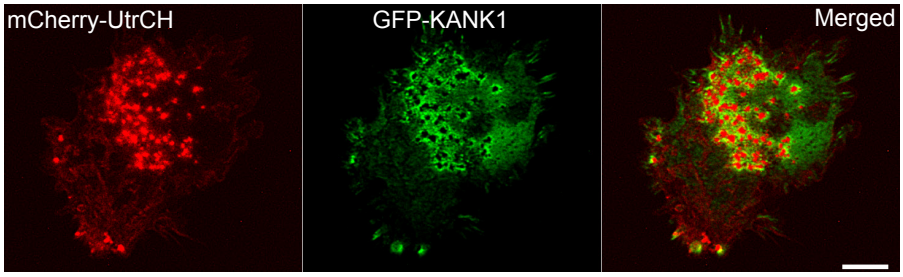

B KANK1-KN expression

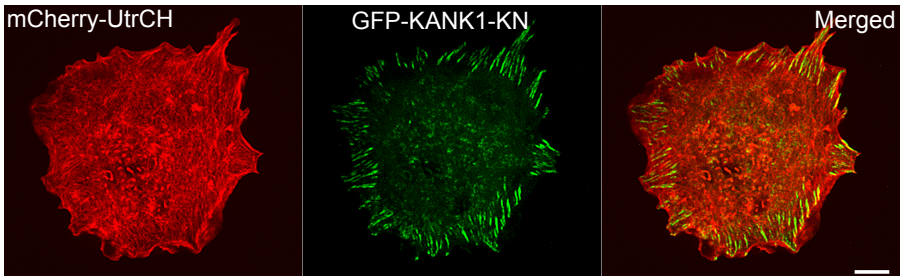

C

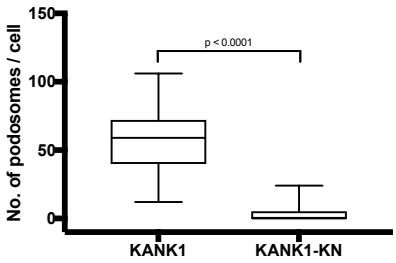

D

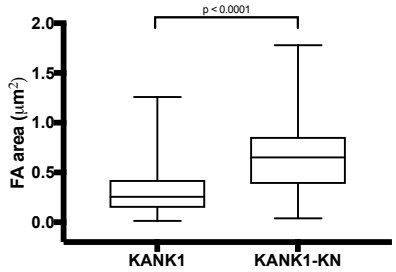

HT-29

E Untreated

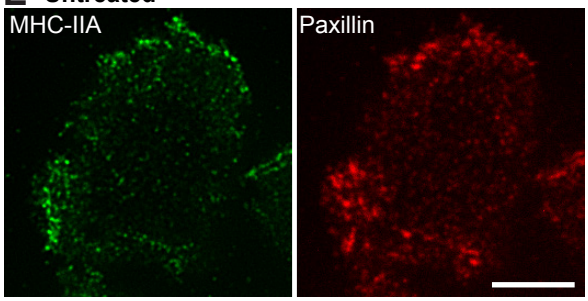

F 1 μM Nz

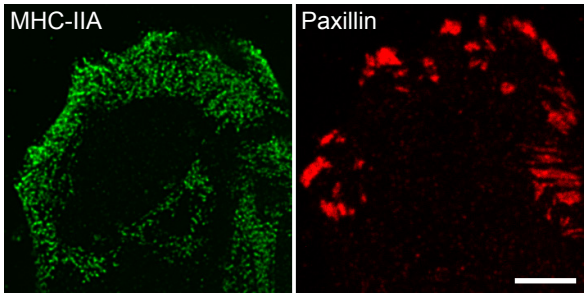

G KANK2-KN expression

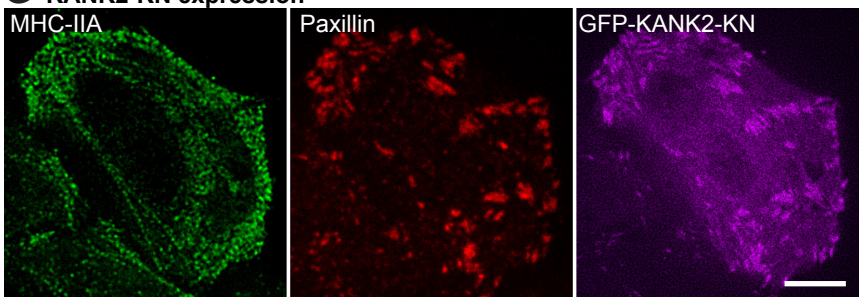

H

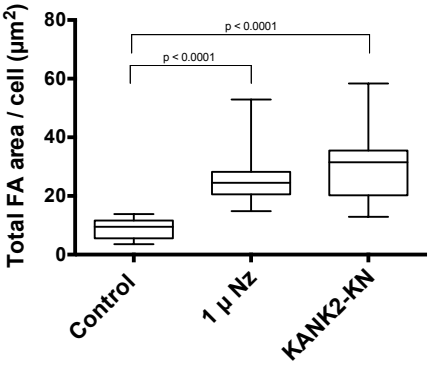

HUVECs

I Control

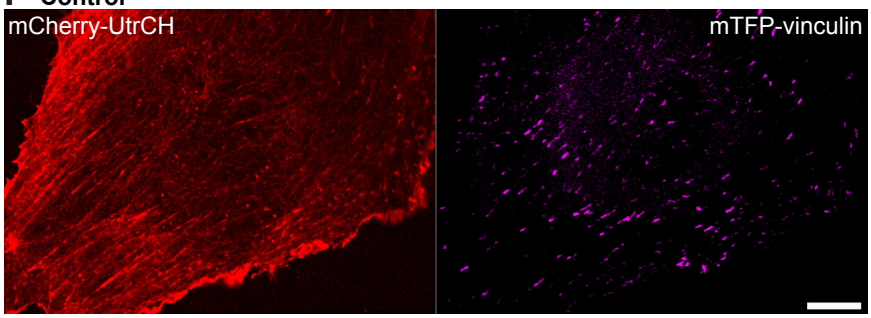

K

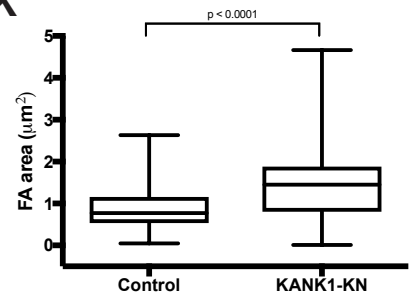

J KANK1-KN expression

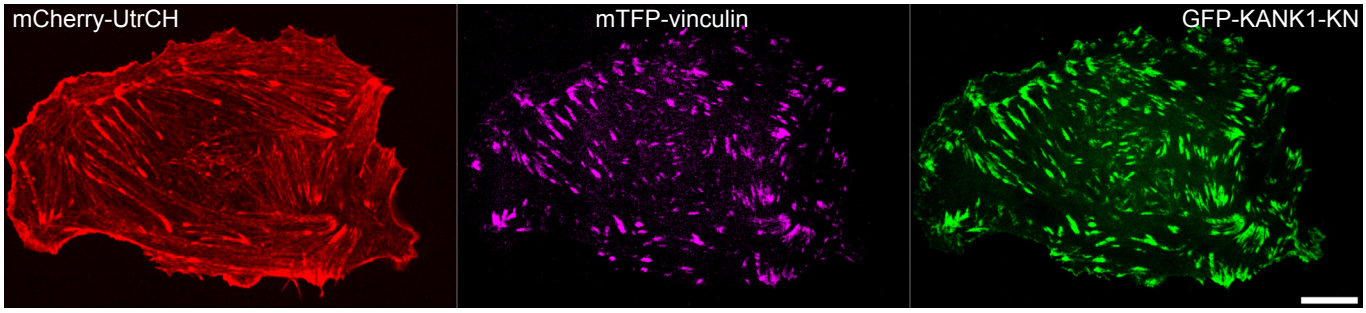

Supplementary Figure 2
Effects of microtubule disconnection from integrin adhesions in different cell types. (A-D) Podosome-forming murine RAW 264.7 macrophages. (A) Localization of GFP-KANK1 (green) and F-actin labeled by mCherry-UtrCH (red) in phorbol 12-myristate 13-acetate (PMA)-stimulated RAW 264.7 cell. GFP-KANK1 localized to the adhesive rings surrounding the actin cores of podosomes and in focal adhesion-like structures at the cell periphery (merged image). (B) Cell overexpressing GFP-KANK1-KN (green) did not form podosomes and display prominent KN-positive focal adhesion-like structures upon stimulation with PMA. Actin is labeled by mCherry-UtrCH (red). Scale bars, 5 μm. Each condition was triple-repeated. (C) The number of podosomes per cell in control and KN-overexpressing cells (box-and-whiskers plots; n≥26 cells for each condition). (D) The average areas of focal adhesion-like structures in control and KN-overexpressing cells visualized by GFP-KANK1 and GFP-KANK1-KN, respectively (box-and-whiskers plots; n=8 cells for each condition). (E-H) Human colon adenocarcinoma cell line HT-29. Immunofluoresence labeling of myosin-IIA heavy chain (MHC-IIA) (green) and focal adhesions labeled by paxillin (red) in untreated (E), nocodazole-treated (F), and GFP-KANK2-KN (purple) overexpressing cells (G). Both disruption of microtubules and their disconnection from integrin adhesions by GFP-KANK2-KN overexpression resulted in increase of myosin-IIA filaments number and focal adhesion size. Nz=nocodazole. Scale bars, 5 μm. (H) The quantification of total focal adhesion area per cell (box-and-whiskers plots; n≥23 cells for each condition; three independent experiments). (I-K) Human umbilical vein endothelial cells (HUVECs). F-actin labeled by mCherry-UtrCH (red) and focal adhesions labeled by mTFP-vinculin (purple) in control (I) and GFP-KANK1-KN (green) overexpressing (J) cells. Each condition was triple-repeated. (K) Overexpression of GFP-KANK1-KN induced increase in average focal adhesion area (n=12 cells for each condition). Scale bars, 10 μm. In C, D, H and K, the p-values calculated using two-tailed Student's *t*-test are indicated.

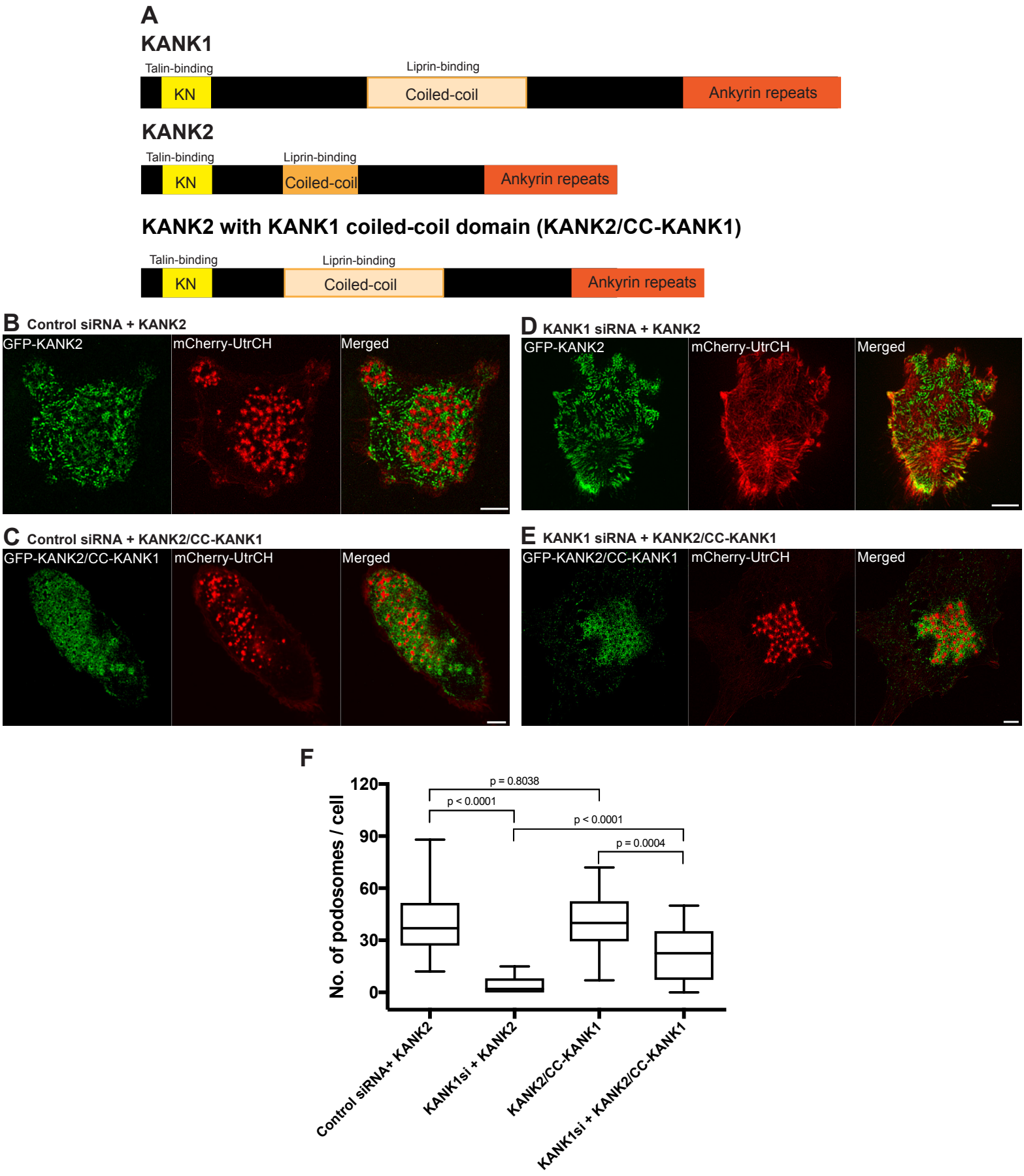
A
KANK1
Talin-binding
Liprin-binding
KN
Coiled-coil
Ankyrin repeats
KANK2
Talin-binding
Liprin-binding
KN
Coiled-coil
Ankyrin repeats
KANK2 with KANK1 coiled-coil domain (KANK2/CC-KANK1)
Talin-binding
Liprin-binding
KN
Coiled-coil
Ankyrin repeats
B Control siRNA + KANK2
GFP-KANK2
mCherry-UtrCH
Merged
D KANK1 siRNA + KANK2
GFP-KANK2
mCherry-UtrCH
Merged
C Control siRNA + KANK2/CC-KANK1
GFP-KANK2/CC-KANK1
mCherry-UtrCH
Merged
E KANK1 siRNA + KANK2/CC-KANK1
GFP-KANK2/CC-KANK1
mCherry-UtrCH
Merged
F
No. of podosomes / cell
120
90
60
30
0
p = 0.8038
p < 0.0001
p < 0.0001
p = 0.0004
Control siRNA+ KANK2
KANK1si + KANK2
KANK2/CC-KANK1
KANK1si + KANK2/CC-KANK1

Supplementary Figure 3

Liprin-binding coiled coil domain of KANK1 is responsible for the differential effect of KANK1 and KANK2 on podosomes in THP1 cells. (A) A diagram depicting the domain structures of KANK1, KANK2, and a chimeric protein KANK2/CC-KANK1, designed as KANK2, in which the liprin-binding coiled-coil domain was replaced by that of KANK1. In particular, the residues 188-238 of KANK2 corresponding to its coiled-coil domain [35] were substituted with the residues 257-500 of KANK1 corresponding to its coiled-coil domain [34]. (B-E) The effects of expression of full-length KANK2 and KANK2/CC-KANK1 on podosomes in THP1 cells containing or lacking KANK1. (B) Expression of GFP-KANK2 (green) in cell transfected with control siRNA did not affect podosomes labeled by mCherry-UtrCH (red). GFP-KANK2 is poorly localized to podosomes. (C) GFP-KANK2/CC-KANK1 strongly localize to podosomes in cell transfected with control siRNA. (D) Expression of GFP-KANK2 (green) in KANK1-depleted cell did not rescue podosomes. (E) Expression of GFP-KANK2/CC-KANK1 in KANK1-depleted cell rescued podosomes. The GFP-KANK2/CC-KANK1 is localized to the rescued podosomes. Scale bars, 5μm. Each condition was repeated twice. (F) Quantification of the effect of full-length GFP-KANK2 and GFP-KANK2/CC-KANK1 on podosome number in control and KANK1 knockdown cells (box-and-whiskers plots; n≥25 cells for each condition). KANK2/CC-KANK1 but not full-length KANK2 expressions significantly increased the podosome number in KANK1-depleted cells. The average number of podosomes in KANK1-depleted cells expressing KANK2/CC-KANK1 was however still lower than in cells containing KANK1. The p-values calculated using two-tailed Student's *t*-test are indicated.

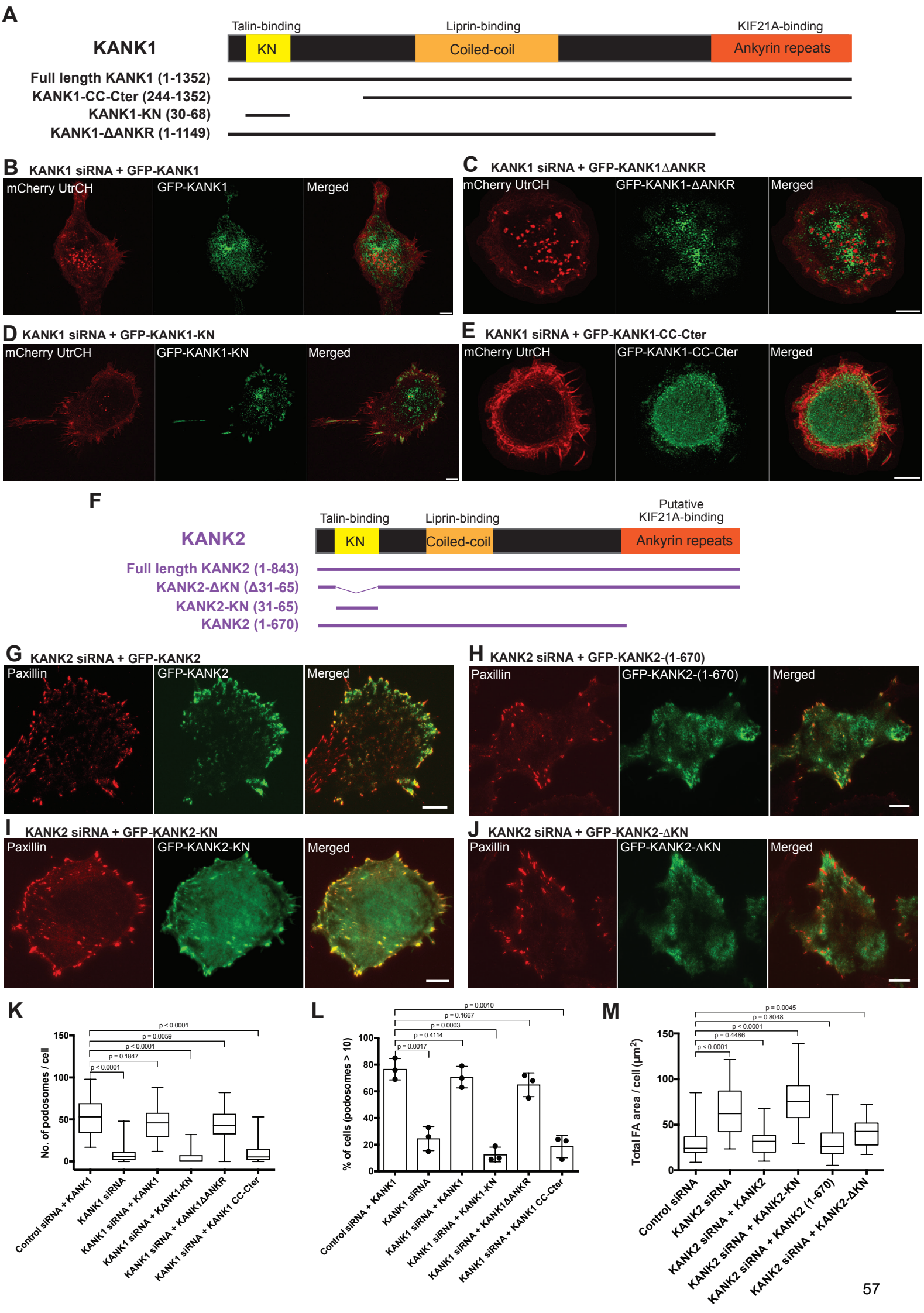
A
KANK1
Talin-binding
KN
Liprin-binding
Coiled-coil
KIF21A-binding
Ankyrin repeats
Full length KANK1 (1-1352)
KANK1-CC-Cter (244-1352)
KANK1-KN (30-68)
KANK1-ΔANKR (1-1149)
B KANK1 siRNA + GFP-KANK1
mCherry UtrCH
GFP-KANK1
Merged
C KANK1 siRNA + GFP-KANK1ΔANKR
mCherry UtrCH
GFP-KANK1-ΔANKR
Merged
D KANK1 siRNA + GFP-KANK1-KN
mCherry UtrCH
GFP-KANK1-KN
Merged
E KANK1 siRNA + GFP-KANK1-CC-Cter
mCherry UtrCH
GFP-KANK1-CC-Cter
Merged
F
KANK2
Talin-binding
KN
Liprin-binding
Coiled-coil
Putative
KIF21A-binding
Ankyrin repeats
Full length KANK2 (1-843)
KANK2-ΔKN (Δ31-65)
KANK2-KN (31-65)
KANK2 (1-670)
G KANK2 siRNA + GFP-KANK2
Paxillin
GFP-KANK2
Merged
H KANK2 siRNA + GFP-KANK2-(1-670)
Paxillin
GFP-KANK2-(1-670)
Merged
I KANK2 siRNA + GFP-KANK2-KN
Paxillin
GFP-KANK2-KN
Merged
J KANK2 siRNA + GFP-KANK2-ΔKN
Paxillin
GFP-KANK2-ΔKN
Merged
K
No. of podosomes / cell
p < 0.0001
p = 0.0059
p < 0.0001
p = 0.1847
p < 0.0001
Control siRNA + KANK1
KANK1 siRNA
KANK1 siRNA + KANK1
KANK1 siRNA + KANK1-KN
KANK1 siRNA + KANK1ΔANKR
KANK1 siRNA + KANK1 CC-Cter
L
% of cells (podosomes > 10)
p = 0.0010
p = 0.1667
p = 0.0003
p = 0.4114
p = 0.0017
Control siRNA + KANK1
KANK1 siRNA
KANK1 siRNA + KANK1
KANK1 siRNA + KANK1-KN
KANK1 siRNA + KANK1ΔANKR
KANK1 siRNA + KANK1 CC-Cter
M
Total FA area / cell (μm²)
p = 0.0045
p = 0.8048
p < 0.0001
p = 0.4486
p < 0.0001
Control siRNA
KANK2 siRNA
KANK2 siRNA + KANK2
KANK2 siRNA + KANK2-KN
KANK2 siRNA + KANK2 (1-670)
KANK2 siRNA + KANK2-ΔKN

Supplementary Figure 4

Rescuing the phenotypes of KANK1 and KANK2-depleted cells by the respective deletion mutants. (A) A diagram depicting the domain structures of KANK1 and presenting its deletion mutants as described in Ref [34]. (B-E) KANK1 depleted THP1 cells. In each triple panel, the images of podosome cores visualized by actin labeling with mCherry-UtrCH (red), localization of GFP fusion constructs of KANK1 or its deletion mutants (green), and the merged images are shown. (B and C) Full-length GFP-KANK1 (B) and GFP-KANK1ΔANKR (C) rescued podosomes in the KANK1-depleted cells. (D and E) GFP-KANK1-KN (D) and GFP-KANK1-CC-Cter (E) did not rescue podosomes in KANK1-depleted cells. Scale bars, 5 μm. Each condition was triple-repeated. (F) A diagram depicting the domain structures of KANK2 and its deletion mutants as described in Ref [35]. Putative binding domain for KIF21A is indicated by analogy with KANK1. (G-J) KANK2 depleted HT1080 cells. In each triple panel, the images of focal adhesions visualized by paxillin antibody staining (red), localization of GFP fusion constructs of KANK2 or its deletion mutants (green), and the merged images are shown. Full-length GFP-KANK2 (B) and GFP-KANK2 (1-670) (C) demonstrate focal adhesions of normal size while GFP-KANK2-KN (D) and GFP-KANK2ΔKN (E) show large focal adhesions similarly to KANK2-depleted cells (See Figure 1F). Each condition was triple-repeated. Scale bars, 10 μm. (K, L) The number of podosomes per cell (box-and-whiskers plots; n≥30 cells for each condition) (K) and percentage of cells with ≥10 podosomes (mean ± SD; n=3 independent samples). (L) in THP1 cells treated as indicated are presented as box-and-whiskers and mean ± SD, respectively. The data on control siRNA + GFP-KANK1-transfected cells and KANK1 siRNA-transfected cells are the same as in Figure 1S and 1T and represent the pooled results of 6 and 7 experiments, respectively. The other data represent the pooled results of not less than 3 independent experiments. (M) The total focal adhesion areas per cell in HT1080 cells treated as indicated are presented. The data on control siRNA and KANK2 siRNA-transfected cells are the same as in Figure 1R and represent the pooled results of three independent experiments (box-and-whiskers plots; n≥24 cells for each condition). The p-values calculated using two-tailed Student's *t*-test are indicated in all graphs.

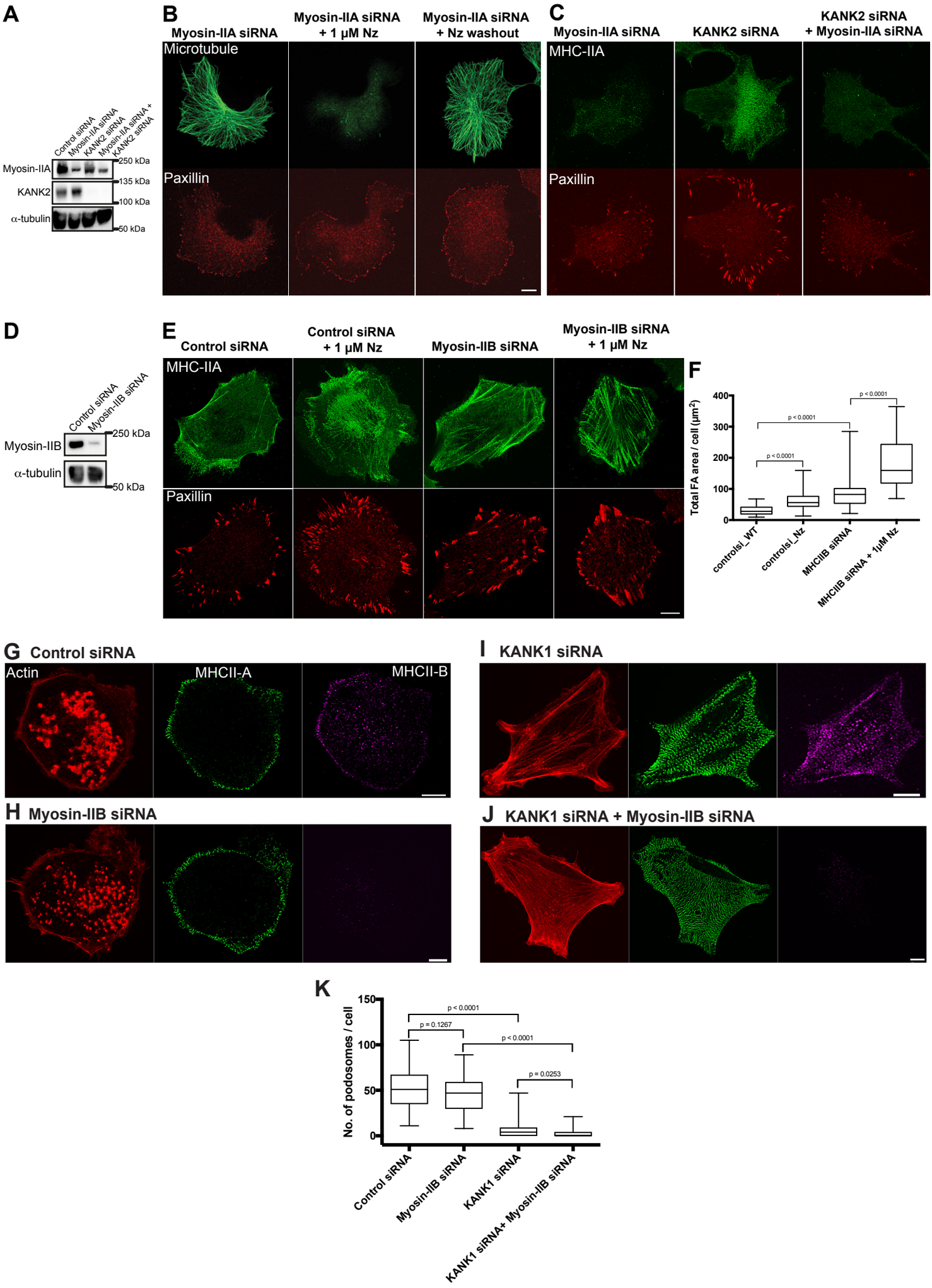
A
Control siRNA
Myosin-IIA siRNA
KANK2 siRNA
Myosin-IIA siRNA + KANK2 siRNA
Myosin-IIA
KANK2
α-tubulin
250 kDa
135 kDa
100 kDa
50 kDa
B
Myosin-IIA siRNA
Myosin-IIA siRNA + 1 μM Nz
Myosin-IIA siRNA + Nz washout
Microtubule
Paxillin
C
Myosin-IIA siRNA
KANK2 siRNA
KANK2 siRNA + Myosin-IIA siRNA
MHC-IIA
Paxillin
D
Control siRNA
Myosin-IIB siRNA
Myosin-IIB
α-tubulin
250 kDa
50 kDa
E
Control siRNA
Control siRNA + 1 μM Nz
Myosin-IIB siRNA
Myosin-IIB siRNA + 1 μM Nz
MHC-IIA
Paxillin
F
Total FA area / cell (μm²)
400
300
200
100
0
p < 0.0001
p < 0.0001
p < 0.0001
controlsi_WT
controlsi_Nz
MHCIIB siRNA
MHCIIB siRNA + 1μM Nz
G Control siRNA
Actin
MHCII-A
MHCII-B
H Myosin-IIB siRNA
I KANK1 siRNA
J KANK1 siRNA + Myosin-IIB siRNA
K
No. of podosomes / cell
150
100
50
0
p < 0.0001
p = 0.1267
p < 0.0001
p = 0.0253
Control siRNA
Myosin-IIB siRNA
KANK1 siRNA
KANK1 siRNA+ Myosin-IIB siRNA

Supplementary Figure 5

Myosin-IIA but not myosin-IIB knockdown abolished effect of microtubule disruption/disconnection on integrin-based adhesions. (A) Western blot data showing depletion of myosin-IIA and KANK2 in HT1080 cells upon transfection with specific siRNAs. α-tubulin was used as loading control. (B) Each column represents the individual myosin-IIA knockdown HT1080 cell treated as indicated. The microtubules were labeled with α-tubulin antibody staining (green) and focal adhesions in the same cells with antibody to paxillin (red). The focal adhesion size in myosin-IIA knockdown cell is small and did not change upon microtubule disruption by nocodazole or outgrowth after nocodazole washout. (C) Myosin-IIA knockdown abolished the effect of KANK2 knockdown on focal adhesion size. The cells were labeled with myosin-IIA heavy chain (green) and paxillin (red) antibodies. KANK2 knockdown cell showed augmented focal adhesions and myosin-II filaments, while double myosin-IIA and KANK2 knockdown cell demonstrated reduced focal adhesion size. (D) Western blot data showing depletion of myosin-IIB in HT1080 cells upon transfection with MYH10 siRNA. α-tubulin was used as loading control. (E) Myosin-IIB knockdown did not prevent increase of focal adhesion size in nocodazole-treated cell. The cells were labeled with antibodies to myosin-IIA and paxillin as in (C). Note that knockdown of myosin-IIB by itself increased the amount of myosin-IIA filaments and the areas of focal adhesions. However, the nocodazole treatment significantly increased the total area of focal adhesions in cells transfected with either control or myosin-IIB siRNA. Images are representative of two independent experiments. Scale bars in B, C and E, 10 μm. (F) Quantification of the results shown in (E). Total areas of focal adhesions per cells in cells treated as indicated are shown (box-and-whiskers plots; n≥40 cells for each condition) as box-and-whiskers plot. (G-J) THP1 cells labeled by phalloidin to visualize actin (red), and by myosin-IIA (green) and myosin-IIB (purple) heavy chain antibodies. (G) Cell transfected with control siRNA, demonstrated numerous actin-positive podosomes and peripherally localized myosin-IIA and myosin-IIB containing filaments. (H) The knockdown of myosin-IIB affected neither podosomes nor myosin-IIA-containing filaments. (I) KANK1 knockdown disrupted podosomes and induced formation of actin bundles and myosin-IIA filament stacks. The distribution of myosin-IIB essentially followed that of myosin-IIA. (J) The double knockdown of KANK1 and myosin-IIB led to complete disruption of podosomes and enhancement of actin bundles and myosin-IIA filament stacks. Scale bars, 5 μm. Each condition was repeated twice. (K) Quantification of podosomes number in cells (box-and-whiskers plots; n≥35 cells for each condition) treated as indicated in (G-J). Nz=nocodazole. The p-values calculated using two-tailed Student's *t*-test are indicated in both graphs.

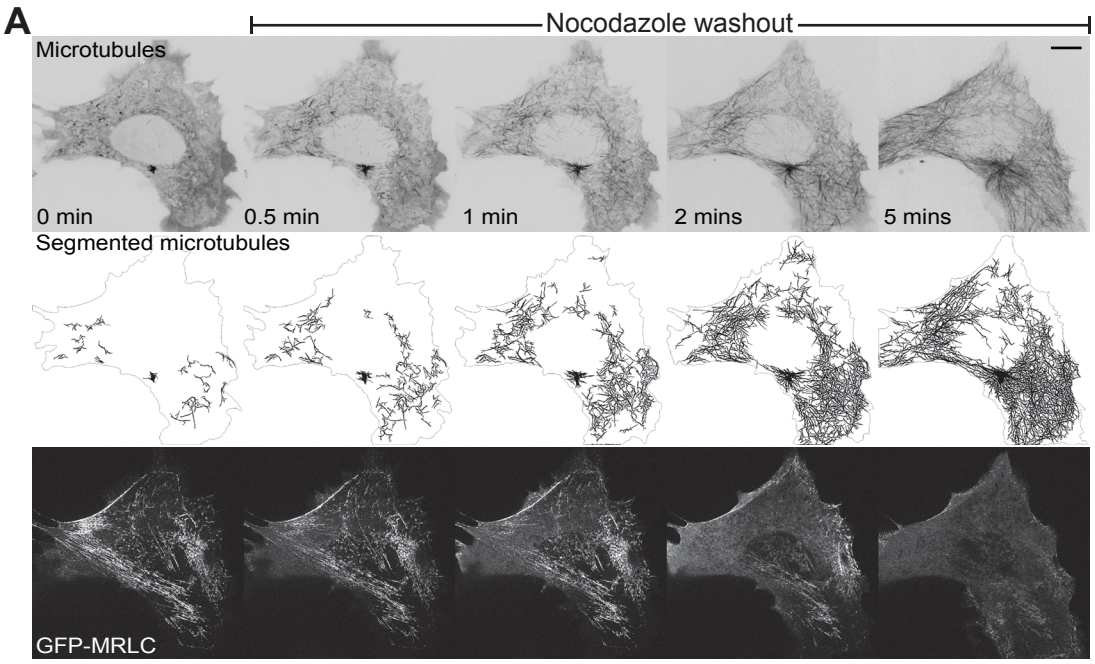
A
Nocodazole washout
Microtubules
0 min
0.5 min
1 min
2 mins
5 mins
Segmented microtubules
GFP-MRLC

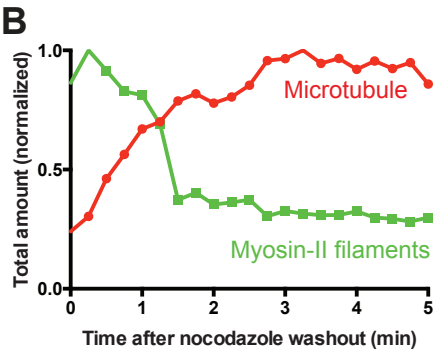
B
Total amount (normalized)
Microtubule
Myosin-II filaments
Time after nocodazole washout (min)

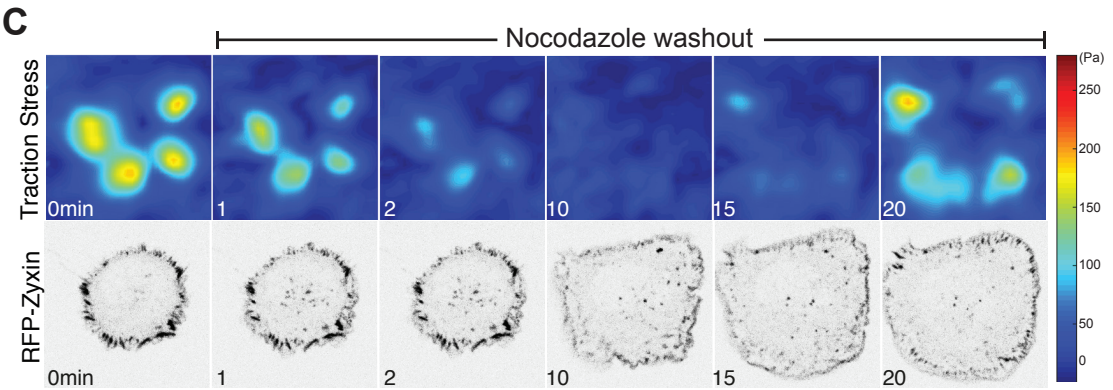
C
Nocodazole washout
Traction Stress
RFP-Zyxin
0min
1
2
10
15
20
(Pa)

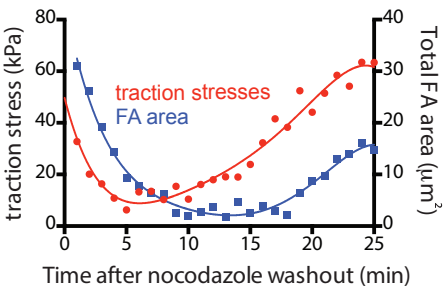
D
traction stress (kPa)
Total FA area (μm²)
traction stresses
FA area
Time after nocodazole washout (min)

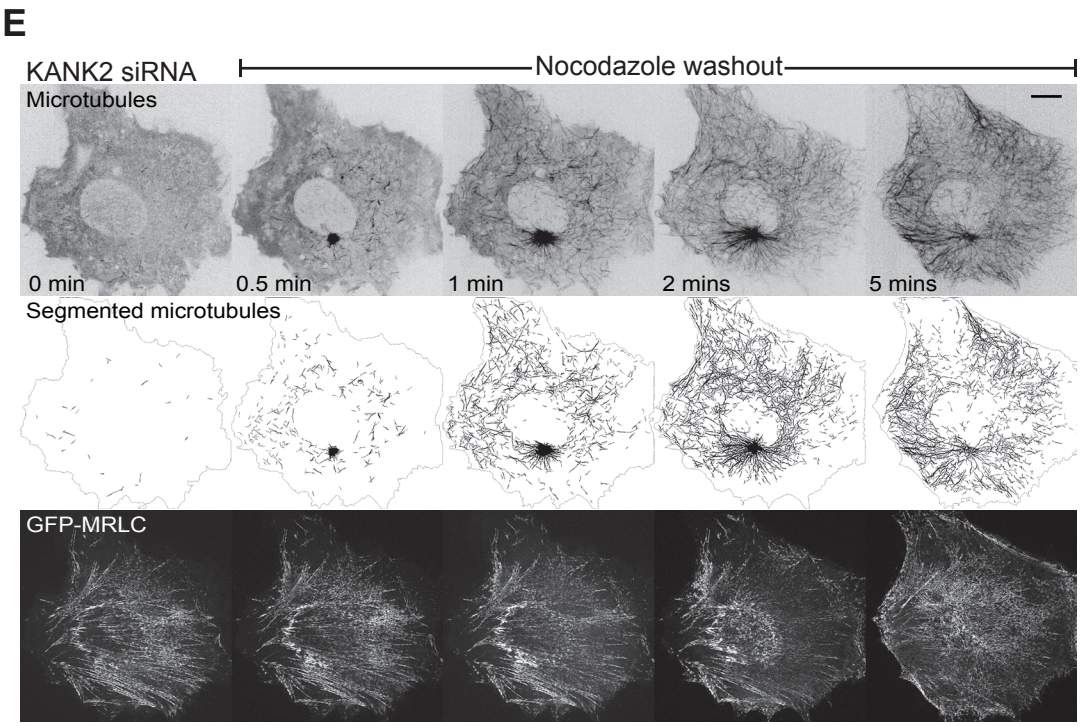
E
KANK2 siRNA
Nocodazole washout
Microtubules
0 min
0.5 min
1 min
2 mins
5 mins
Segmented microtubules
GFP-MRLC

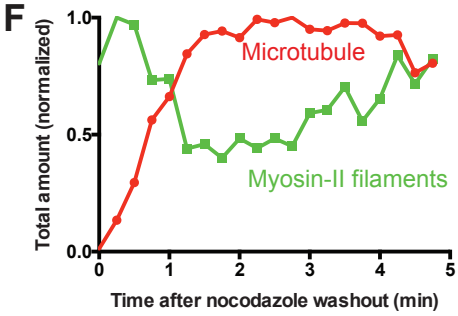
F
Total amount (normalized)
Microtubule
Myosin-II filaments
Time after nocodazole washout (min)

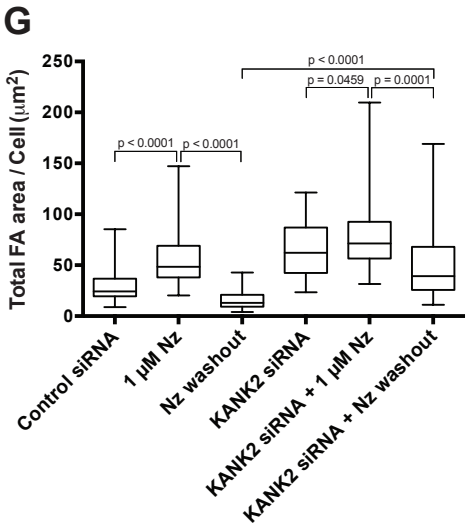
G
Total FA area / Cell (μm²)
p < 0.0001
p < 0.0001
p < 0.0001
p = 0.0459
p = 0.0001
Control siRNA
1 μM Nz
Nz washout
KANK2 siRNA
KANK2 siRNA + 1 μM Nz
KANK2 siRNA + Nz washout

Supplementary Figure 6

Enhancement of microtubule targeting to focal adhesions brings about disassembly of myosin-II filaments and focal adhesions. (A) Time-lapse observations of microtubules (upper row), computationally segmented microtubules (second row) and myosin-II filaments (bottom row) in the course of microtubule outgrowth after nocodazole washout in HT1080 cell. Time after the nocodazole washout is indicated in each frame. Microtubules and myosin-II filaments were labeled by mApple-MAP4 and GFP-MRLC, respectively. Inverted images of microtubule labeling are shown. Note that recovery of microtubules is accompanied by disappearance of myosin-II filaments. See Supplementary Movie 7. (B) Quantification of the changes in fluorescence intensity of microtubules (red) and myosin-II filaments (green) shown in (A). For details of the quantification procedures, see Materials and Method. (C) Changes in traction forces exerted by cell in the course of microtubule recovery following nocodazole washout. The traction forces are presented in the upper row in spectrum scale shown on the right. The corresponding images of cells with focal adhesions labeled with RFP-zyxin are presented in the bottom row, along with the time in minutes after nocodazole washout. The traction forces and focal adhesion size strongly decreased following nocodazole washout but recovered in about 20 minutes thereafter. See Supplementary Movie 8. (D) Changes in sum of the absolute values of traction forces (kPa) and total focal adhesion area (μm^2) per cell shown in (C). The drop and subsequent increase of traction forces (red) preceded the drop and increase in focal adhesion area (blue). (E) KANK2 knockdown suppresses the effect of microtubule outgrowth on the amount of myosin-II filaments. Microtubules (upper row), computationally segmented microtubules (second row), myosin-II filaments (bottom row) in the same cell were labeled as indicated in (A). Time after nocodazole washout is indicated in the upper row. See Supplementary Movie 9. Note that in spite of microtubule outgrowth, the decrease of myosin-II filament fluorescence was less pronounced than in control cell shown in (A). (F) Quantification of the changes in fluorescence intensity of microtubules (red) and myosin-II filaments (green) as in (B). Nz-nocodazole. Sequences shown in (A-F) are representative of n≥3 independent experiments. Scale bars in all panels correspond to 10 μm. (G) Changes in the total area of focal adhesions after nocodazole treatment and washout in control and KANK2 knockdown cells shown as box-and-whiskers plots (n≥40 cells for each condition). The cells treated as indicated were fixed and stained with paxillin antibody to visualize focal adhesions. The p-values calculated using two-tailed Student's *t*-test are indicated.

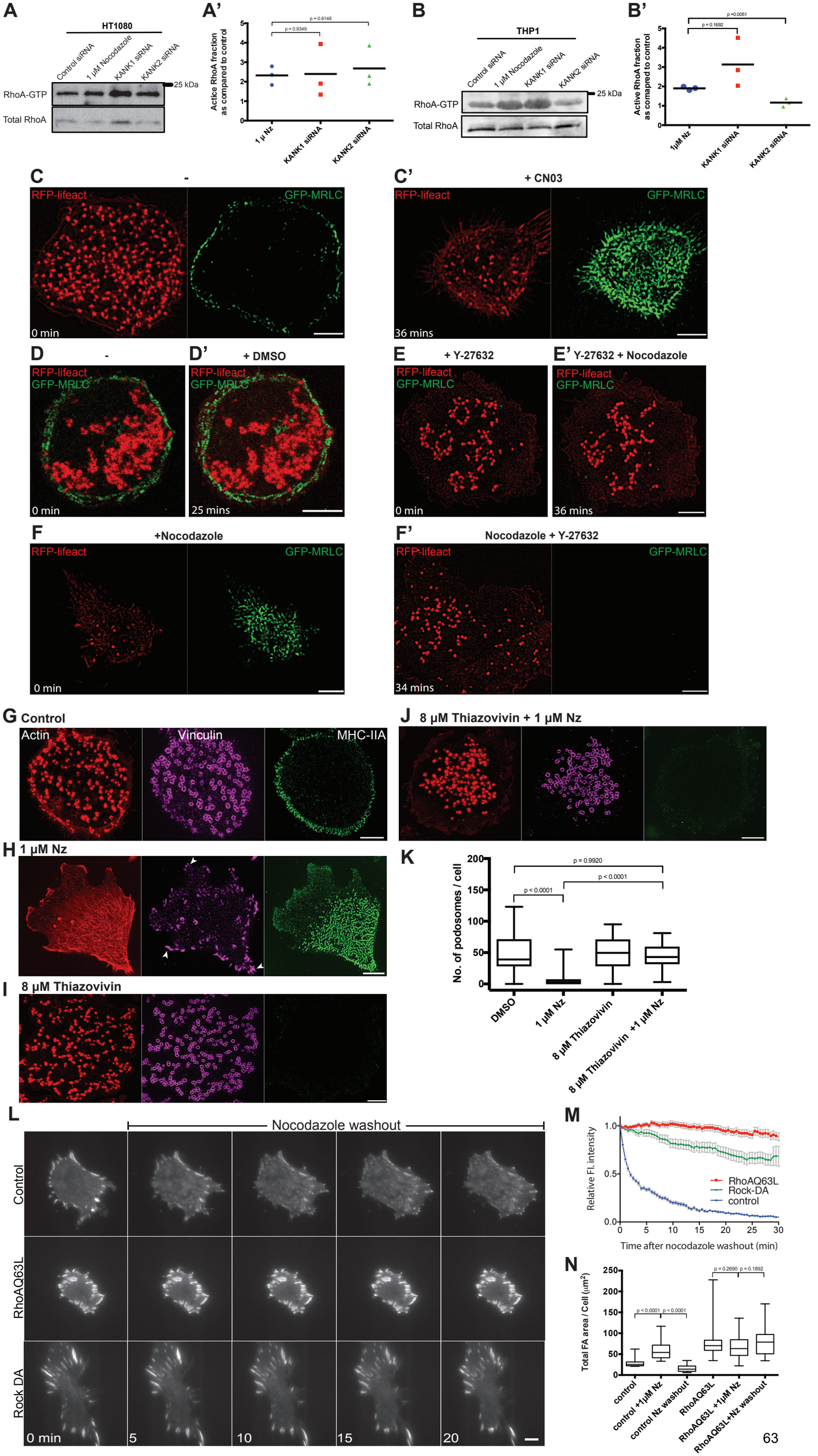
A
HT1080
Control siRNA
1 μM Nocodazole
KANK1 siRNA
KANK2 siRNA
RhoA-GTP
Total RhoA
25 kDa
A'
Actice RhoA fraction as compared to control
p = 0.6148
p = 0.9349
1 μ Nz
KANK1 siRNA
KANK2 siRNA
B
THP1
Control siRNA
1 μM Nocodazole
KANK1 siRNA
KANK2 siRNA
RhoA-GTP
Total RhoA
25 kDa
B'
Active RhoA fraction as compared to control
p =0.0051
p = 0.1692
1μM Nz
KANK1 siRNA
KANK2 siRNA
C
-
RFP-lifeact
GFP-MRLC
0 min
C'
+ CN03
RFP-lifeact
GFP-MRLC
36 mins
D
-
RFP-lifeact
GFP-MRLC
0 min
D'
+ DMSO
RFP-lifeact
GFP-MRLC
25 mins
E
+ Y-27632
RFP-lifeact
GFP-MRLC
0 min
E'
Y-27632 + Nocodazole
RFP-lifeact
GFP-MRLC
36 mins
F
+Nocodazole
RFP-lifeact
GFP-MRLC
0 min
F'
Nocodazole + Y-27632
RFP-lifeact
GFP-MRLC
34 mins
G
Control
Actin
Vinculin
MHC-IIA
J
8 μM Thiazovivin + 1 μM Nz
H
1 μM Nz
K
No. of podosomes / cell
p = 0.9920
p < 0.0001
p < 0.0001
DMSO
1 μM Nz
8 μM Thiazovivin
8 μM Thiazovivin +1 μM Nz
I
8 μM Thiazovivin
L
Nocodazole washout
Control
RhoAQ63L
Rock DA
0 min
5
10
15
20
M
Relative Fl. intensity
RhoAQ63L
Rock-DA
control
Time after nocodazole washout (min)
N
Total FA area / Cell (μm²)
p < 0.0001
p < 0.0001
p = 0.2690
p = 0.1892
control
control +1μM Nz
control Nz washout
RhoAQ63L
RhoAQ63L +1μM Nz
RhoAQ63L+Nz washout

Supplementary Figure 7

Microtubule disruption or disconnection from integrin adhesions affect the adhesions via activation of RhoA-ROCK axis. (A and B) Results of pull-down assays showing effects of KANK1 and KANK2 knockdowns on RhoA activation in HT1080 and THP1 cells as compared to the effects of nocodazole treatment. Western blots of RhoA-GTP level and of total RhoA in the corresponding samples are shown in the upper and lower rows, respectively. (A' and B') The ratios between the amounts of RhoA-GTP to total RhoA in the sample estimated as a ratio between intensities of corresponding bands. The results normalized to the value of such ratio in untreated cells transfected with control siRNA are presented in the graphs. Each treatment was assessed by triplicate measurements. The mean values are indicated as horizontal bars. (A, A') The knockdown of either KANK1 or KANK2 in HT1080 cells led to 2-fold increase of average RhoA-GTP level as compared to control, similar to nocodazole treatment. The differences between KANK1 and KANK2 knockdown effects as compared to that of nocodazole are non-significant. (B, B') The knockdown of KANK1 but not KANK2 in THP1 cells led to increase of RhoA-GTP level similar to nocodazole treatment. Each condition was triple-repeated. The p-values calculated using two-tailed Student's *t*-test are indicated in both A' and B' graphs (mean ± SD; n=3 independent experiments). (C-F) Podosomes were visualized by RFP-lifeact (red) and myosin-II filaments were labeled by GFP-MRLC (green) in THP1 cells. (C, C') Effect of RhoA activation. Podosomes and myosin-II filaments in the same cell before (C) and 36 minutes following (C') addition of Rho activator, CN03. Note the assembly of new myosin-II filaments and the disappearance of podosomes. See Supplementary Movie 10. (D, D') DMSO, control. Merged images of podosomes and myosin-II filaments before (D) and after (D') incubation with DMSO. See Supplementary Movie 11. (E-K) ROCK inhibition prevents the effect of nocodazole. (E, E') Cell was pre-treated with Y-27632 for 30 minutes before addition of nocodazole at 0 minute (E) and further incubated in the presence of both compounds for 36 minutes (E'). Treatment with Y-27632 disrupted myosin-II filaments and prevent disruptive effect of nocodazole on podosomes (cf. Figures 1H and 3A). See Supplementary Movie 13. (F, F') Cell pre-treated with nocodazole for 30 minutes before addition of Y-27632 at 0 minute (F) and further incubated in the presence of both compounds for 34 minutes (F'). Addition of Y-27632 resulted in the disassembly of myosin-II filaments, and subsequent recovery of podosomes. See Supplementary Movie 14. Each condition was triple-repeated. See quantification of effects shown in C-F in Figures 4C and D. (G-K) Inhibition of ROCK by thiazovivin. (G-J) The actin cores and adhesive rings of podosomes were visualized by staining of F-actin by phalloidin and vinculin by corresponding antibody. Myosin-II filaments were stained by antibody to myosin-IIA heavy chain. (G) DMSO-treated cell (control); (H) Cell treated with nocodazole (Nz) for 1 hour; note the disruption of podosomes, appearance

of focal adhesion-like structures (arrowheads) and burst of myosin-II filament assembly. (I) Treatment with ROCK inhibitor thiazovivin for 1hour disrupted myosin-II filaments. (J) Cell pre-treated with thiazovivin for 30 minutes and further incubated with nocodazole and thiazovivin for 1 hour demonstrated intact podosomes. Scale bars in C-J, 5 μm. Each condition was repeated twice. (K) Box-and-whiskers plots showing the numbers of podosomes per cell (n≥40 cells for each condition) indicated in G-J. (L-N) Constitutively active RhoA and ROCK1 prevented the disruption of focal adhesions following microtubule outgrowth in HT1080 cells. (L) Time-lapse sequences showing focal adhesion dynamics after nocodazole washout in control cell (top row), cell expressing constitutive active RhoA-Q63L (middle row) and cell expressing dominant active ROCK (rat Rok-alpha 1-543aa). The focal adhesions labeled by mApple-paxillin were visualized by TIRF microscopy. The cells were pre-treated with nocodazole for 1 hour. Nocodazole washout led to disassembly of the focal adhesions, while constitutively active RhoA and ROCK prevented this process. Images are representative of two independent experiments. Scale bars, 10 μm. See Supplementary Movie 16. (M) Intensities of mApple-paxillin fluorescence in focal adhesions (n≥34 for each condition; mean ± SEM) normalized to the intensity level in the first frame, in control, RhoA-Q63L expressing and ROCK1-DA expressing cells shown in (L). (N) Total area of focal adhesions per cell visualized by paxillin antibody staining in control and RhoA-Q63L expressing cells are shown in box-and-whiskers plots. The cells were either untreated, nocodazole-treated for 1 hour, or fixed after 30 minutes following nocodazole washout. Nz-nocodazole. n≥14 cells from two independent experiments were measured for each type of treatment. The p-values calculated using two-tailed Student's *t*-test are indicated.

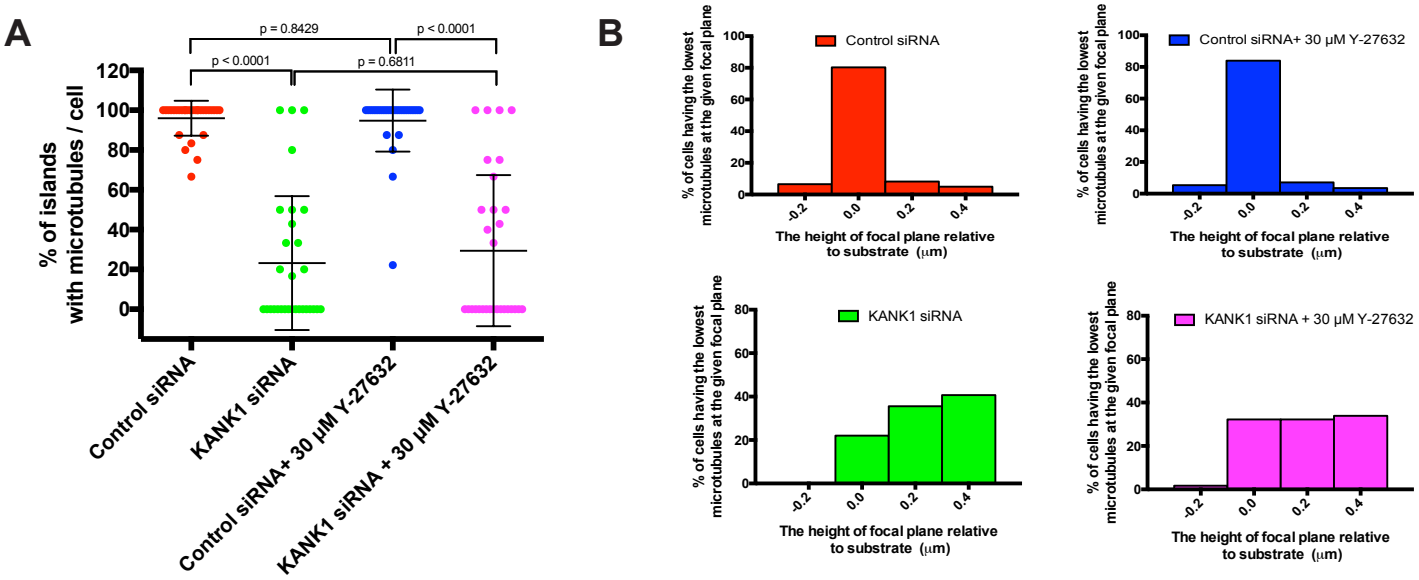

Supplementary Figure 8

Quantification of the localization of microtubule tips to the podosomes or focal adhesion-like structures in THP1 cells plated on micropatterned adhesive islands (see Figure 4I-L). (A) Percentage of adhesive islands with microtubule tips seen at z=0 focal plane. Each dot corresponds to individual cell (n=30 cells were scored for each type of treatment). The mean ± SD values are shown. The p-values calculated using two-tailed non-parametric Mann–Whitney test are indicated. (B) The histograms representing fractions of the cells having the lowest microtubule tips at indicated focal planes (n≥56 cells were scored for each type of treatment).

HT1080 fibrosarcoma

A Control siRNA

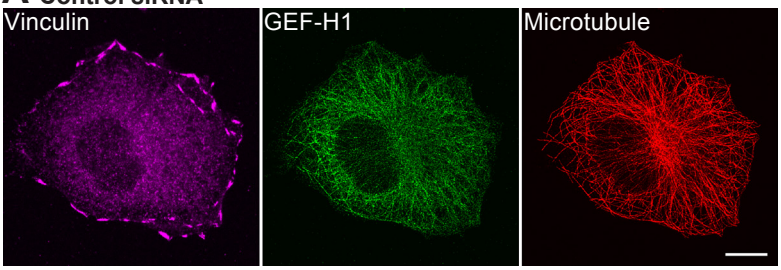

C KANK2 siRNA

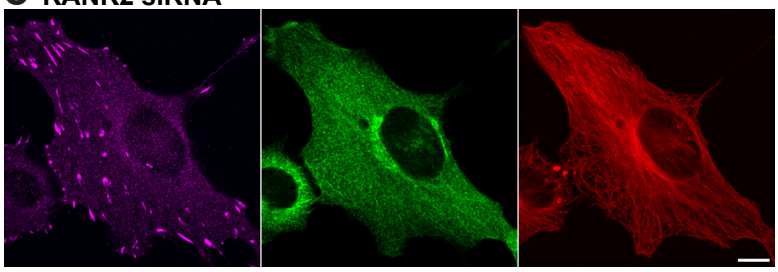

B 1 μM Nz

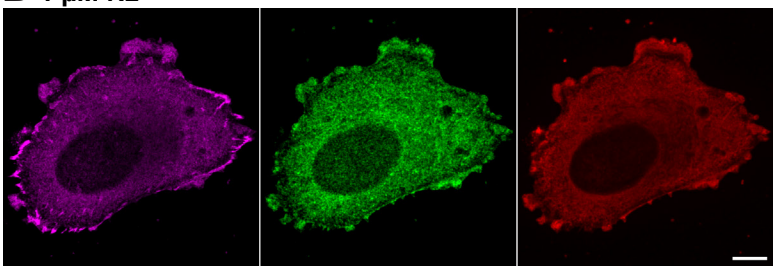

D KANK1 and KANK2 siRNA

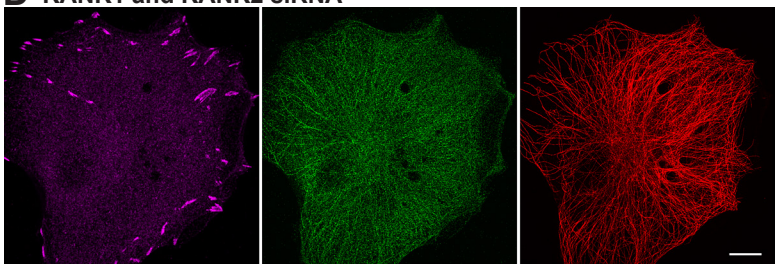

HUVECs

E

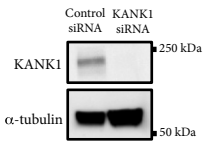

F Control siRNA

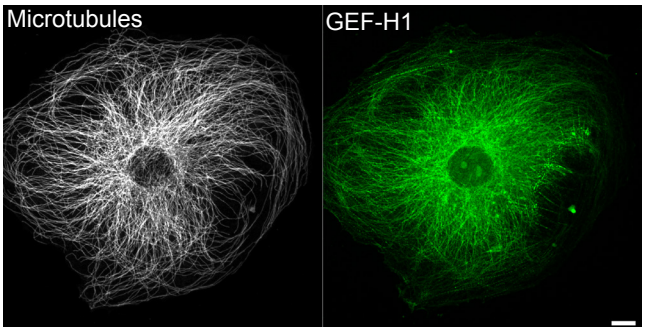

G KANK1 siRNA

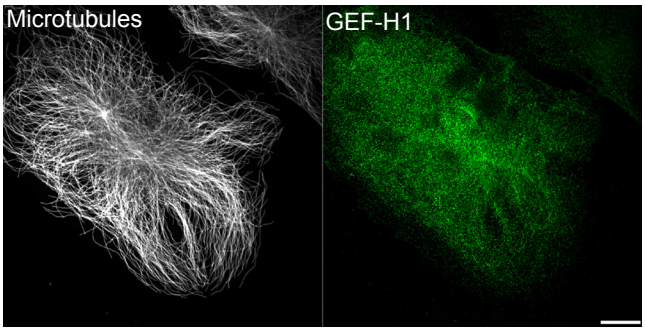

THP1 macrophages

H Control siRNA

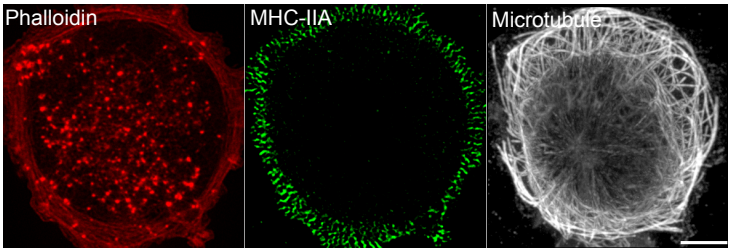

I GEF-H1 siRNA

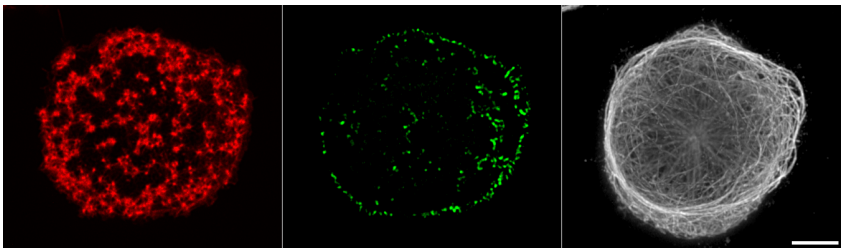

J Control siRNA + 1 μM Nocodazole

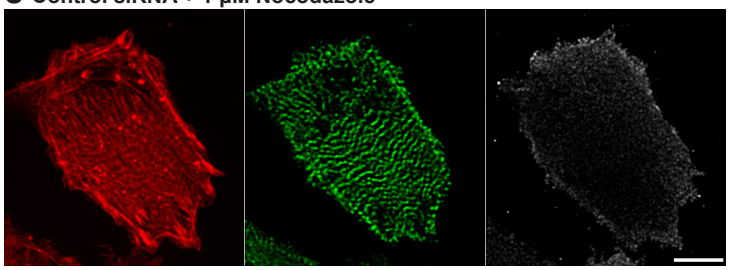

K GEF-H1 siRNA + 1 μM Nocodazole

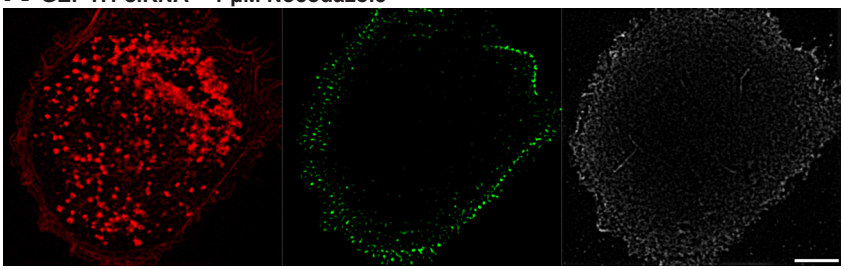

L KANK1 siRNA

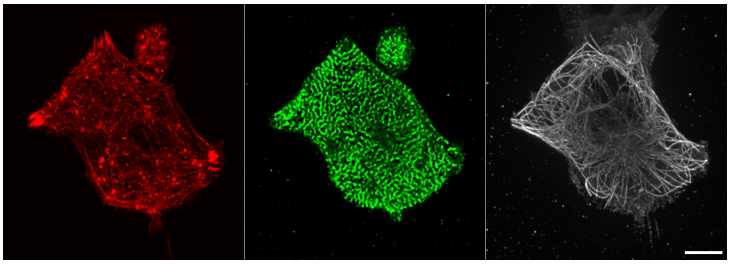

M GEF-H1 siRNA + KANK1 siRNA

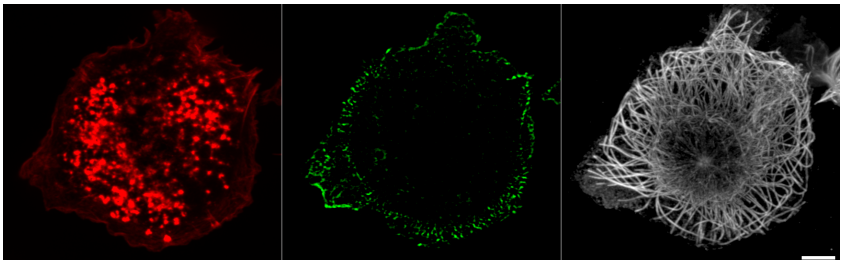

Supplementary Figure 9

Function of GEF-H1 in different cell types. (A-G) Release of GEF-H1 from microtubules upon microtubule disruption or disconnection from focal adhesions. (A-D) Focal adhesions (vinculin, purple), GEF-H1 (green) and microtubules (α-tubulin, red) were labeled by corresponding antibodies in HT1080 cells. (A) Control cell formed peripheral focal adhesion; GEF-H1 was localized to microtubules. (B) Disruption of microtubules by nocodazole (Nz) treatment for 1 hour resulted in augmentation of focal adhesions and diffused localization of GEF-H1. (C and D) KANK2 knockdown (C) or KANK1 and KANK2 double knockdown (D) resulted in appearance of larger and non-peripherally localized focal adhesions (cf. Figure 1 and Supplementary Figure 1) and diffused localization of GEF-H1. Microtubule network is apparently intact in C and D. Images are representative of three independent experiments. (E) Western blot analysis of KANK1 levels in human endothelial cells (HUVECs) transfected with control and KANK1 siRNAs. α-tubulin was used as the loading control. (F and G) Microtubules (white) and GEF-H1 (green) visualized by α-tubulin and GEF-H1 antibodies, respectively, in cells transfected with control siRNA (F) and KANK1 siRNA (G). Depletion of KANK1 resulted in diffused GEF-H1 localization. Scale bars, 10μm. Each condition was repeated twice. (H-M) Effect of GEF-H1 knockdown in THP1 cells (data supplementary to Figure 5E-P). Actin (red), myosin-IIA filaments (green) and microtubules (white) were visualized by staining with phalloidin, myosin-IIA heavy chain and α-tubulin antibodies, respectively. Control (H) and GEF-H1 knockdown (I) THP1 cells demonstrated intact podosomes cores, peripheral myosin-II filaments and well-developed microtubule arrays. (J and K) Nocodazole (Nz) treatment for 1 hour disrupted podosomes and enhanced the amount of myosin-II filaments in control (J) but not in GEF-H1 knockdown (K) cells, even though the disruption of microtubules was complete in both cases. (L and M) KANK1 knockdown led to disassembly of podosomes and increase in the amount of myosin-IIA filaments (L) but cells lacking both GEF-H1 and KANK1 demonstrated intact podosomes and low level of myosin-II filaments (M). The microtubules are well preserved in both cases. Each condition was repeated twice. Scale bars, 5 μm.

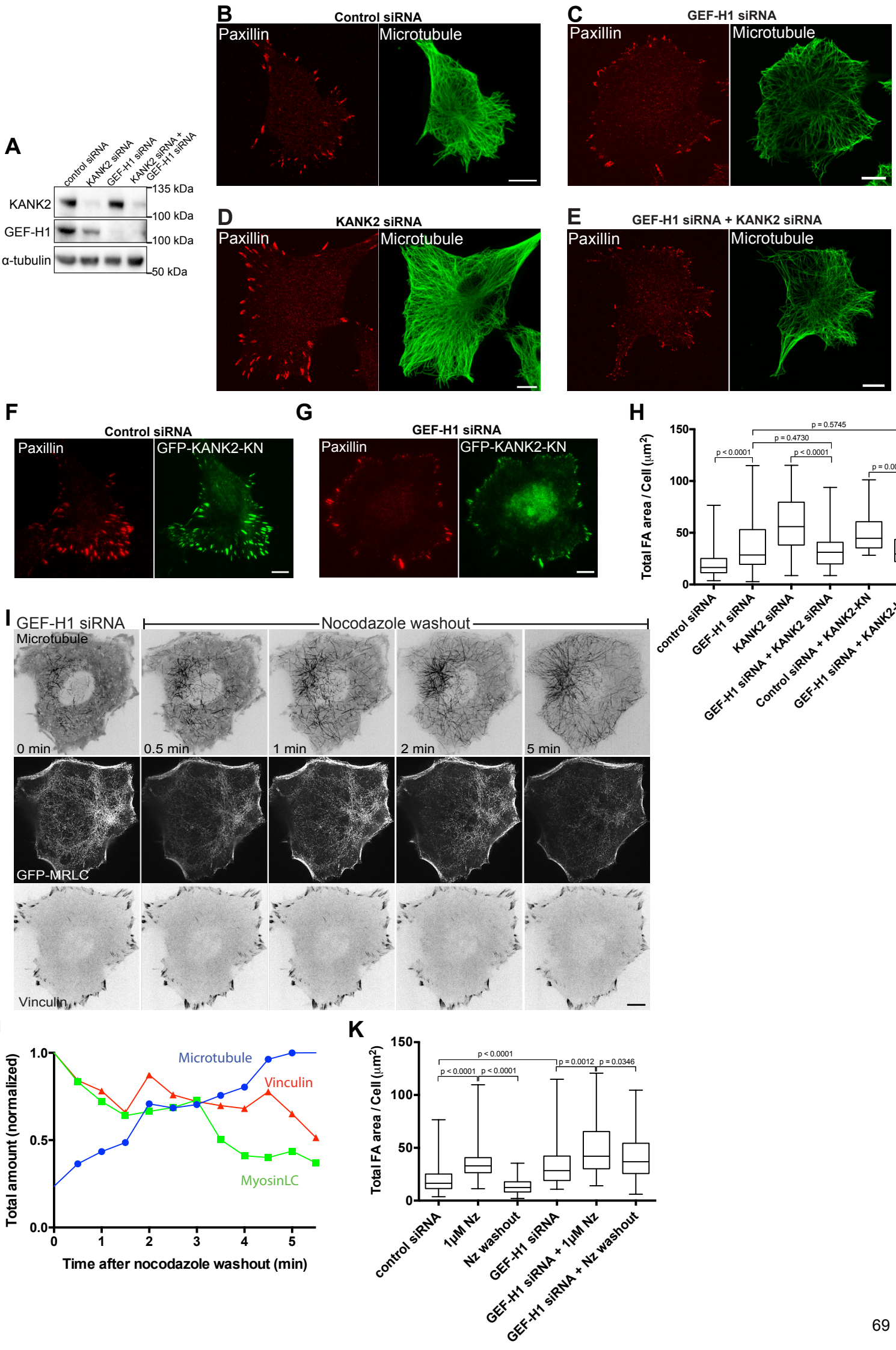
A
control siRNA
KANK2 siRNA
GEF-H1 siRNA
KANK2 siRNA + GEF-H1 siRNA
KANK2
GEF-H1
α-tubulin
135 kDa
100 kDa
100 kDa
50 kDa
B
Control siRNA
Paxillin
Microtubule
C
GEF-H1 siRNA
Paxillin
Microtubule
D
KANK2 siRNA
Paxillin
Microtubule
E
GEF-H1 siRNA + KANK2 siRNA
Paxillin
Microtubule
F
Control siRNA
Paxillin
GFP-KANK2-KN
G
GEF-H1 siRNA
Paxillin
GFP-KANK2-KN
H
Total FA area / Cell (μm²)
p = 0.5745
p = 0.4730
p < 0.0001
p < 0.0001
p = 0.0068
control siRNA
GEF-H1 siRNA
KANK2 siRNA
GEF-H1 siRNA + KANK2 siRNA
Control siRNA + KANK2-KN
GEF-H1 siRNA + KANK2-KN
I
GEF-H1 siRNA
Nocodazole washout
Microtubule
0 min
0.5 min
1 min
2 min
5 min
GFP-MRLC
Vinculin
J
Total amount (normalized)
Microtubule
Vinculin
MyosinLC
Time after nocodazole washout (min)
K
Total FA area / Cell (μm²)
p < 0.0001
p < 0.0001
p < 0.0001
p = 0.0012
p = 0.0346
control siRNA
1μM Nz
Nz washout
GEF-H1 siRNA
GEF-H1 siRNA + 1μM Nz
GEF-H1 siRNA + Nz washout

Supplementary Figure 10

GEF-H1 knockdown prevented the effects of microtubule disconnection from focal adhesions and microtubule outgrowth on focal adhesions in HT1080 cells. (A) Western blot demonstrating siRNA-mediated depletion of GEF-H1, KANK2, and both of them in HT1080 cells. α-tubulin is used as loading control. (B-E) Focal adhesions (paxillin, red) and microtubules (α-tubulin, green) in HT1080 cells transfected with control (B), GEF-H1-targeted (C), KANK2-targeted (D) siRNAs, or with both KANK2- and GEF-H1- targeted siRNAs (E). KANK2 knockdown increased the size of focal adhesions in control but not in GEF-H1 knockdown cell. The integrity of microtubules was not affected in any cases. (F and G) GEF-H1 knockdown prevented increase in focal adhesion area induced by expression of GFP-KANK2-KN. (F) Cell transfected with control siRNA and GFP-KANK2-KN (green) demonstrates large and numerous paxillin-positive focal adhesions (red) containing KANK2-KN. (G) The cell transfected with GEF-H1 siRNA and GFP-KANK2-KN has lower total focal adhesion area, similarly to cells transfected with GEF-H1 siRNA alone (see C). Images are representative of two independent experiments. Scale bars, 10 μm. (H) Quantification of the total focal adhesion area per cell in conditions corresponding to that shown in box-and-whiskers plots (B-G). n≥20 cells from two independent experiments were measured for each type of treatment. (I) The sequence of images showing the GEF-H1 knockdown cell labeled for microtubules (upper panels), myosin-II filaments (middle panels) and focal adhesions (bottom panels) in the course of microtubule outgrowth after nocodazole washout. The microtubules, myosin-II filaments and focal adhesions were labeled with mApple-MAP4, GFP-MRLC and mTFP-vinculin, respectively. See Supplementary Movie 17. The images of microtubules and focal adhesions are reversed. Unlike the strong disruptive effect of microtubule outgrowth on myosin-II filaments and focal adhesions in control cells (cf. Supplementary Figure 6A and B), the recovery of microtubules in GEF-H1 knockdown cell was accompanied by only partial disruption of myosin-II filaments and focal adhesions (see quantification in J). Scale bar, 10 μm. (J) The dynamics of total fluorescence intensity of the microtubules, myosin-II filaments and focal adhesions in cell shown in (I) is presented in blue, green and red plots, respectively. Images and graph are representative of two independent experiments. (K) The measurements of total focal adhesion area per cell in control and GEF-H1 knockdown cells upon nocodazole treatment and washout are shown in box-and-whiskers plots. n≥60 cells were assessed for each type of treatment from three independent experiments. The cells were fixed and stained with antibodies to paxillin after respective treatments. Nz=nocodazole. The p-values calculated using two-tailed Student's *t*-test are indicated.

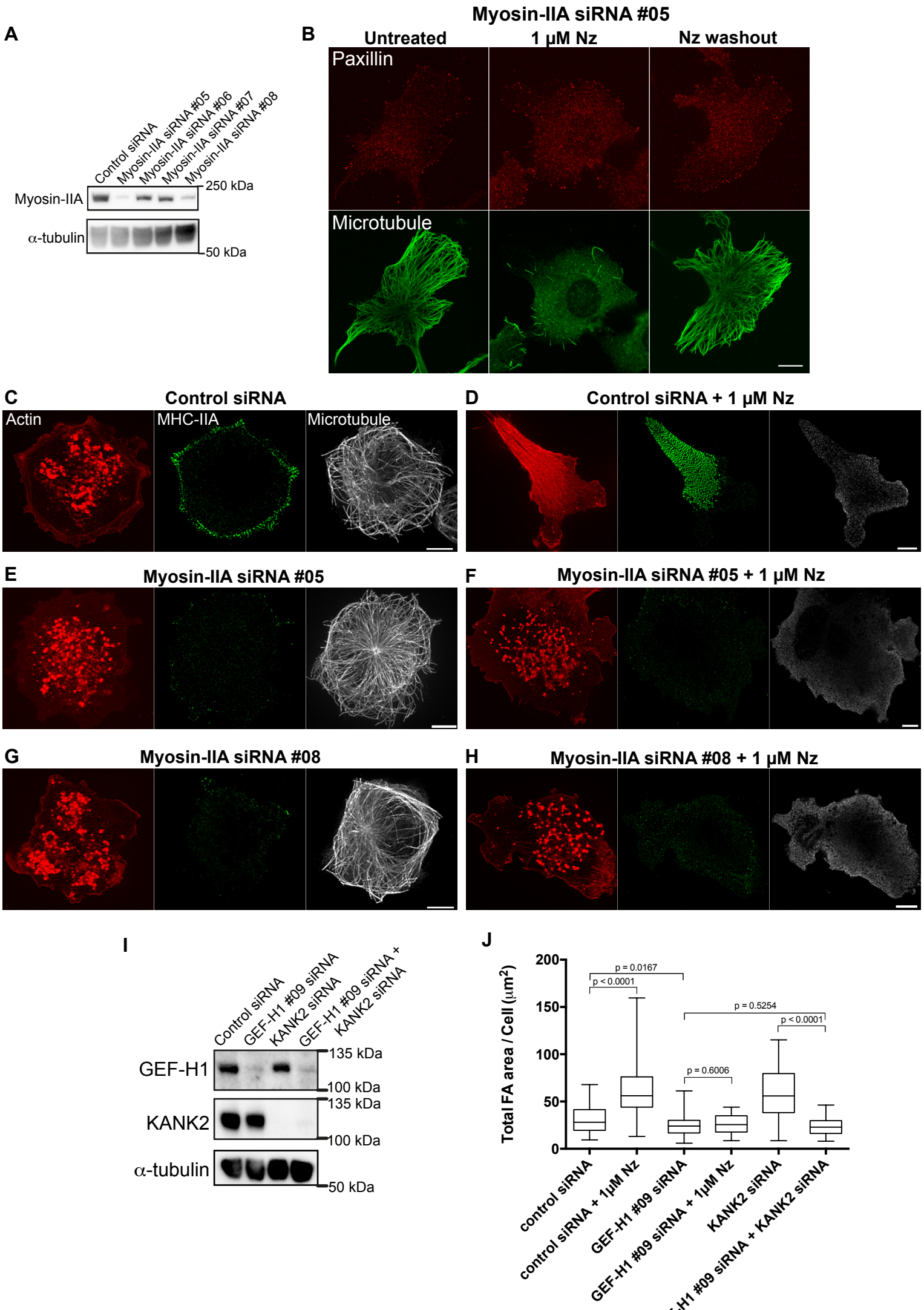
A
Control siRNA
Myosin-IIA siRNA #05
Myosin-IIA siRNA #06
Myosin-IIA siRNA #07
Myosin-IIA siRNA #08
Myosin-IIA
250 kDa
α-tubulin
50 kDa
B
Myosin-IIA siRNA #05
Untreated
1 μM Nz
Nz washout
Paxillin
Microtubule
C
Control siRNA
Actin
MHC-IIA
Microtubule
D
Control siRNA + 1 μM Nz
E
Myosin-IIA siRNA #05
F
Myosin-IIA siRNA #05 + 1 μM Nz
G
Myosin-IIA siRNA #08
H
Myosin-IIA siRNA #08 + 1 μM Nz
I
Control siRNA
GEF-H1 #09 siRNA
KANK2 siRNA
GEF-H1 #09 siRNA + KANK2 siRNA
GEF-H1
135 kDa
100 kDa
KANK2
135 kDa
100 kDa
α-tubulin
50 kDa
J
Total FA area / Cell (μm²)
200
150
100
50
0
p = 0.0167
p < 0.0001
p = 0.5254
p < 0.0001
p = 0.6006
control siRNA
control siRNA + 1μM Nz
GEF-H1 #09 siRNA
GEF-H1 #09 siRNA + 1μM Nz
KANK2 siRNA
GEF-H1 #09 siRNA + KANK2 siRNA

Supplementary Figure 11

Verification of the effects of Dharmacon smartpool siRNAs against myosin-IIA and GEF-H1 in experiments with individual siRNAs. (A) Western blot data showing effects of individual siRNAs on myosin-IIA heavy chain (MYH9) expression in HT1080 cells. The information corresponding to individual siRNAs (#05-#08) is presented in Materials and Methods. α-tubulin was used as loading control. (B) Cell transfection with myosin-IIA siRNA #05 prevented the effects of nocodazole and nocodazole washout on focal adhesions in HT1080 cells. Focal adhesions (red) and microtubules (green) were immunolabeled with paxillin and α-tubulin antibodies, respectively. Images are representative of two independent experiments. Scale bar, 10 μm. (C-H) Myosin-II siRNAs #05 and #08 prevented the disruption of podosomes upon addition of nocodazole in THP1 cells. Cells transfected with indicated siRNAs were labeled for actin by phalloidin (red) to visualize podosomes, and immunostained for myosin-IIA heavy chain (green) and α-tubulin (white) to visualize myosin-IIA filaments and microtubules, respectively. (C and D) Treatment with nocodazole of cells transfected with control siRNA resulted in disappearance of podosomes and formation of numerous myosin-II filaments. (E-H) Transfection of THP1 cells with either myosin-IIA siRNA #05 (E and F) or #08 (G and H) abolished effect of nocodazole on podosomes in spite of disruption of microtubules. The effects of individual siRNAs #05 and #08 did not differ from the effect of Dharmacon smartpool presented in Figure 3 and Supplementary Figure 5. Scale bars, 5 μm. Each condition was repeated twice. (I and J) Individual siRNA to GEF-H1 (#09) abolished the effect of nocodazole and KANK2 knockdown on focal adhesions in HT1080 cells. (I) Western blot showing the effect of individual siRNA #09 on GEF-H1 expression in control and KANK2 knockdown cells. α-tubulin was used as a loading control. (J) Total focal adhesion area in control, nocodazole (Nz)-treated and KANK2-depleted HT1080 cells, nontransfected or transfected with GEF-H1 siRNA #09 (box-and-whiskers plots; n≥40 cells for each condition in two independent experiments). The GEF-H1 siRNA #09 prevented the increase of focal adhesion area by nocodazole or KANK2 depletion similarly or stronger to the Dharmacon smartpool against GEF-H1 as shown in Supplementary Figure 10. The information corresponding the GEF-H1 siRNA #09 is presented in Materials and Methods. The p-values calculated using two-tailed Student's *t*-test are indicated.

A

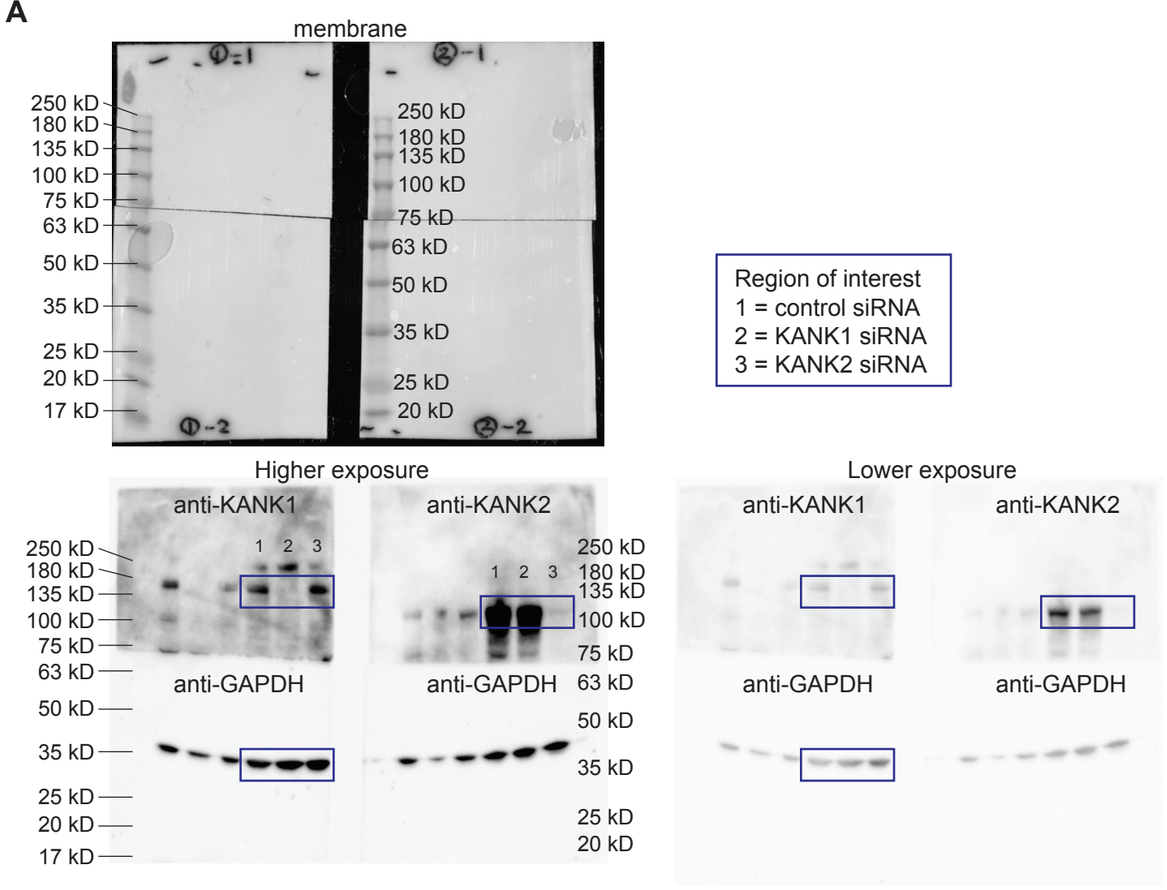
membrane
250 kD
180 kD
135 kD
100 kD
75 kD
63 kD
50 kD
35 kD
25 kD
20 kD
17 kD
Higher exposure
anti-KANK1
anti-KANK2
anti-GAPDH
1 2 3
Lower exposure
Region of interest
1 = control siRNA
2 = KANK1 siRNA
3 = KANK2 siRNA

B

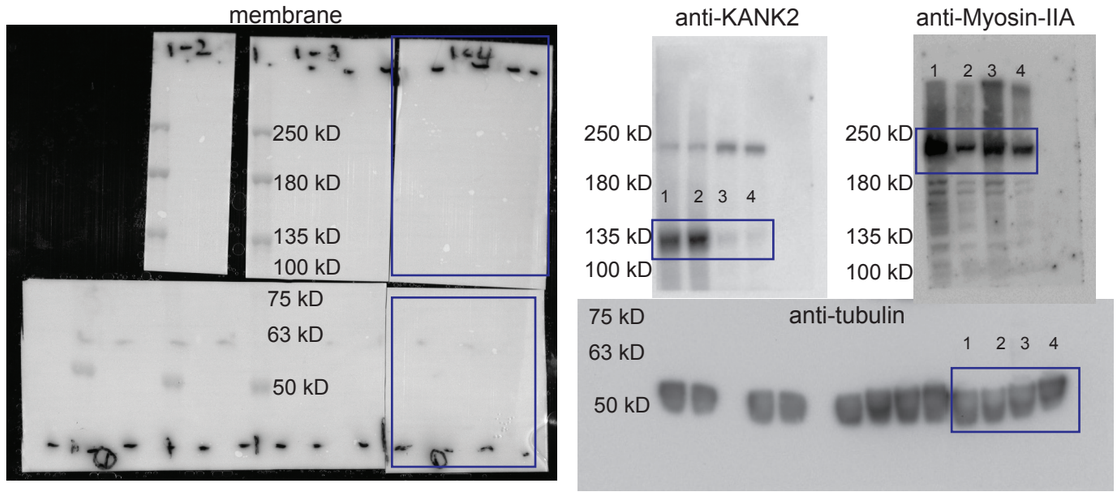
membrane
250 kD
180 kD
135 kD
100 kD
75 kD
63 kD
50 kD
anti-KANK2
anti-Myosin-IIA
anti-tubulin
1 2 3 4
Region of interest
1 = control siRNA
2 = Myosin-IIA siRNA
3 = KANK2 siRNA
4 = Myosin-IIA siRNA + KANK2 siRNA

C

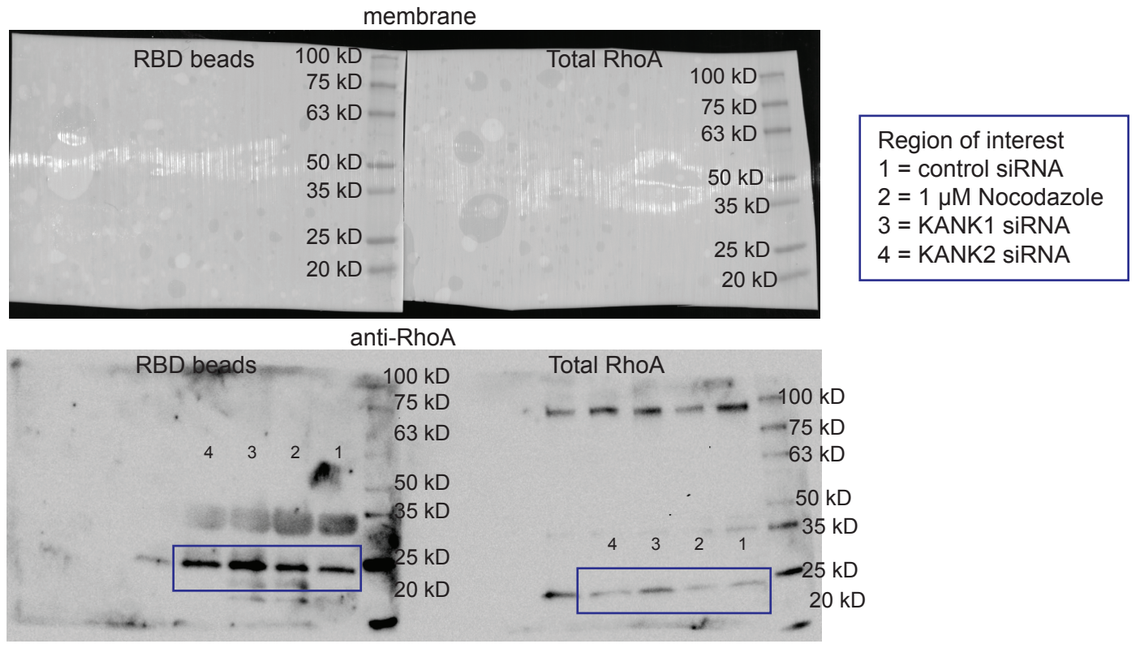
membrane
RBD beads
Total RhoA
100 kD
75 kD
63 kD
50 kD
35 kD
25 kD
20 kD
anti-RhoA
4 3 2 1
Region of interest
1 = control siRNA
2 = 1 μM Nocodazole
3 = KANK1 siRNA
4 = KANK2 siRNA

D

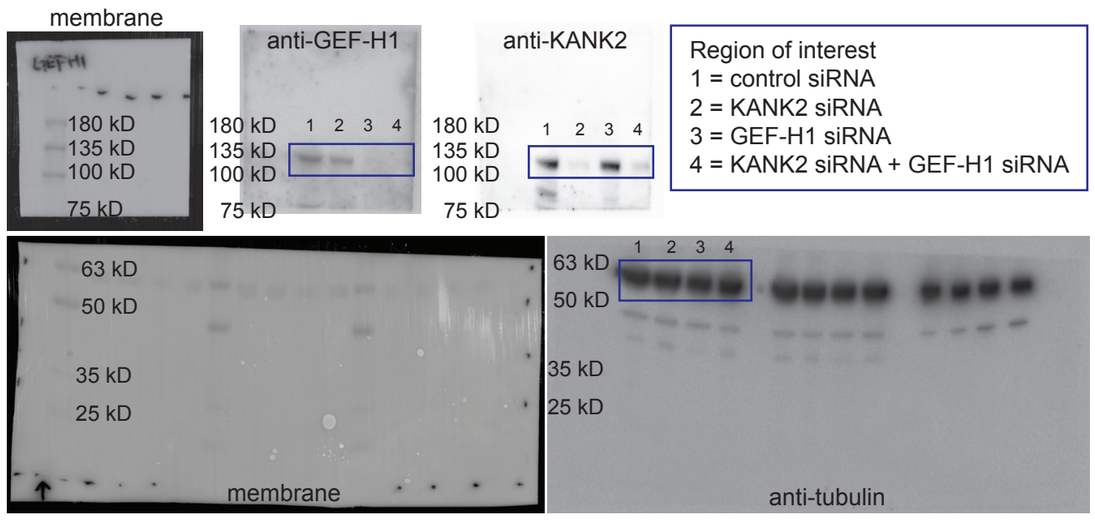
membrane
anti-GEF-H1
anti-KANK2
180 kD
135 kD
100 kD
75 kD
1 2 3 4
63 kD
50 kD
35 kD
25 kD
membrane
anti-tubulin
Region of interest
1 = control siRNA
2 = KANK2 siRNA
3 = GEF-H1 siRNA
4 = KANK2 siRNA + GEF-H1 siRNA

Supplementary Figures 12

Uncropped images of western blots of HT1080 cells showed in Figure 1D (A), Supplementary Figure 5A (B), Supplementary Figure 7A (C) and Supplementary Figure 10A (D). See detailed explanation in the legends to the corresponding figures. The boxed areas (blue frames) show the cropped images.

A Higher exposure

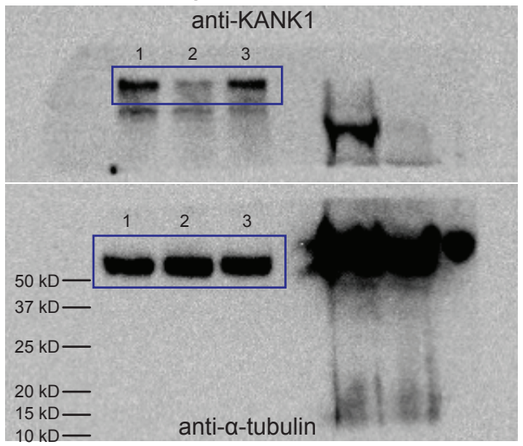

Region of interest
1 = Control siRNA
2 = KANK1 siRNA
3 = KANK2 siRNA

A' Lower exposure

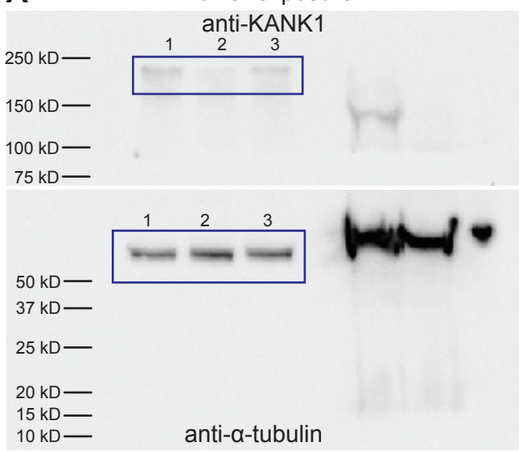

Region of interest
1 = Control siRNA
2 = KANK1 siRNA
3 = KANK2 siRNA

B Higher exposure

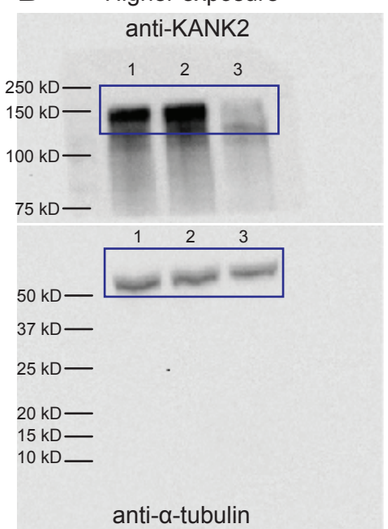

B' Lower exposure

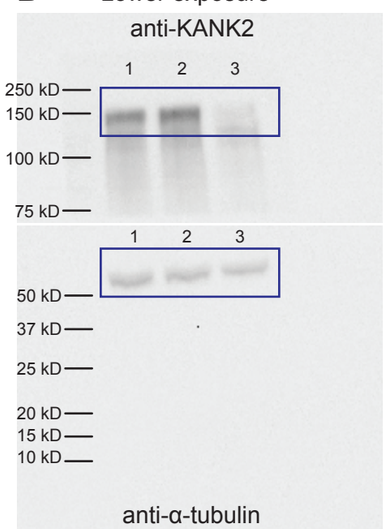

Region of interest
1 = Control siRNA
2 = KANK1 siRNA
3 = KANK2 siRNA

C

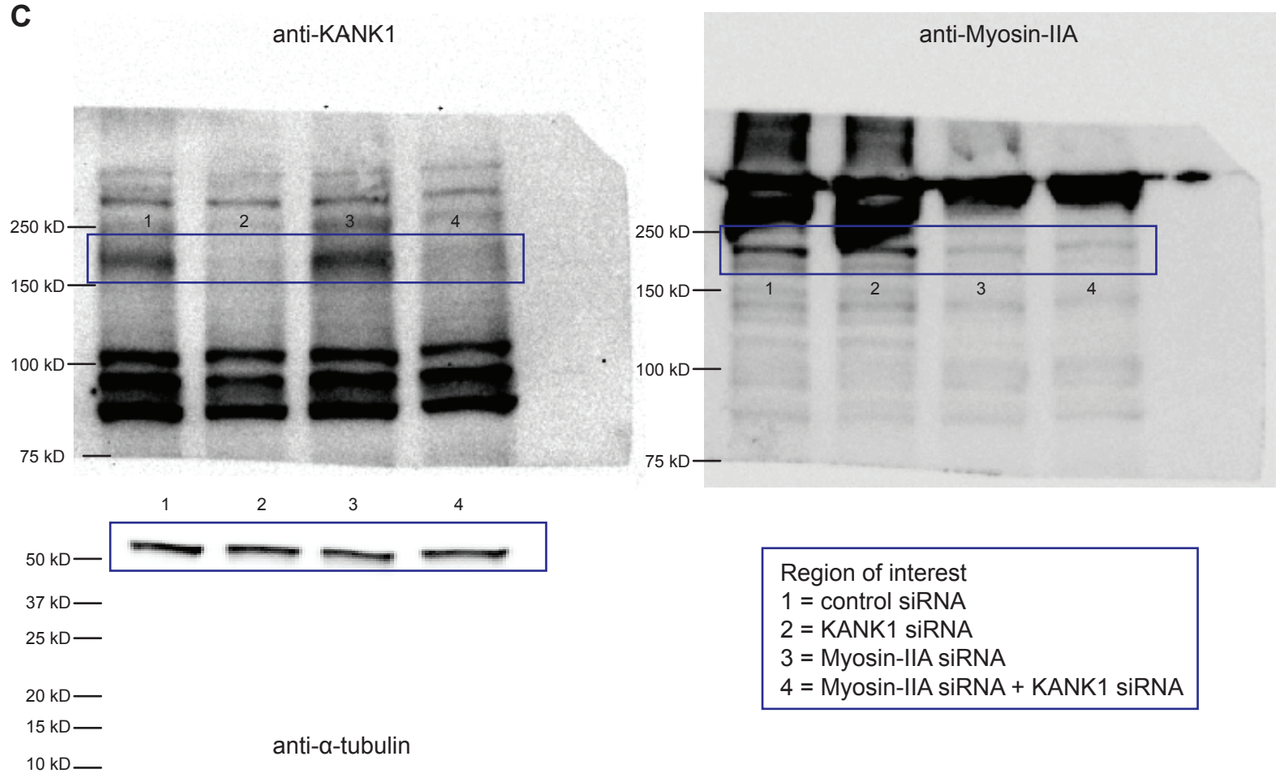

Region of interest
1 = control siRNA
2 = KANK1 siRNA
3 = Myosin-IIA siRNA
4 = Myosin-IIA siRNA + KANK1 siRNA

D

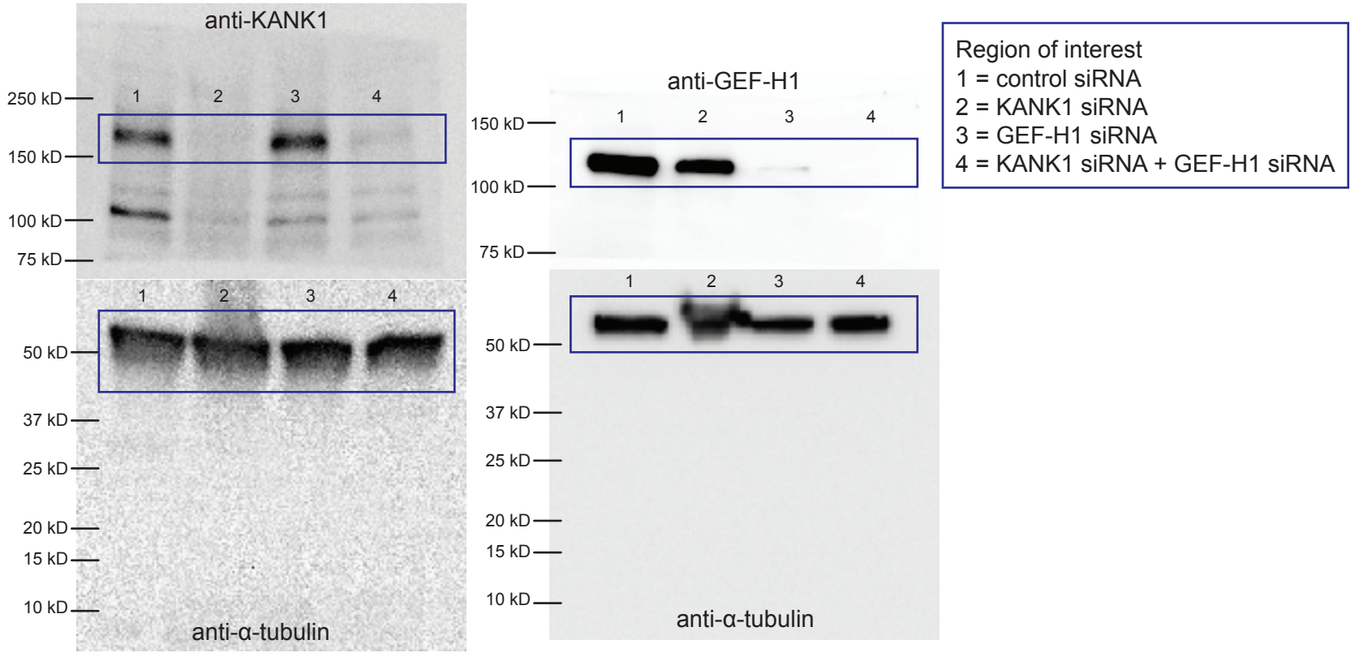

Region of interest
1 = control siRNA
2 = KANK1 siRNA
3 = GEF-H1 siRNA
4 = KANK1 siRNA + GEF-H1 siRNA

Supplementary Figure 13

Uncropped images of western blots of THP1 cells showed in Figure 1I (A and B), Figure 3I (C) and Figure 5E (D). See detailed explanation in the legends to the corresponding figures. The boxed areas (blue frames) show the cropped images.

Supplementary Table 1

Gene expression profile of HT1080 and THP1 cells presented as fragments per kilobase million (FPKM) values. See materials and method section for details of the quantification.

Gene ID	Protein	FPKM values	
		HT1080	**THP1**
23189	KANK1	5.46	6.74
25959	KANK2	18.6	71.97
256949	KANK3	0.46	0.23
163782	KANK4	1.37	-
23332	CLASP1	8.37	10.23
3688	Integrin β1	547.88	69.23
3689	Integrin β2	0.61	217.96
7094	Talin-1	98.26	80.24
7414	Vinculin	81.37	22.35
8496	Liprin-β1	65.6	8.29
60	β-actin	3876.02	4328.99
999	Cadherin-1	0.15	0.67

Supplementary movie legends

Supplementary movie 1
The microtubule plus ends of HT1080 cell transfected with control siRNA are accumulated at focal adhesions concentrated within adhesive islands

Cell with focal adhesion labeled with GFP-vinculin (red) and microtubule plus tips labeled with mKO-EB3 (green) was imaged using SIM. Single plane close to the substrate is shown. The frames were recorded at 1-second intervals over a period of 3 minutes. Display rate is 10 frames/sec. The superimposition of frames from this movie is shown in Figure 2F (middle and right images). Scale bar, 10 μm. Typical sequence is shown; 21 cells from n=2 independent experiments were examined.

Supplementary movie 2
The microtubule plus ends were randomly distributed over adhesive islands and spaces between them in HT1080 cell depleted of KANK1 and KANK2

A representative cell of three independent experiments is shown. Cell with focal adhesion labeled with GFP-vinculin (red) and microtubule plus tips labeled with mKO-EB3 (green) was imaged using SIM. Single plane close to the substrate is shown. The frames were recorded at 1-second intervals over a period of 3 minutes. Display rate is 10 frames/sec. The superimposition of frames from this movie is shown in Figure 2G (middle and right images). Scale bar, 10 μm. Typical sequence is shown; 18 cells from n=2 independent experiments were examined.

Supplementary movie 3
Microtubule outgrowth induced transient disassembly of focal adhesions in HT1080 cell

The imaging started immediately after nocodazole washout. The cell with microtubules labeled with GFP-ensconsin (green) and focal adhesions labeled with mApple-paxillin (red) was imaged using a spinning disk confocal microscopy. For microtubules, z-projection of all focal planes is shown; for focal adhesions, single plane near the substrate is shown. The frames were recorded at 30-seconds intervals over a period of 30 minutes. Display rate is 10 frames/sec. Scale bar, 10 μm. Typical sequence is shown; 9 cells from n=4 independent experiments were examined.

Supplementary movie 4
Rapamycin-induced linking of two parts of KANK1 molecule triggered disassembly of focal adhesions in HT1080 cell

Addition of 1 μg/ml rapamycin promoted the accumulation of FKBP-ΔKN-mEmerald (red) to KN-containing focal adhesions (mApple-KN-FRB, green). The enforced dimerization by rapamycin resulted in a transient disassembly of focal adhesions marked by mTFP-vinculin (inverted black and white images). Single plane close to the substrate is shown. The frames

were recorded at 30-second intervals over a period of 20 minutes using SIM. Display rate is 5 frames/sec. The movie corresponds to the time-lapse series shown in Figure 2I. Scale bar, 10 μm. Typical sequence is shown; 27 cells from n=6 experiments were examined.

Supplementary movie 5
Microtubule disruption triggered massive assembly of myosin-II filaments and disassembly of podosomes in THP1 cell

Disruption of podosomes labeled by RFP-lifeact (red, left) in THP1 cell treated with 1 μM nocodazole was accompanied by a massive burst of myosin-II filament assembly that aligned in stacks, as visualized by GFP-MRLC (green, right) using SIM. Single plane close to the substrate is shown. The frames were recorded at 15-second intervals over a period of 30 minutes using SIM. Display rate is 10 frames/sec. The movie corresponds to the time-lapse series shown in Figure 2A. Scale bar, 5 μm. Typical sequence is shown; 45 cells from n=5 experiments were examined.

Supplementary movie 6
Microtubule disruption triggered massive assembly of myosin-II filaments and augmentation of focal adhesion in HT1080 cell

Myosin-II filament formation accompanies focal adhesion augmentation in HT1080 cell treated with 1 μM nocodazole. Focal adhesions are labeled with mApple-paxillin (red), myosin-II filaments are labeled with GFP-MRLC (green) and imaged using SIM. The imaging started immediately after nocodazole addition. Single plane close to the substrate is shown. The frames were recorded at 1-minute intervals over a period of 30 minutes. Display rate is 10 frames/sec. The movie corresponds to the time-lapse series shown in Figure 3B. Scale bar, 10 μm. Typical sequence is shown; 19 cells from n=2 experiments were examined.

Supplementary movie 7
Microtubule outgrowth induced disassembly of myosin-II filaments in HT1080 cell

Microtubules are labeled with mApple-MAP4 (left) and myosin II filaments are labeled with GFP-MRLC (right) and imaged using SIM. The imaging started immediately after nocodazole washout. For microtubules, z-projection of all focal planes is shown; for myosin-II filaments, single plane near the substrate is shown. The frames were recorded at 15 seconds intervals over a period of 10 minutes. Display rate is 10 frames/sec. The movie corresponds to the time-lapse series shown in Supplementary Figure 6A. Scale bar, 10 μm. Typical sequence is shown; 16 cells from n=3 experiments were examined.

Supplementary movie 8
Transient decrease in traction forces after microtubule outgrowth in HT1080 cell

Focal adhesions are labeled with RFP-Zyxin (right) and imaged using spinning disk confocal microscopy. Single plane close to the substrate is shown. The imaging started immediately after nocodazole washout. Traction stresses (left) computed as described in Materials and Method section are presented in spectrum scale (Pa); the scale is shown on the farmost left. The frames were recorded at 1-minute intervals over a period of 31 minutes. Display rate is 10 frames/sec. The movie corresponds to the time-lapse series shown in Supplementary Figure 6C. Scale bar, 10 μm. Typical sequence is shown; 13 cells from n≥3 experiments were examined.

Supplementary movie 9
KANK2 knockdown suppressed disassembly of myosin-II filaments induced by microtubule outgrowth in HT1080 cell

The imaging started immediately after nocodazole washout. Microtubules are labeled with mApple-MAP4 (left), myosin II filaments are labeled with GFP-MRLC (right) and imaged using SIM. For microtubules, z-projection of all focal planes is shown; for myosin-II filaments, single plane near the substrate is shown. The frames were recorded at 15-second intervals over a period of 5 minutes. Display rate is 10 frames/sec. The movie corresponds to the time-lapse series shown in Supplementary Figure 6E. Scale bar, 10 μm. Typical sequence is shown; 13 cells from n=3 experiments were examined.

Supplementary movie 10
Activation of RhoA by CN03 augmented myosin-II filament formation and podosome disruption in THP1 cell

Disruption of podosomes labeled by RFP-lifeact (red, left) in THP1 cell treated with 1 μg/ml CN03 was accompanied by an increased assembly of myosin-II filaments visualized by GFP-MRLC (green, right), similar to nocodazole-treated cell. Single plane close to the substrate is shown. The frames were recorded at 1-minute intervals over a period of 40 minutes using SIM. Display rate is 10 frames/sec. The movie corresponds to the time-lapse series shown in Supplementary Figure 7C. Scale bar, 5 μm. Typical sequence is shown; 12 cells from n=3 experiments were examined.

Supplementary movie 11
Dynamics of podosomes and myosin-II filaments in control THP1 cell

Podosomes were labeled by RFP-lifeact (red) in THP1 cell treated with 0.2% DMSO. Note that myosin-II filaments visualized by GFP-MRLC (green) are localized to the peripheral rim of the cell and are absent at sites of podosome assemblies. Single plane close to the substrate is shown. The frames were recorded at 10-seconds intervals over a period of 30 minutes using SIM. Display rate is 10 frames/sec. The movie corresponds to the time-lapse series shown in Supplementary Figure 7D. Typical sequence is shown; 10 cells from n=3 experiments were examined.

Supplementary movie 12
ROCK inhibition by Y-27632 did not affect podosome dynamics in THP1 cell

Inhibition of ROCK by addition of 30 μM Y-27632 induced disassembly of myosin-II filaments visualized by GFP-MRLC (green) but did not affect podosome dynamics in THP1 cell. Podosomes are labeled by RFP-lifeact (red) and imaged using SIM. Single plane close to the substrate is shown. The frames were recorded at 10-seconds intervals over a period of 30 minutes. Display rate is 10 frames/sec. The movie corresponds to the time-lapse series shown in Figure 4A. Scale bar, 5 μm. Typical sequence is shown; 25 cells from n=3 experiments were examined.

Supplementary movie 13
Inhibition of ROCK by Y-27632 disrupted myosin-II filaments and prevented nocodazole-induced disassembly of podosomes in THP1 cell

The imaging started at the 30th minute after addition of 100 μM Y-27632 and was continued for another hour in the presence of both Y-27632 and 1 μM nocodazole. Single plane close to the substrate is shown. The frames were recorded at 2-minute intervals over a period of 40 minutes. Podosomes and myosin II filaments are labeled with RFP-lifeact (red) and GFP-MRLC (green), respectively, and imaged by SIM. The movie corresponds to the time-lapse series shown in Supplementary Figure 7E. Scale bar, 5 μm. Typical sequence is shown; 32 cells from n=3 experiments were examined.

Supplementary movie 14
Disruption of myosin-II filaments by Y-27632 resulted in recovery of podosomes in THP1 cell pre-treated with nocodazole.

Disassembly of myosin-II filaments by 30 μM Y-27632 results in recovery of podosomes in THP1 cell pre-treated with nocodazole for 30 minutes as visualized by SIM. Podosomes and myosin II filaments are labeled with RFP-lifeact (red) and GFP-MRLC (green), respectively, and imaged by SIM. The imaging started at the 30th minute after addition of nocodazole and was continued for another hour in the presence of both Y-27632 and 1 μM nocodazole. Single plane close to the substrate is shown. The frames were recorded at 2-minute intervals over a period of 40 minutes. Display rate is 10 frames/sec. The movie corresponds to the time-lapse series shown in Supplementary Figure 7F. Scale bar, 5 μm. Typical sequence is shown; 30 cells from n=3 experiments were examined.

Supplementary movie 15
Disruption of myosin-II filaments by Y-27632 resulted in recovery of podosomes in KANK1-depleted THP1 cell

Inhibition of ROCK by treatment with 30 μM Y-27632 in KANK1-depleted THP1 cell induced the formation of *de novo* podosomes, approximately 30 minutes after addition of the drug. Podosomes and myosin-II filaments are labeled with RFP-lifeact (red) and GFP-MRLC (green), respectively, and imaged by SIM. Single plane close to the substrate is shown. The frames were recorded at 30-second intervals over a period of 60 minutes using SIM. Display rate is 10 frames/sec. The movie corresponds to the time-lapse series shown in Figure 4B. Scale bar, 5 μm. Typical sequence is shown; 20 cells from n=3 experiments were examined.

Supplementary movie 16
Constitutively active RhoA and ROCK prevented the disruption of focal adhesions upon microtubule outgrowth in HT1080 cells

Control cell (left) and cells expressing constitutive active form of RhoA (middle) or ROCK (right) are imaged just after nocodazole washout by TIRF microscopy. Focal adhesions are labeled with mApple-paxillin. The frames were recorded at 30-second intervals over a period of 30 minutes. Display rate is 10 frames/sec. The movie corresponds to the time-lapse series shown in Supplementary Figure 7L. Scale bar, 10 μm. Typical sequence is shown; 17 cells (control), 22 cells (CA-RhoA) and 10 cells (CA-ROCK) from n≥3 experiments were examined.

Supplementary movie 17
GEF-H1 knockdown suppressed disruption of myosin-II filaments and prevented disassembly of focal adhesions upon microtubule outgrowth in HT1080 cell

The imaging started immediately after nocodazole washout. Microtubules are labeled with mApple-MAP4 (left), myosin II filaments are labeled with GFP-MRLC (right); focal adhesions are labeled with mTFP-vinculin (right), and were imaged using SIM. For microtubules, z-projection of all focal planes is shown; for myosin-II filaments and focal adhesions, single planes near the substrate are shown. The frames were recorded at 15 seconds intervals over a period of 10 minutes. Display rate is 10 frames/sec. The movie corresponds to the time-lapse series shown in Supplementary Figure 10I. Scale bar, 10 μm. Typical sequence is shown; 13 cells from n=3 experiments were examined.

Supplementary references

1 Wittmann, T. & Waterman-Storer, C. M. Cell motility: can Rho GTPases and microtubules point the way? *Journal of cell science* **114**, 3795-3803 (2001).

2 Small, J. V., Geiger, B., Kaverina, I. & Bershadsky, A. How do microtubules guide migrating cells? *Nature reviews. Molecular cell biology* **3**, 957-964, doi:10.1038/nrm971 (2002).

3 Stehbens, S. & Wittmann, T. Targeting and transport: how microtubules control focal adhesion dynamics. *The Journal of cell biology* **198**, 481-489, doi:10.1083/jcb.201206050 (2012).

4 Kaverina, I. & Straube, A. Regulation of cell migration by dynamic microtubules. *Seminars in cell & developmental biology* **22**, 968-974, doi:10.1016/j.semcdb.2011.09.017 (2011).

5 Linder, S., Wiesner, C. & Himmel, M. Degrading devices: invadosomes in proteolytic cell invasion. *Annual review of cell and developmental biology* **27**, 185-211, doi:10.1146/annurev-cellbio-092910-154216 (2011).

6 Bouchet, B. P. & Akhmanova, A. Microtubules in 3D cell motility. *Journal of cell science* **130**, 39-50, doi:10.1242/jcs.189431 (2017).

7 Krylyshkina, O. *et al.* Modulation of substrate adhesion dynamics via microtubule targeting requires kinesin-1. *The Journal of cell biology* **156**, 349-359, doi:10.1083/jcb.200105051 (2002).

8 Rodionov, V. I. *et al.* Microtubule-dependent control of cell shape and pseudopodial activity is inhibited by the antibody to kinesin motor domain. *The Journal of cell biology* **123**, 1811-1820 (1993).

9 Even-Ram, S. *et al.* Myosin IIA regulates cell motility and actomyosin-microtubule crosstalk. *Nature cell biology* **9**, 299-309, doi:10.1038/ncb1540 (2007).

10 Joo, E. E. & Yamada, K. M. MYPT1 regulates contractility and microtubule acetylation to modulate integrin adhesions and matrix assembly. *Nature communications* **5**, 3510, doi:10.1038/ncomms4510 (2014).

11 Ezratty, E. J., Bertaux, C., Marcantonio, E. E. & Gundersen, G. G. Clathrin mediates integrin endocytosis for focal adhesion disassembly in migrating cells. *The Journal of cell biology* **187**, 733-747, doi:10.1083/jcb.200904054 (2009).

12 Ezratty, E. J., Partridge, M. A. & Gundersen, G. G. Microtubule-induced focal adhesion disassembly is mediated by dynamin and focal adhesion kinase. *Nature cell biology* **7**, 581-590, doi:10.1038/ncb1262 (2005).

13 Juanes, M. A. *et al.* Adenomatous polyposis coli nucleates actin assembly to drive cell migration and microtubule-induced focal adhesion turnover. *The Journal of cell biology*, doi:10.1083/jcb.201702007 (2017).

14 Ren, X. D., Kiosses, W. B. & Schwartz, M. A. Regulation of the small GTP-binding protein Rho by cell adhesion and the cytoskeleton. *The EMBO journal* **18**, 578-585, doi:10.1093/emboj/18.3.578 (1999).

15 Chang, Y. C., Nalbant, P., Birkenfeld, J., Chang, Z. F. & Bokoch, G. M. GEF-H1 couples nocodazole-induced microtubule disassembly to cell contractility via RhoA. *Molecular biology of the cell* **19**, 2147-2153, doi:10.1091/mbc.E07-12-1269 (2008).

16 Krendel, M., Zenke, F. T. & Bokoch, G. M. Nucleotide exchange factor GEF-H1 mediates cross-talk between microtubules and the actin cytoskeleton. *Nature cell biology* **4**, 294-301, doi:10.1038/ncb773 (2002).

17 Kaverina, I., Rottner, K. & Small, J. V. Targeting, capture, and stabilization of microtubules at early focal adhesions. *The Journal of cell biology* **142**, 181-190 (1998).
18 Kopp, P. *et al.* The kinesin KIF1C and microtubule plus ends regulate podosome dynamics in macrophages. *Molecular biology of the cell* **17**, 2811-2823, doi:10.1091/mbc.E05-11-1010 (2006).
19 Efimova, N. *et al.* Podosome-regulating kinesin KIF1C translocates to the cell periphery in a CLASP-dependent manner. *Journal of cell science* **127**, 5179-5188, doi:10.1242/jcs.149633 (2014).
20 Cornfine, S. *et al.* The kinesin KIF9 and reggie/flotillin proteins regulate matrix degradation by macrophage podosomes. *Molecular biology of the cell* **22**, 202-215, doi:10.1091/mbc.E10-05-0394 (2011).
21 Zhu, X., Efimova, N., Arnette, C., Hanks, S. K. & Kaverina, I. Podosome dynamics and location in vascular smooth muscle cells require CLASP-dependent microtubule bending. *Cytoskeleton* **73**, 300-315, doi:10.1002/cm.21302 (2016).
22 Riveline, D. *et al.* Focal contacts as mechanosensors: externally applied local mechanical force induces growth of focal contacts by an mDia1-dependent and ROCK-independent mechanism. *The Journal of cell biology* **153**, 1175-1186 (2001).
23 Oakes, P. W. & Gardel, M. L. Stressing the limits of focal adhesion mechanosensitivity. *Curr Opin Cell Biol* **30**, 68-73, doi:10.1016/j.ceb.2014.06.003 (2014).
24 Vicente-Manzanares, M., Ma, X., Adelstein, R. S. & Horwitz, A. R. Non-muscle myosin II takes centre stage in cell adhesion and migration. *Nature reviews. Molecular cell biology* **10**, 778-790, doi:10.1038/nrm2786 (2009).
25 Bershadsky, A. D. *et al.* Assembly and mechanosensory function of focal adhesions: experiments and models. *European journal of cell biology* **85**, 165-173, doi:10.1016/j.ejcb.2005.11.001 (2006).
26 Gardel, M. L., Schneider, I. C., Aratyn-Schaus, Y. & Waterman, C. M. Mechanical integration of actin and adhesion dynamics in cell migration. *Annual review of cell and developmental biology* **26**, 315-333, doi:10.1146/annurev.cellbio.011209.122036 (2010).
27 Vicente-Manzanares, M. & Horwitz, A. R. Adhesion dynamics at a glance. *Journal of cell science* **124**, 3923-3927, doi:10.1242/jcs.095653 (2011).
28 Prager-Khoutorsky, M. *et al.* Fibroblast polarization is a matrix-rigidity-dependent process controlled by focal adhesion mechanosensing. *Nature cell biology* **13**, 1457-1465, doi:10.1038/ncb2370 (2011).
29 Bhuwania, R. *et al.* Supervillin couples myosin-dependent contractility to podosomes and enables their turnover. *Journal of cell science* **125**, 2300-2314, doi:10.1242/jcs.100032 (2012).
30 Cervero, P., Wiesner, C., Bouissou, A., Poincloux, R. & Linder, S. Lymphocyte-specific protein 1 regulates mechanosensory oscillation of podosomes and actin isoform-based actomyosin symmetry breaking. *Nature communications* **9**, 515, doi:10.1038/s41467-018-02904-x (2018).
31 Rafiq, N. B. *et al.* Podosome assembly is controlled by the GTPase ARF1 and its nucleotide exchange factor ARNO. *The Journal of cell biology* **216**, 181-197, doi:10.1083/jcb.201605104 (2017).

32 Dulyaninova, N. G., Ruiz, P. D., Gamble, M. J., Backer, J. M. & Bresnick, A. R. S100A4 regulates macrophage invasion by distinct myosin-dependent and myosin-independent mechanisms. *Molecular biology of the cell* **29**, 632-642, doi:10.1091/mbc.E17-07-0460 (2018).
33 van Helden, S. F. *et al.* PGE2-mediated podosome loss in dendritic cells is dependent on actomyosin contraction downstream of the RhoA-Rho-kinase axis. *Journal of cell science* **121**, 1096-1106, doi:10.1242/jcs.020289 (2008).
34 Bouchet, B. P. *et al.* Talin-KANK1 interaction controls the recruitment of cortical microtubule stabilizing complexes to focal adhesions. *eLife* **5**, doi:10.7554/eLife.18124 (2016).
35 Sun, Z. *et al.* Kank2 activates talin, reduces force transduction across integrins and induces central adhesion formation. *Nature cell biology* **18**, 941-953, doi:10.1038/ncb3402 (2016).
36 Bulinski, J. C., Odde, D. J., Howell, B. J., Salmon, T. D. & Waterman-Storer, C. M. Rapid dynamics of the microtubule binding of ensconsin in vivo. *Journal of cell science* **114**, 3885-3897 (2001).
37 Tee, Y. H. *et al.* Cellular chirality arising from the self-organization of the actin cytoskeleton. *Nature cell biology* **17**, 445-457, doi:10.1038/ncb3137 (2015).
38 Hu, S. *et al.* Long-range self-organization of cytoskeletal myosin II filament stacks. *Nature cell biology* **19**, 133-141, doi:10.1038/ncb3466 (2017).
39 Burkel, B. M., von Dassow, G. & Bement, W. M. Versatile fluorescent probes for actin filaments based on the actin-binding domain of utrophin. *Cell motility and the cytoskeleton* **64**, 822-832, doi:10.1002/cm.20226 (2007).